EXPLANATORY SUPPLEMENT

TO THE

IRAS SERENDIPITOUS

SURVEY CATALOG

S. G. KLEINMANN

R. M. CUTRI

E. T. YOUNG

F. J. LOW

F. C. GILLETT

1986

IRAS
SERENDIPITOUS SURVEY CATALOG

Explanatory Supplement

S. G. Kleinmann
University of Massachusetts

R. M. Cutri
E. T. Young
F. J. Low
University of Arizona

F. C. Gillett
National Optical Astronomy Observatories

TABLE OF CONTENTS

	Page
I. INTRODUCTION	
II. POINTED OBSERVATION DATABASE	
A. Characteristics	II-1
B. Scheduling of Pointed Observations	II-3
C. Pointed Observation Processing	II-3
D. Beam Size Effects	II-7
E. Photometry	II-9
III. SSC DATA PROCESSING	
A. Grid Pair Selection	III-1
B. Source Confirmation	III-2
C. Position and Flux Density Refinement	III-7
C.1. Position Refinement	III-7
C.2. Flux Density Refinement	III-8
D. Confusion Processing	III-8
E. Band Merging	III-9
E.1. Positional Tests	III-9
E.2. Position Refinement	III-10
F. Effective Grid Areas	III-10
G. Identification of Overlapping Fields	III-14
H. Associations with Other Astronomical Catalogs	III-14
IV. ANALYSIS OF THE SSC	
A. Confirmation, Reliability and Sensitivity Limits	IV-1
A.1. Confirmation Tuning and Confirmation Rates	IV-1
A.2. Reliability of Confirmed Sources	IV-6
A.3. Band Merging Reliability	IV-7
A.4. Sensitivity Limits	IV-7
B. Association Statistics	IV-11
C. Absolute Positional Accuracy	IV-21
D. Photometric Accuracy	IV-22
D.1. Accuracy of Relative Flux Densities	IV-22
D.2. Accuracy of Absolute Flux Densities	IV-22
D.3. Flux Density Uncertainty	IV-26
E. Sky Coverage and Source Densities	IV-27
F. General Catalog Statistics	IV-36
V. FORMATS OF THE IRAS SERENDIPITOUS SURVEY CATALOG	
A. Introduction	V-1
B. Machine Readable Version	V-1
C. Printed Version	V-8

VI. ADDITIONAL CONSIDERATIONS

A. Effects of High Source Density VI-1
B. Asteroids VI-1
C. Redundant Sources VI-4

VII. REFERENCES

VIII. ACKNOWLEDGEMENTS

APPENDIX A: TABLE OF OVERLAPPING FIELDS

I. INTRODUCTION

In 1983 the sky was surveyed by the Infrared Astronomical Satellite (IRAS) in four broad spectral bands centered at 12, 25, 60 and 100 μm. During the course of the 300 day mission, about two-thirds of the satellite time was used to carry out an unbiased sky survey which led to the production of the IRAS Point Source Catalog (IRAS/PSC) containing 245,889 sources. That catalog, along with many other aspects of the mission, are described in the IRAS Catalogs and Atlases Explanatory Supplement (1985) [Referenced below as the "Main IRAS Supplement"]. A portion of the remaining mission was used to conduct a series of Pointed Observations, usually directed at objects of interest, and using the various capabilities of the satellite. Many of these Pointed Observations were performed by repeatedly scanning the 0.5 deg. wide survey detector array over the selected object. These scans were combined to produce a sensitive map of area about one deg.^{2} around the selected source (or, in some cases, a targeted "blank" field). By spatially coadding the repeated scans comprising each Pointed Observation a large data base was generated. Young et al. (1985) have described these data, the Pointed Observation program and the associated data processing at the Infrared Processing and Analysis Center (IPAC).

This document describes the IRAS Serendipitous Survey Catalog (IRAS/SSC) which has been constructed using the fortuitous observations at 12, 25, 60, and 100 μm of 43,866 point-like sources that happened to lie in 1813 of the individual fields included in the Pointed Observation program. Because the Pointed Observations resulted in longer integration times for each source in the field than was possible in the all- sky survey mode, the limiting sensitivity for the IRAS/SSC is typically better than that of the IRAS/PSC by a factor of about 4. Also, the photometric accuracy, especially for faint sources, is improved relative to that of the IRAS/PSC. The amount of sky sampled in the SSC is nearly 1400 deg.^{2} but because of uneven sensitivity across the Pointed Observation fields, the effective sky coverage is 1108 deg.^{2}. Excluding certain areas of great scientific interest to the team who planned the observations (specifically, the Galactic plane and the Magellanic Clouds), the Pointed Observations were widely distributed on the sky. Positional association of the SSC sources with those in the PSC reveal that 11,129 are in both IRAS catalogs; also, 5470 SSC sources have been cataloged at other wavelengths.

The positional accuracy of the SSC is not as high as that of the PSC, in part because of the restricted geometry of the observations themselves and also because of compromises made in processing the data. In those cases where more accurate positions are critically needed, it may be possible to obtain better results through re-processing the observations at one of the IRAS data centers.

The main objective of the Serendipitous Survey was to extend the detection threshold for point sources over a finite but significant portion of the sky so that those sources could be studied individually. No attempt has been made to construct an unbiased sample by removing the targeted sources or by correcting either for the non-random sky coverage or for the uneven depth of the survey corresponding to different characteristics of the several observing modes. Because most of the SSC sources are faint and because it was inherently difficult to achieve a uniform level of completeness in this program, it was decided to emphasize high reliability and photometric accuracy. These important SSC objectives were achieved by retaining only those sources which were detected in each of two independent Pointed Observations and by averaging the two measurements. No fields were included where only a single Pointed Observation was available. This strategy also provided a means for rejecting some asteroids and any other moving objects.

Frequently, independent observations were made of nearly the same region of sky and were treated in this catalog as separate fields; this practice resulted in partially redundant data sets. These overlapping fields are noted in the SSC to facilitate their further study. Because each of the 1813 fields in the SSC is unique in the sense that it may differ from other fields, both according to the observing mode that was used and in the wide range of source densities encountered, the catalog is presented field-by-field along with data pertinent to each field. Enough information is retained to permit the user to reorganize the source lists as needed. Those fields which overlap other fields are cross referenced. The fields are ordered by the right ascensions of their centers and the source list within each field is also ordered by right ascension.

An important objective of this catalog is to present a list of reliable sources found in all the selected Pointed Observation fields despite effects of high source density and/or complex backgrounds. In those heavily crowded fields where source confusion degrades the sensitivity, reliability, completeness, positional accuracy or photometric accuracy, the guiding philosophy has been as follows:

(a) accept some degradation,

(b) flag sources where confusion may have affected the confirmation process,

(c) indicate the local density of sources for each wavelength band,

(d) provide information on the effects of confusion so that the user is both warned and equipped to make valid scientific judgments.

This policy has the result that many of the SSC fields and sources must be analyzed with particular care by the user, but it also means that many faint sources are included in crowded regions of scientific interest.

In summary, the main features of the SSC relative to the PSC are as follows:

1. Enhanced sensitivity for point-like sources in all four wavelength bands over a few percent of the sky.
2. Excellent reliability in low surface density fields.
3. Uneven sky coverage and completeness.
4. Reduced positional accuracy.
5. Improved photometric accuracy.
6. Much greater depth in crowded fields at the expense of reliability and accuracy.

The user of the SSC should be aware of the following considerations. First, a set of high latitude, unique, less crowded fields, selected as described in Section IV, was used in much of the current analysis. This subset of the catalog is comprised of 450 fields containing 5100 sources. Second, for these high latitude fields, reliability of order 99% was achieved for sources brighter than the flux density limits of 100, 150, 120, and 400 mJy for the 12, 25, 60, and 100 μm bands, respectively; note that even within these fields the completeness limits vary. Third, the measured positional accuracy of SSC sources defines a search box with dimensions of 30" x 180" at 12 μm, increasing to 60" x 140" at 60 μm. The orientation of each search box is indicated by the grid orientation angle given in the appropriate field header. Fourth, for the high latitude subset of fields, the systematic photometric errors introduced by the absolute calibration are nearly identical with those in the PSC. The remaining systematic errors and uncertainties due to lack of reproducibility are less than $\pm$10% on average for sources detected with high signal-to- noise, and the

effects of noise are well quantified within each field. Fifth, for lower latitude fields, or fields where the underlying background has a complex structure, the reliability, completeness, positional, and photometric accuracies may be substantially degraded and each field must be analyzed with caution. Sixth, as in the PSC many sources are slighty extended and will have erroneous flux densities; other IRAS data bases such as the INTN mode grids (Young et al, 1985) should be used for the study of small extended sources.

In the preparation and presentation of the SSC, an effort was made, so far as possible, to conform to conventions established in the preparation and presentation of the PSC. In the following sections only that information not found in the Main IRAS Supplement (1985) or in the Users Guide to IRAS Pointed Observation Products (Young et al. 1985) and needed for the use of this catalog will be given. This includes: information on the Pointed Observation data base from which the point sources were extracted and the extraction process (Section II), on the data processing used to develop the SSC from the list of extracted sources (Section III), on the reliability and sensitivity of the SSC, its positional and photometric accuracy and certain statistical properties (Section IV), on the format and content of the SSC in its machine-readable and printed forms (Section V), warnings to the user concerning confusion effects, asteroids and redundant sources (Section VI), and a table of overlapping fields (Appendix A).

II. POINTED OBSERVATIONS DATABASE

The Pointed Observation database described by Young et al. (1985) is available from the National Space Science Data Center (NSSDC) and at the IRAS data centers. IPAC and the two data centers in Europe provide software and facilities for detailed analysis. The SSC is based on processing of the Pointed Observation data at IPAC including extraction of the point sources which comprise the input to the SSC production software described in Section III; this section describes the Pointed Observation database and key aspects of the processing at IPAC.

A. Characteristics

All of the IRAS Pointed Observations were made using command sequences (macros) stored in the satellite's computer. The macros are designated by a three letter code giving the generic class of observation, a two-digit number identifying the specific type and a single letter indicating the version. Although the number of macros is large, the vast majority of the survey array observations were made with only a few of these macros. For the Serendipitous Survey, only observations made with the DPS or TPS class macros have been included since these were the only macro classes which provided significant areal coverage combined with improved sensitivity. Moreover, these macros were by far the most important numerically, comprising ~90% of the Pointed Observation program. In these macros, the satellite repeatedly scanned an area of sky using the entire survey array, producing infrared maps of the observed region 0.5 deg. wide and of different lengths ranging from 0.6 to 6 degrees. The scan rate adopted was one-half the survey scan rate of 3.85 arcmin/sec. Variations included the number of scans and the size of the cross-scan step between scans; these are indicated by different numbers in the macro name. Characteristics of these macros are given in Table II.A. The improvement in signal-to-noise ratio (SNR) compared to the PSC, was computed from the increased integration time afforded by the macro.

Table II.A. DPS and TPS Macro Characteristics

Macro Name	Number of Scans	Scan Length (Arcmin)	Cross Step (Arcmin)	SNR Gain	Catalog Code
DPS02B	6	96	0.3	4.8	A
DPS05B	3	360	1.0	3.5	B
DPS52B	6	96	0	4.8	C
TPS52B	6	96	0	4.8	L
DPS55B	3	360	0	3.5	D
DPS60B	4	60	0.8	4.0	E
DPS60C	5	48	0.4	4.4	K
DPS60D	5	48	0.4	4.4	F
DPS60M	5	48	0.4	4.4	M
DPS61C	12	48	0.2	6.9	G
DPS61D	15	48	0.2	7.7	H
DPS62D	9	96	0.4	6.0	I
DPS63D	3	96	0.8	3.5	J

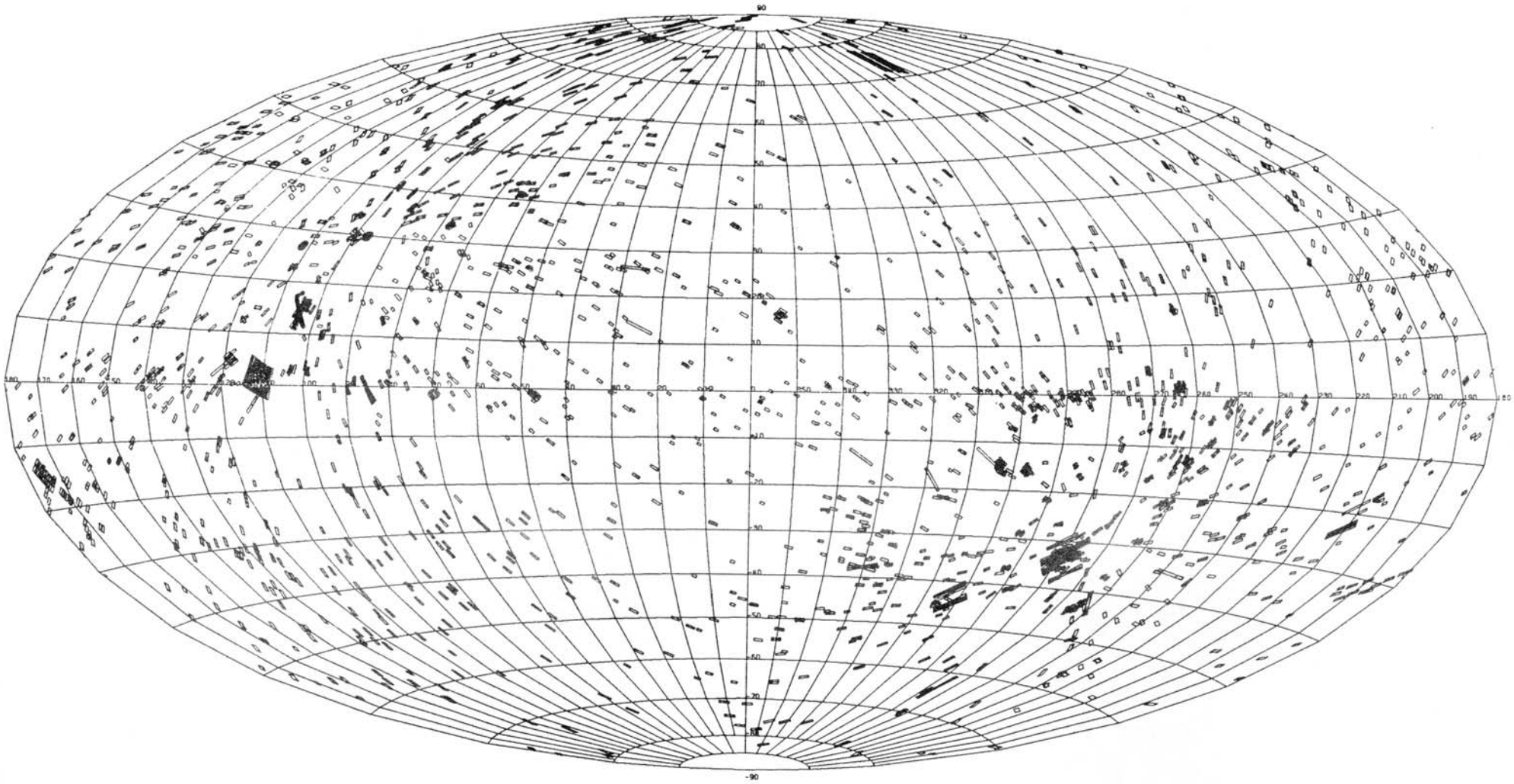

Figure II.A Locations of IRAS Pointed Observations in Galactic Coordinates.

B. Scheduling of Pointed Observations

The all-sky survey was given first priority in the selection of satellite observing time; the Pointed Observations were inserted into the satellite operations plan on the basis of an internal priority rating system and sky viewing constraints. As a method of deciding on the targets for the Pointed Observations, the Joint IRAS Science Working Group (JISWG) selected targets of scientific interest and assigned their relative priorities. In practice, the complexities of the scheduling and the overall highest priority assigned to the survey, coupled with the limited area in which the telescope could point at any given time, meant that Pointed Observations were not carried out on priority standing alone. Additionally, a large list of blank fields evenly spaced on the sky was available if no higher priority targets were suitable during a given observing period.

In particular, a further guideline used in scheduling of the Pointed Observations was designed to allow discrimination of transient phenomena in the IRAS bands such as asteroids, earth satellites, and dust particles. An attempt was made to repeat each observation at least once. To increase the integration time some observations were repeated many times. It is this strategy which permits the SSC to be based on the "confirmation" process described in Section III.B.

The coverage of the Pointed Observations on the sky in galactic coordinates is depicted in Figure II.A. The user of the Serendipitous Survey is reminded that sky coverage is not strictly random for two reasons. First, the targeted positions usually contained a source of specific scientific interest. Second, constraints due to the survey strategy and the satellite design strongly affected the sky available for Pointed Observations. Because of the orbital motion of the satellite, and the various pointing constraints (including Earth limb and Sun avoidance), the observations tended to concentrate near the ecliptic poles (l = 96 deg., b = +30 deg. and l =276 deg., b = -30 deg.) where most of the observing time was available.

C. Pointed Observation Processing

The detector output and positional data for the Pointed Observations were processed by the Deep Sky Coadd Observations Processor (DSCO) at the IPAC. The primary output of the processor is a set of eight two-dimensional arrays of numbers (called maps), produced by positionally coadding the detector data. The eight maps represent the signal and the noise in each of the four IRAS bands for the region of sky covered by the observation. The eight maps comprise a "grid".

Two kinds of grids were produced, FLUX mode and intensity or INTN mode grids. INTN grids are unfiltered and preserve the total intensity information of the observed region. For the FLUX grids, the detector data are filtered with a zero-sum bandpass filter centered on the point source spatial frequency. This processing technique suppresses the extended spatial scale information and achieves the highest sensitivity for the detection of point sources in uncomplicated fields. Because the IRAS Serendipitous Survey is intended to produce a catalog of faint point sources, only FLUX mode grids were used for the SSC processing.

The important process steps in producing FLUX grids are:

1. Removal of residual radiation hits and other glitches from the data.
2. Bandpass filtering of the detector data.
3. Mapping the detector samples to a spatial grid using the refined pointing data from the satellite.

4. Binning the data in a two-dimensional spatial array.
5. Computing the weighted flux and noise estimates for each pixel in the grid.
6. Extracting sources from grids.
7. Applying suitable calibration factors.

High frequency noise spikes such as charged particle hits are removed using a simple algorithm that compares the power in a high frequency (or glitch) band to the power in a band centered on the point source frequency. If the glitch is of sufficient amplitude and if the ratio of the power in the glitch band to the power in the source band exceeds a predetermined threshold, three samples are removed from the data stream. Note that a point source contains at least six samples. This filter successfully removes over 90% of the narrow glitches from the data.

In the next stage of processing, the data stream is passed through a digital zero-sum filter centered on the point source spatial frequency. The filter consists of a running 18-sample weighted average of the detector values. The weights for each of the first six and final six points are -1/12 and for the middle six points are +1/6. Thus, for smooth backgrounds, the filter output is zero. A position for the output point is assigned based on the mid position of the input samples. Figure II.B shows the resultant in-scan profile for a point source.

After filtering, the grid coordinates of the detector center at the sample time are computed. The data value is coadded to each grid cell whose center falls within a specified in-scan and cross-scan distance from the detector center. The cell sizes used in the maps are given in Table II.B. These values were set in part by the detector field of view, but mainly by the spatial smoothing applied in the DSCO processor.

Table II.B. Grid Pixel Sizes

Band (μm)	In-Scan (Arcmin)	Cross-Scan (Arcmin)
12	0.25	0.60
25	0.25	0.60
60	0.50	0.60
100	1.00	0.60

Following the filtering and binning process, maps of the signal and the noise are generated for each wavelength band. The signal grid consists of the weighted averages of the detector data in each grid cell (or pixel). The weighting gives minimum variance for the samples added into a pixel. If f_i is a flux sample added into a pixel and n_i is the noise estimate associated with that sample, the averaged flux <f> of M samples is given by:

$$<f> = \frac{\sum f_i \, w_i}{\sum w_i} \qquad \text{II.1}$$

where the weighting factor $w_i=(n_i)^{-2}$. For each detector, the noise is estimated using a median estimator similar to the type used in the production of the PSC. Median noise estimates are described in Section V.C.2 of the Main IRAS Supplement. The median of all the individual detector noise estimates for a given band defines the median noise in that band.

The noise map is generated by combining the sample variance with the detector noise weights for each pixel. The chi-square for a pixel is defined as:

$$\chi^2 = \sum f_i{}^2 w_i - \left(\sum w_i\right) <f>^2 \qquad \text{II.2}$$

The estimated local noise $<\sigma>$ is then:

$$<\sigma> = \left(\frac{1+\chi^2}{M \sum w_i}\right)^{1/2} \qquad \text{II.3}$$

This local noise is nearly equal to the minimum variance estimate for a small number of scans, but approaches the sample variance/$\sqrt{M}$ for a large number of scans. In complex fields it is sensitive to structure and can be artificially high in such areas.

The sources for the Serendipitous Survey were extracted with a simple threshold extractor which used both the signal and local noise maps to identify sources. The signal map is scanned for contiguous groups of pixels above a predetermined flux threshold. This threshold is expressed in terms of the median noise for the grid and has been set at 3.0 for this catalog. At the corresponding positions in the local noise grid, the initial source extraction required the signal to local noise ratio to be greater than 2.5.

Once contiguous regions above the thresholds are identified, an attempt is made to separate partially overlapping sources. A rethresholding technique is used to identify and separate these sources. This new extraction threshold is the original threshold plus a contribution from the median signal-to- noise ratio over the region to be separated. The user is cautioned that only well defined sources of roughly equal intensity are reliably separated by this algorithm. The Serendipitous Survey includes many examples, primarily in fields where the source density is high, of overlapping sources that have not been separated by the rethresholding technique. For such sources, the extracted position is then a flux weighted average of the positions of the constituent sources.

A correlation coefficient for an extracted source was calculated using a point source profile based on observations of the asteroid Egeria. A typical profile is shown in Figure II.B. This template was obtained from half survey rate observations which were binned at twice the normal pixel resolution and then resampled evenly using a cubic spline interpolation technique. The calculation of the correlation coefficient was similar to that for the PSC described in Section V.C.4 of the Main IRAS Supplement, except that the slope and baseline were zero due to the bandpass filtering of the data (see the Main IRAS Supplement for the definition of these quantities).

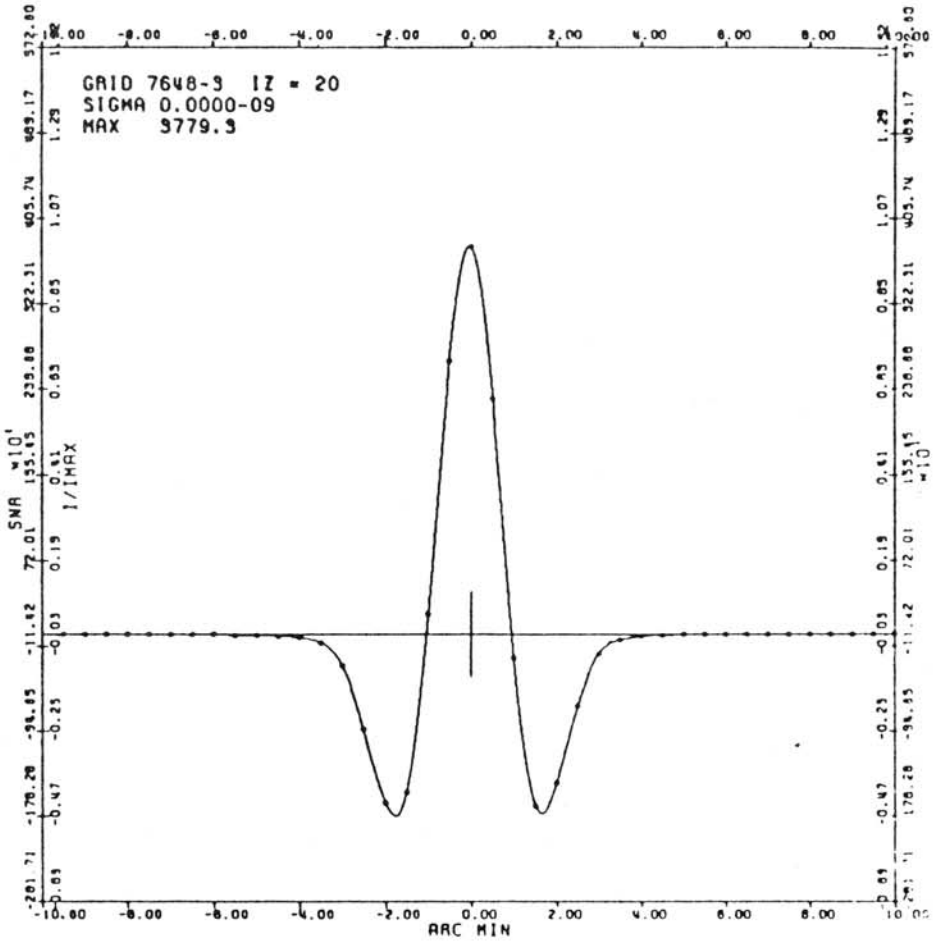

FLUX In-Scan Point Source Signature, 60 um Band

Figure II.B The SSC point source response function at 60 μm illustrating the result of FLUX filtering.

D. Beam Size Effects

The presence of negative sidelobes in the FLUX filtered point spread function complicates the analysis of high source density regions. Although the solid angle "covered" by the full filtered point spread function is nearly three times the geometrical solid angle of the detector, the beam size appropriate for estimating effects of confusion is significantly smaller. Unlike a more typical beam profile, with only positive sidelobes, the character of the confusion effects in the SSC depend on the source density in a non-monotonic fashion. It is possible to distinguish two cases, the first case applies to moderately crowded fields and the second to more heavily crowded situations.

Two competing effects will modify the source extractions from a FLUX filtered grid. In the first case, at moderate source densities, weak sources within the negative sidelobes of another source (within 60", 60", 120", and 240" for the 12, 25, 60, and 100 μm bands, respectively) are reduced in flux. At these source densities, the primary penalty is a loss of completeness. For the second case, the source density is high enough for multiple sources to occur within the central filter peak. Then the extracted fluxes will often be higher than the true fluxes, leading to the usual effects of confusion. Given the filter parameters chosen for Pointed Observations processing, the effective beam size associated with this second case is very nearly the geometrical solid angle of the detector.

To illustrate these two effects, the response of a one- dimensional FLUX filter was simulated for source distributions of various densities and log N vs log F power laws. Figure II.C shows the results from a simulation at 60 μm in which the density of sources brighter than 100 mJy is 20/deg.^{2} and a -1.5 power law is assumed for the relationship between source density and flux. The solid line represents the assumed underlying source distribution at 15" in-scan resolution. The dotted line represents the output of the FLUX filter. As can be seen from the comparison, the brighter sources will be extracted with slightly underestimated fluxes. Only at lower thresholds, and hence higher source densities, are there cases of merged sources producing flux overestimates. Note that at 60 μm a density of 20 sources/deg. ^{2} corresponds to 27 beams/source using the geometric area of the beam appropriate for case 2. For comparison, the point source catalog used a confusion processing threshold of 25 beams/source (cf. Main IRAS Supplement, Section VIII-C). Table II.C summarizes the source densities where the two potential confusion effects become important; the threshold is set at 25 beams/source and the -1.5 power law is assumed as in the simulation.

Table II.C. Confusion Thresholds (Sources/Deg.^{2})[1]

Band (μm)	Case 1	Case 2
12	18	44
25	16	41
60	9	22
100	4	10

NOTE:

[1] The density of sources with $F_\nu > 0.1$ Jy.

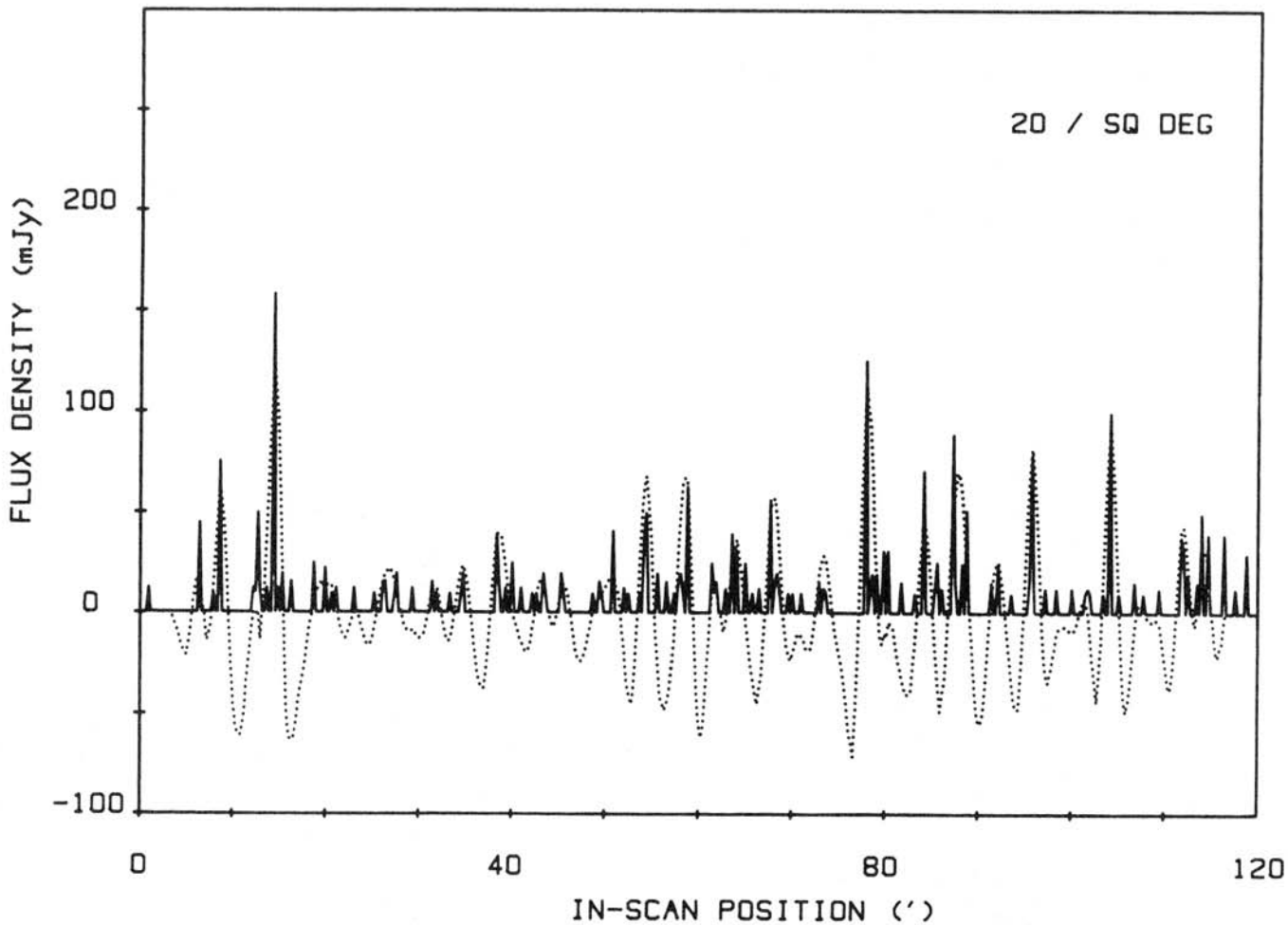

Figure II.C Solid curve represents a simulated one-dimensional source distribution for: log N vs log F slope = -1.5, and 20 sources/deg.^{2} at F(60 μm) > 0.1 Jy. Dotted curve represents the FLUX filtered output. Two effects of confusion are shown: (a) amplitudes of sources within the negative sidelobes of other sources are reduced, (b) higher amplitude single sources occur in the output when multiple sources fall within the positive beam.

E. Photometry

The flux density estimate for an extracted source is calculated from its peak amplitude above the baseline. Extended sources will have systematically low flux densities on FLUX grids. The SSC has been calibrated to the same absolute flux density scale as the PSC. This calibration is based on observations of standard stars and selected asteroids. Details of the absolute calibration can be found in Section VI.C of the Main IRAS Supplement and here in Section IV.D. Flux densities are given in units of Janskys at wavelengths of 12, 25, 60 and 100 μm assuming a continuum flux density distribution which is inversely proportional to frequency. Color correction tables for other energy distributions are given in the Main IRAS Supplement. Because of the wide bandwidths of the IRAS spectral filters, these color corrections are generally quite significant and must be applied to the tabulated values in the SSC.

Corrections have been applied to remove a number of known systematic errors in the processed data. In particular, non- linear effects which depend on the flux of the source and the macro have been corrected. Additionally, there is a background-dependent correction that has not been applied to the Serendipitous Survey sources. We have assumed, instead, that the sources were all measured at a low background characteristic of high ecliptic and galactic latitudes. The error in making this assumption is generally less than 2% in the flux density.

The photometric accuracy of extracted point sources is dependent on the details of the observation. The various sources of uncertainty and bias in the photometric accuracy are discussed separately below.

1. The absolute calibration, in the sense of a knowledge of the flux densities of a set of standard stars and asteroids, has an estimated uncertainty of 2, 5, 5 and 10 percent in the 12, 25, 60 and 100 μm bands, respectively (see Chapter VI of the Main IRAS Supplement). This does not include: (a) uncorrected systematic errors, (b) the effects of noise or (c) lack of reproducibility caused by various instrumental instabilities or pointing errors.
2. The IRAS detector array showed systematic variation in response as a function of cross-scan track with a peak-to-peak amplitude of $\pm$ 10%, 6%, 9%, and 10% in the 12, 25, 60 and 100 μm bands, respectively. Because the current IRAS processing does not correct for this effect and because serendipitous sources are found on all possible tracks, some sources suffer errors.
3. For the IRAS detector sampling rates, use of the peak amplitude above baseline for the determination of flux density results in a maximum error of 10% and a typical error of 2 to 5% independent of the signal to noise ratio of the source. For bright sources, a template fit can give more precise photometric results. We have chosen, however, to use the peak estimate since it gives a more reliable flux estimate for sources with low signal-to-noise ratio.
4. It is expected that the uncertainties introduced by corrections for the frequency dependent responsivity and the non- linearity of the load resistors are less than 3%, for all the 12 and 25 μm sources and for 25 and 60 μm sources fainter than the primary IRAS reference source NGC 6543 (108 and 129 Jy at 25 and 60 μm, respectively). However, for the brightest 100 μm sources the responsivity may vary with frequency by as much as 60% (cf. Main IRAS Supplement, Section VI.B.4).
5. The Pointed Observations were calibrated via flashes of an internal reference source. When observations were made near the Galactic plane, in other highly crowded regions, or where the backgrounds are high, the reference flashes were frequently so confused by local structure in the baseline or by discrete sources that they were rejected by the calibration processor, and the

calibration transfer were based on an adjacent reference flash. Approximately 20% of all the Pointed Observations are affected by this rejected reference flash problem. For the 12, 25 and 60 μm bands, the responsivities of the detectors were constant to better than +/-12% (see Figure IV.A.2 of the Main IRAS Supplement), so the worst case error would be ~24%. For the 100 μm band the dispersion in detector responsivities was about twice that of the other bands. In general, however, the errors due to rejected calibration flashes are much smaller than these maximum values.

6. In crowded fields, both cross-scan and in-scan confusion causes errors in both position and flux strength of a source. The zero-sum filter used to produce the FLUX grids increases these effects due to its large negative side lobes; as shown in Figure II.B, these effects extend to nearly one source width on each side of a source in the scan direction.

7. Because the primary purpose of the Pointed Observations was to maximize the sensitivity for weak sources, the majority of the observations were carried out in the high gain mode of the satellite analog electronics. Consequently, a number of very bright sources have erroneous flux densities because of analog to digital converter saturation. The user should refer to the PSC for the flux densities of these very bright sources. A list of grids that have saturated pixels is given in Young et al. (1985).

In summary, taking into account that the two independent observations of each source are averaged, the uncertainties in the flux densities quoted in the Serendipitous Survey are generally of order 10%. Cases where larger errors are anticipated are indicated by flags in the SSC listing, as described in Section III. However, the uncertainties are sufficiently non-Gaussian that each case must be interpreted in the context of the specific observation.

III. SSC DATA PROCESSING

Given the list of point sources that had been extracted from each of the grids included in the Pointed Observation program (Section II), preparation of the SSC required further data processing as follows:

1. Grid Selection: For each field observed, select the two grids which should yield the maximum number of twice-observed sources.
2. Confirmation: Within each grid pair, and within each of the four IRAS bands, discard the sources that were detected with a low correlation coefficient, or low local signal-to-noise (Section II.C). Determine which of the remaining sources were seen near the same position and at approximately the same flux density in both grids.
3. Parameter Refinement: Combine the fluxes and positions of the individual detections to derive an improved position and flux density of each confirmed source.
4. Confusion Processing: For the list of "confirmed" sources found in each of the 4 bands, flag those detected in crowded regions.
5. Band Merging: Combine sources confirmed in two or more bands into a single source, and provide upper limits for bands where confirmed sources were not detected. Derive improved positions for band-merged sources.
6. Cirrus Flagging: Flag fields possibly contaminated by a significant number of spurious point sources related to spatial gradients in the diffuse emission [see Low et al (1984) for a description of infrared cirrus].
7. Effective Area Measurement: Compute the effective areal coverage for each macro type (Section II.A).
8. Redundant Field Indication: Identify those grid pairs which overlapped with other grid pairs and quantify the degree of overlap.
9. Associations: As for the PSC, seek associations between SSC sources in the final band-merged list and sources in other astronomical catalogs.

With the exception of the last step, all of this processing was carried out on a VAX 11/750 computer at the headquarters of the National Optical Astronomy Observatories in Tucson, Arizona. Details are given below.

A. Grid Pair Selection

The first step in the Serendipitous Survey processing was to identify pairs of grids which could later be compared with one another to verify sources. The objective of this selection process was to maximize the number of sources that could be confirmed by finding grids with the maximum percentage of overlapping area coverage and with the least median noise.

In most cases, repeated observations of the same field with the same observing parameters can be readily identified by their observation identification number (OBSID). (The individual observations for a given OBSID can be distinguished by their grid numbers (cf. Young et al. 1985).) Where 3 or more observations had the same OBSID number, the two "best" observations were selected by defining a figure of merit (FOM) designed to maximize the number of 60 μm sources that could be confirmed.

$$FOM = (1 - \Delta\theta)\ n^{-1.5} \qquad \text{III.1}$$

In this equation, $\Delta\theta$ is the difference in position angle between the two grids and n is the median noise in the 60 μm band for the grid having the higher 60 μm median noise. (Hereafter, the grid having the lesser median noise at 60 μm is denoted the "reference grid", while the grid having the higher 60 μm median noise is the "confirming grid".) The first factor in Eqn. III.1 is an estimate of the fractional area of overlap of the two grids, which (for small differences in orientation angle) varies directly as $\Delta\theta$, since the aspect ratio is invariant for grids with the same OBSID. The second factor rests on the assumption that the number of sources, N, detected in the 60 μm Band should increase as

$$N\ (> f_\nu(60\mu m)) = constant \cdot f_\nu(60\mu m)^{-1.5} \qquad \text{III.2}$$

where $f_\nu(60\mu m)$ is the source flux density at 60 μm. (The use of the 60 μm noise as an indicator of the quality of a grid was predicated on earlier analyses of the PSC, which suggested that, because the 60 μm source counts were dominated by galaxies rather than stars or infrared "cirrus", they should be more sensitive to to gains in sensitivity than source counts at other wavelengths.)

For about 60% of the fields observed, only two observations could be paired on the basis of their OBSID number, and for these fields no selection on the basis of overlapping area or noise was applied.

For about 10% of the grids the OBSID was unique. These grids were paired with one another on the basis of the proximity of their field centers. No area or noise selection was applied to the grid pairs that were identified by this process.

In all cases, grids were paired only if their centers coincided to within 5 arcmin.

B. Source Confirmation

The major goal of the confirmation processing was to select, from among the point sources extracted from each observation pair, those sources which exceeded limits of local signal-to-noise and correlation coefficient that were determined to distinguish reliable point sources, and which were detected near the same position and flux on both the reference and confirming grids. This process was carried out separately for each of the four IRAS bands.

As a preliminary step in the confirmation process, all sources lying within two pixels of the grid boundaries were discarded, since such sources are likely to have erroneous fluxes and positions.

Using the resulting list of acceptable sources, the positions of sources within each of the two grids in a pair were compared. This positional discrepancy test actually consists of two tests applied serially, since the fields of view of all of the detectors were non-circular (cf. Table II.B). In particular, most fields of view were elongated in the direction perpendicular to that in which they were scanned across a field, so that the allowable "in-scan" positional discrepancies were generally smaller than the "cross-scan" discrepancies.

Projection of the positional differences of sources onto the cross-scan and in-scan directions was complicated by the fact that the scan directions (or orientation

angles) of the two grids in each grid pair were not identical. Since these differences were usually small, the average orientation angle of the grid pair was used:

$$\langle\theta\rangle = \frac{\theta_r + \theta_c}{2} \qquad \text{III.3}$$

In Eqn. III.3 and hereafter, the subscript "r" refers to the reference grid, while the subscript "c" refers to the confirming grid of the grid pair.

The relevant geometry is shown schematically in Figure III.A. The projection of the difference in position in the in-scan (cross-scan) direction along (across) the direction corresponding to the average orientation angle is related to the right ascension and the declination of the source positions as follows:

$$\Delta y = \Delta r \sin (\phi - \langle\theta\rangle) \qquad \text{III.4a}$$

$$\Delta z = \Delta r \cos (\phi - \langle\theta\rangle) \qquad \text{III.4b}$$

where,

$$\Delta r = \left[(\alpha_r - \alpha_c)^2 + (\delta_r - \delta_c)^2 \right]^{1/2} * Cos\left(\frac{\delta_r + \delta_c}{2} \right) * 3600$$

$$\phi = \tan^{-1}\left(\frac{\delta_r - \delta_c}{\alpha_r - \alpha_c} \right) \qquad \text{for } \delta_r - \delta_c > 0$$

$$\phi = \tan^{-1}\left(\frac{\delta_r - \delta_c}{\alpha_r - \alpha_c} \right) + \pi \qquad \text{for } \delta_r - \delta_c < 0$$

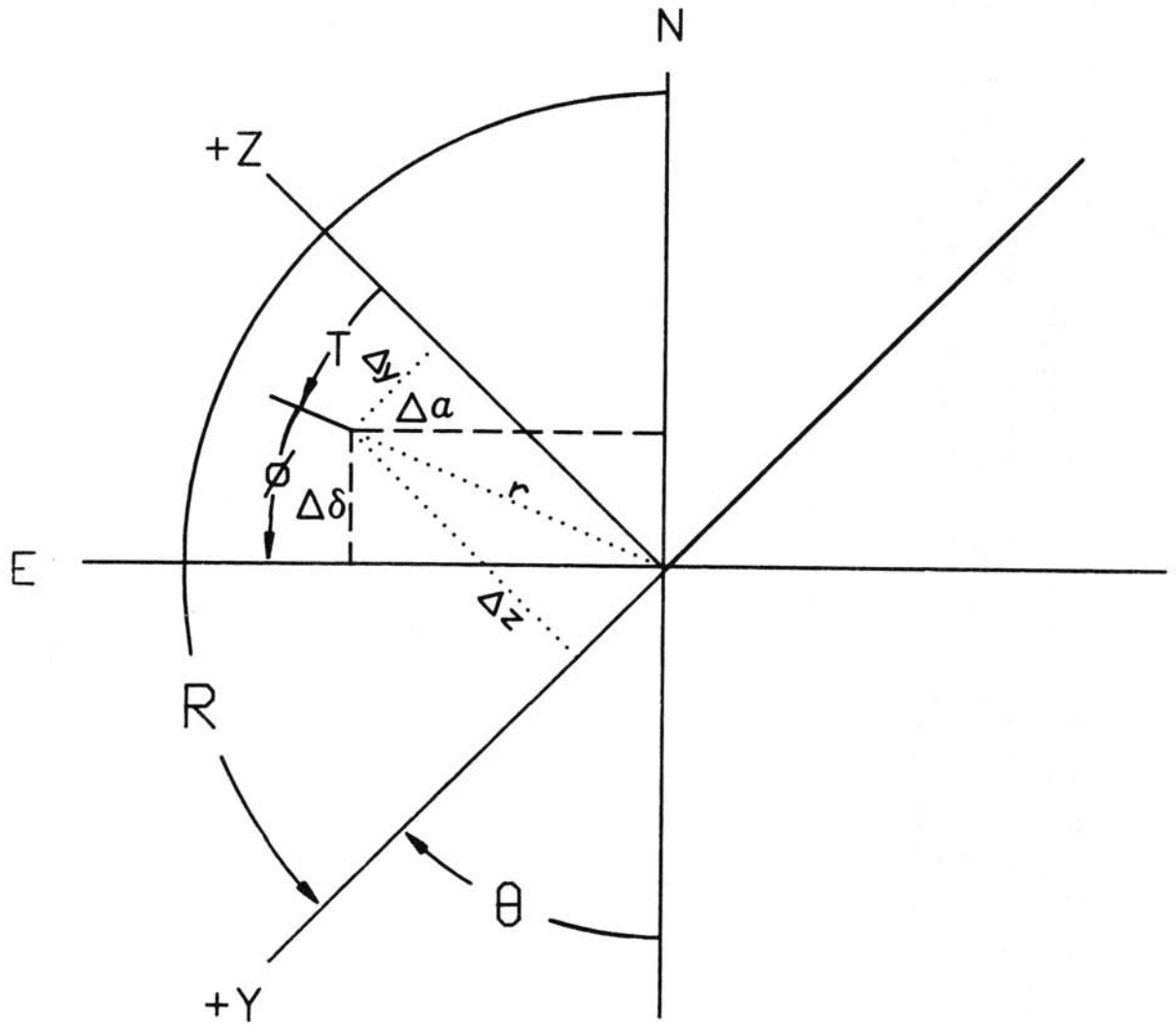

Figure III.A Coordinate system used in SSC; symbols explained in text.

In the above equations, α and δ are the right ascension and declination of each source in radians, Δr is the total positional difference between source i (detected in the reference grid) and source j (detected in the confirming grid) in arcsec, $\Delta\theta$ is the position angle of the vector from source i to source j and Δy and Δz are the in-scan and cross-scan position difference measured parallel and perpendicular to the average scan direction of the grid pair. In order to pass the positional confirmation test, it was required that Δy and Δz not exceed the constraints listed in Table III.A. These limits were determined by examining the distribution of position differences between sources extracted from the two grids. The distribution of valid source confirmations is sharply peaked about zero, while the spurious confirmations show up as a constant level background. The magnitudes of the final confirmation windows were defined by the half-widths of the peaked distributions at the points where they exceed the background distribution by a factor of three. Figure III.B shows the observed distribution of in-scan (y direction) and cross-scan (z direction) separations, as well as the adopted upper limits for positional differences. Only grids with $|\ b\ | > 30$ deg. were used in these determinations to minimize the effects of confusion from high density regions.

Sources passing the positional difference test were then passed on to a filter that checked the flux density ratio; it required

$$0.5 < F_r / F_c < 2.0 \qquad \text{III.5}$$

This test helped to eliminate moving sources that coincided by chance with a source or a noise event.

Sources with acceptable grid positions were then checked to determine whether their correlation coefficients and local signal-to-noise ratios exceeded certain lower limits. These limits were optimized by an empirical procedure described in Section IV.F.1 and are listed in Table III.A.

Differences among the four IRAS bands in the acceptable limits on positional and flux discrepancies, local signal-to- noise ratio and correlation coefficient, among the 4 IRAS bands are due to variations in noise and detector fields of view. In addition, because of a periodic noise pickup in one of the 12 μm detectors, a higher local noise threshold was used for one track in the 12 μm grids. The offending detector showed low level 1 Hz clock pulses from the spacecraft computer at cross scan coordinate 11 (i.e., 11 x 0.6 arcmin from the detector #27 edge). Since these pulses could in some cases repeat from observation to observation, they occasionally mimicked real, but faint, sources. For candidate detections within one cross scan pixel (i.e., +/- 0.6 arcmin) of the "noise track", the local signal-to-noise threshold was set at 5.5.

Table III.A. Confirmation Requirements

Band	Minimum Median SNR	Minimum Local SNR	Minimum Correlation Coefficient	Maximum Position Difference	
				In-Scan (Arcsec)	Cross-Scan (Arcsec)
12 μm	3.0	3.0	0.70	27.5	92.5
12 μm "clock tracks"	3.0	5.5	0.70	27.5	92.5
25 μm	3.0	4.0	0.70	27.5	92.5
60 μm	3.0	2.5	0.70	70.0	142.5
100 μm	3.0	2.5	0.70	142.0	142.5

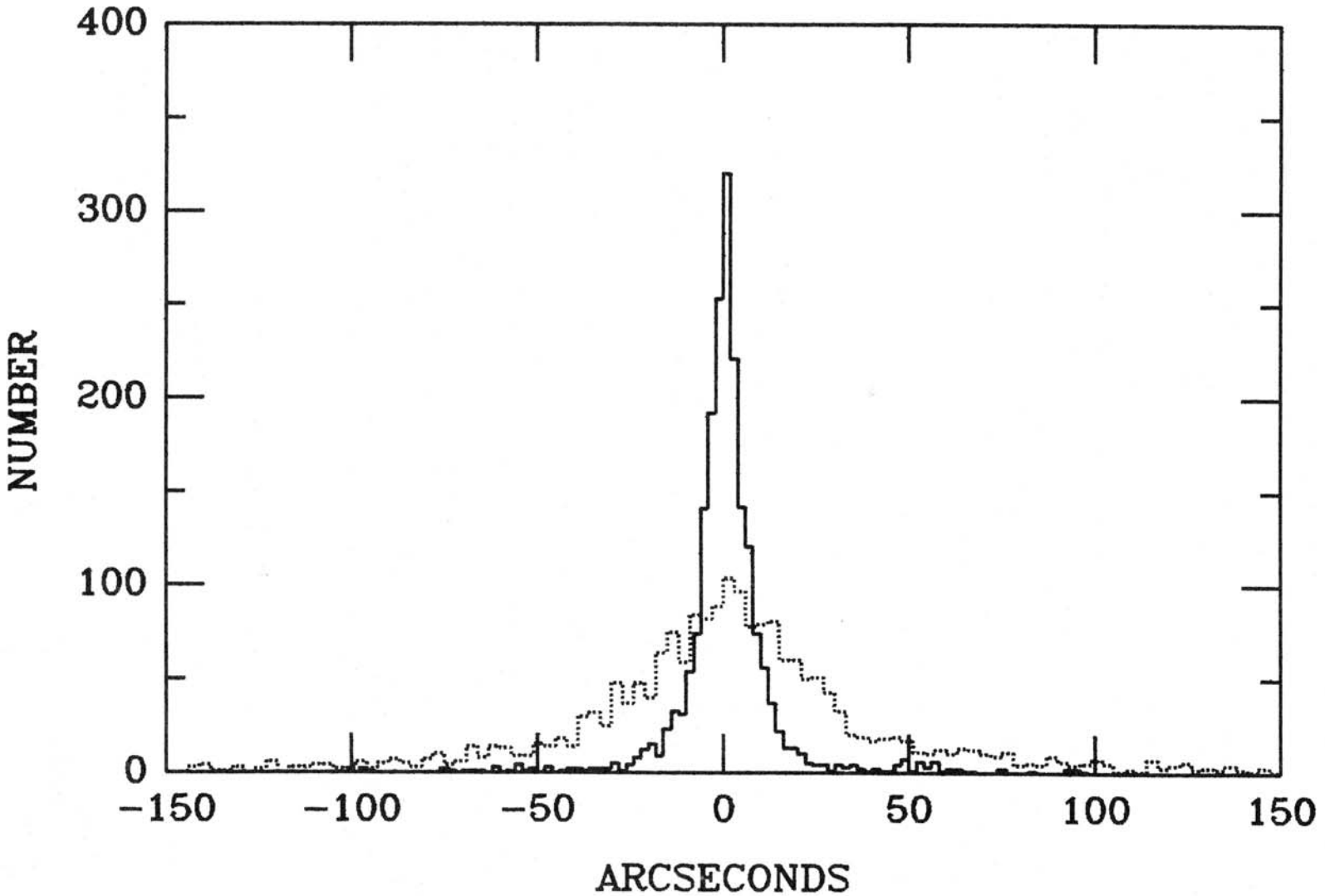

Figure III.B Number of sources versus separation between positions in the reference and confirming grids, in-scan (solid line) and cross-scan (dotted line).

C. Position and Flux Density Refinement

Sources in each grid pair which satisfied all of the criteria listed in Table III.A were identified as high quality sources. A weighted position and flux density was derived for each confirmed source.

Sources which satisfied only the criteria of positional and flux density agreement were retained as medium quality sources, as long as one of the two sources exceeded the limits on local signal-to-noise and correlation coefficients. The positions and flux densities of these medium quality sources were taken from the extraction satisfying all verification criteria. Finally, sources not meeting both the positional and the flux density tests were rejected from further processing in the SSC.

C.1. Position Refinement

Positional uncertainties for all confirmed sources were derived from data obtained in the verification process. The position differences between the pairs of source detections were binned according to the local signal-to-noise (LSNR) of the source in the confirming grid as follows:

$$BIN = integer\ value\ [\ 5 * \log\ (LSNR/MINLSNR)\ ] \qquad \text{III.6}$$

where MINLSNR is the threshold LSNR for each band (Table III.A). Within each bin, rms values for the cross-scan and in-scan position differences of each source pair were computed. The positional uncertainty of all sources detected in a given range (BIN) of local signal-to-noise was then defined to be equal to $2^{-0.5}$ of the derived rms value for the positional differences. Table III.B lists the results.

Table III.B. Assigned Position Uncertainty for Confirmed Sources

LSNR	In-Scan (Arcsec)				Cross-Scan (Arcsec)			
BIN	12 μm	25 μm	60 μm	100 μm	12 μm	25 μm	60 μm	100 μm
0	14.3	11.0	36.5	57.3	55.2	53.6	64.7	66.3
1	11.2	9.7	30.9	50.6	53.1	50.3	63.4	66.1
2	9.5	9.1	22.9	43.2	48.4	47.9	60.1	62.9
3	8.9	8.2	20.1	37.3	46.7	44.7	55.4	58.9
4	7.7	7.2	16.9	29.9	42.1	41.7	51.4	55.4
5	7.2	6.4	14.6	26.0	40.7	37.5	47.3	50.2
6	6.7	6.3	12.7	22.0	37.8	35.8	43.6	46.1
7	6.2	6.1	10.1	20.4	33.2	34.6	38.1	45.3
8	6.2	5.9	9.2	18.0	31.5	31.1	33.0	40.6
9	6.0	6.1	8.5	15.1	28.3	31.7	31.1	35.7
10	5.9	6.4	8.0	13.9	26.6	27.9	28.1	33.8
11	6.3	7.2	8.9	13.5	25.6	28.1	29.6	34.7
12	6.2	7.3	7.7	13.5	22.2	29.1	29.1	32.0

The positions of high quality confirmed sources were refined according to Eqns. III.7a and b, which give increments to the in-scan and cross-scan positions:

$$\delta z = (z_c - z_r) / (1 + \sigma_c^2 (z) / \sigma_r^2 (z)) \qquad \text{III.7.b}$$

$$\delta z = (z_c - z_r) / (1 + \sigma_c^2 (z) / \sigma_r^2 (z)) \qquad \text{III.7.b}$$

The refined equatorial coordinates of the confirmed source are obtained by projecting these increments onto equatorial coordinates:

$$\alpha = \alpha_r + \frac{\delta_y \sin < \theta > + \delta_z \cos < \theta >}{3600 \cos \left(\frac{\delta_r + \delta_c}{2} \right)} \qquad \text{III.8.a}$$

$$\delta = \delta_r + \frac{\delta_z \sin < \theta > - \delta_y \cos < \theta >}{3600} \qquad \text{III.8.b}$$

C.2 Flux Density Refinement

To derive the most accurate flux density for confirmed sources, the flux densities of individual source extractions were combined and weighted according to the median noises in their respective grids, thus:

$$< F > = F_r + (F_c - F_r) / (1 + n_c^2 / n_r^2) \qquad \text{III.9}$$

Here n_r is the median noise in the reference grid, in the band where the source was detected, and n_c is the median noise in the same band in the confirming grid. The refined flux density uncertainty is taken to be

$$< n > = \left(\frac{n_r^2 \, n_c^2}{n_r^2 + n_c^2} \right)^{1/2} \qquad \text{III.10}$$

D. Confusion Processing

Potentially confused sources were flagged during the confirmation processing, by counting the number of confirmed sources which occurred within a specified range in the cross-scan and in-scan directions. The processing steps are identical to those used in the confirmation processing itself, except that the source positions from the reference grid and from the confirming grid are both replaced by the refined positions of confirmed sources, and the confusion windows in Δy and Δz are taken to be a factor of two larger than the confirmation windows given in Table III.A.

E. Band Merging

The process of identifying sources that were detected in two or more IRAS bands, and of setting upper limits on the fluxes of sources not detected in all four of the IRAS bands, is called band merging. The process of band merging relied solely on positional coincidence, and used positional tests similar to those used in the confirmation processing (Section III.B). The sources selected for band merging were limited to the high quality confirmed sources. However, in cases where a high quality Band i source had no apparent counterpart among the high quality Band j sources, the list of medium quality sources in Band j was scanned for a possible positional coincidence. In cases where no band merger candidate could be found among either the high or medium quality sources, an upper limit to the flux in the merging band was derived from the median noise in the reference grid, nr. In most cases the upper limit is taken to be 4.5 x n_r. Upper limits at 12 μm for sources located near the region which suffered "clock interference" (Section III.B) are given as 5.5 x n_r.

The band merge process was executed in the same order as that of the PSC (Main IRAS Supplement, Chapter V.D.3) as shown repeated in Table III.C. In particular, it began by attempting to band merge the high quality sources detected at 12 μm with those detected at 25 μm. If a merger was found, the position and positional uncertainty of the source was refined (cf. Section III.E.2), and a merger was then sought among the high quality sources from 60 μm etc. Sources that had been band merged were flagged, and were not available for band-merging with other high quality sources. Thus, in the second pass of the band merging process, mergers were sought only for high quality sources detected at 25 μm that had not been previously merged with any source detected at 12 μm.

The final stage of the band merge processing was a count of the number of 100 μm sources that could not be merged with any other sources detected at other wavelengths. The areal density of these sources is taken to be an indication of the presence of infrared cirrus in the region.

Table III.C. Order of Band Merging

Primary Band (μm)	Secondary Band (μm)		
12	25,	60,	100
25	12,	60,	100
60	25,	100,	12
100	60,	25,	12

E.1 Positional Tests for Band Merging

The test for positional coincidence in band merging is similar to that used in the confirmation processing. However, in the band merging process, the positional difference is tested against the combined positional uncertainties of the potential merging sources in the in scan and cross scan directions. That is, for a source in Band i to merge with a source in Band j, it is required that:

$$\Delta\, y_{ij} < 4 * \sigma_{ij}(y) \qquad \text{III.11.a}$$

$$\Delta z_{ij} < 4 * \sigma_{ij}(z) \qquad \text{III.11.b}$$

where $\sigma_{ij}(y)$ and $\sigma_{ij}(z)$, the total uncertainties in the in-scan and cross-scan directions, are computed from the uncertainties of the two potentially merging sources:

$$\sigma_{ij}(y) = \left[\frac{\sigma_i^2(y)\,\sigma_j^2(y)}{\sigma_i^2(y) + \sigma_j^2(y)} \right]^{1/2} \qquad \text{III.12.a}$$

$$\sigma_{ij}(z) = \left[\frac{\sigma_i^2(z)\,\sigma_j^2(z)}{\sigma_i^2(z) + \sigma_j^2(z)} \right]^{1/2} \qquad \text{III.12.b}$$

In cases where more than one high quality source might satisfy the positional coincidence test, the merger having the least positional discrepancy is used.

E.2 Position and Position Uncertainty Refinement

After each successful band merger, i.e., after a band merger of two high quality sources, the position and positional uncertainty of a merged source were refined using the same algorithms applied in the confirmation processing (Eqns. III.7 and III.8). However, in the case of the band merging process, the subscript 1 refers to the source seen in the primary band (the left-most column in Table III.B), while the subscript 2 refers to the secondary band in which the band merger was sought. After a source has been band merged once, then the subscript 1 refers to the refined position and positional uncertainty. The refinement of positions and positional uncertainties (in cases where two high quality sources were band merged) occurred immediately after each band merger, and thus tightly constrains mergers of sources in more than two bands.

If a high quality source could not be merged with any other high quality source, but was found to be located near a medium quality source, then the medium quality source was used to estimate the flux in the band in which a merger was sought. However, the position and positional uncertainty of the high quality source was retained as the parameters of the "primary" band, and no position refinement was executed.

F. Effective Field Areas

The effective sky coverage of the fields used in the SSC processing is smaller than the areas deduced from the scan geometries of individual grids alone. This reduction in area is due to imperfect overlap of the reference and confirming grids and to non uniform sensitivities across the focal plane detector array.

The nominal grid area is the geometric area covered by the Pointed Observation scans (as specified by the macro type; see Table II.A) minus the two pixel borders (Section III.B), and is given by

$$A = (ny - 4)\,(nz - 4) * S_y * S_z \qquad \text{III.13}$$

where ny and nz are the number of in-scan and cross-scan pixels in the map, respectively, and S_y and S_z are the in-scan and cross-scan pixel sizes as listed in Table II.B. The nominal grid areas for each macro type are listed in Table III.D. For Eqn. III.13, it is assumed that the two grids which comprise the confirming pair have identical areas. This assumption is accurate for about 90% of the grid pairs, but there are examples where one grid may be up to 10 pixels shorter in the in-scan direction than its companion grid. Such discrepancies should amount to no more than a ~10% effective area loss for those few fields.

The effective area for each SSC field, A', was estimated as the product of the nominal geometric grid area, A, with several correction factors, as follows:

$$A' = A * C_1\,(dy,dz) * C_2\,(\Delta\theta) * W(y) * W(z) \qquad \text{III.14}$$

Factors C_1 and C_2 are purely geometric corrections which compensate for small positional offsets and scan angle differences between the reference and confirming grids, and will be different for each grid pair. For small offsets these factors are approximated by:

$$C_1 = (1 - 2dy/y) * (1 - 2dz/z) \qquad \text{III.15.a}$$

and

$$C_2 = (1 - \tan \Delta\theta) \qquad \text{III.15.b}$$

where dy and dz are the in-scan and cross-scan grid offsets, y and z are the in-scan and cross-scan lengths, which vary between macro types, and $\Delta\theta$ is the difference in orientation angle. In general, positional agreements between grid centers is excellent; 99% of the SSC fields have dy < 15" and dz < 45". The range of scan angle differences in the grid pairs is also relatively small, typically < 6 degrees. However, there are a few cases with $\Delta\theta$ up to ~25 degrees.

Because the local sensitivity is a function of position on the grid, the effective area over which the maximum sensitivity can be attained is smaller than the geometric grid overlap area. To estimate the correction for this effect, the "equivalent widths" of the grids in the in-scan and cross-scan directions, W(y) and W(z), were evaluated. These equivalent widths are defined to be the size that a uniform sensitivity grid would have so that the integral of its sensitivity over its area would be equal to the integral of the actual sensitivity profile over the geometric grid area. For use in equation III.14 the equivalent width is normalized to the geometric width, thus a uniform sensitivity grid would have W(y) = W(z) = 1.0.

To determine the actual sensitivity profiles it was assumed that the net sensitivity could be traced by counting the numbers of sources detected at each position

on the grid; a uniform sensitivity grid representing many observations of randomly distributed sources should exhibit flat source distributions in both the in-scan and cross-scan directions. The actual distributions were evaluated by sorting all of the SSC fields into one of four macro classes defined by the macro scan lengths given in Table II.A, and for each macro class counting the numbers of confirmed sources which occurred at each in-scan and cross-scan grid position. As an illustration, the grid positions of all 12 um sources found in fields with DPS02B, 52B, 62D and 63D are histogrammed in Figure III.C. A roll-off in sensitivity towards the edges of the grids is manifested by the decrease in number of sources/unit area. The sharp peaks in the distributions are the result of the pointing procedure which consistently placed the targeted objects of each observation on the most sensitive detectors.

From these histograms the values of the grid equivalent widths for each macro class were determined using the following equations:

$$W(y) = 1/(ny-4) * \left(\frac{\sum n_p(y) \Delta p_y}{N_{Ymax}} \right) \qquad \text{III.16.a}$$

$$W(z) = 1/(nz-4) * \left(\frac{\sum n_p(z) \Delta p_z}{N_{zmax}} \right) \qquad \text{III.16.b}$$

where $n_p(y)$ and $n_p(z)$ are the number of sources found in a given in-scan and cross-scan position bin, Δp_y and Δp_z are the sizes of the position bins in pixels, and Nymax and Nzmax are the mean number of sources found within the most sensitive region of the grid (defined as the region with the highest source density). In equations III.16a and 16b the sums are taken over all position bins, and Ny_{max} and Nz_{max} are equal to the level of the "continuum" on either side of the targeted source peaks. In Table III.D the resulting values of W(y) and W(z) are listed for each macro type.

The effective field area was calculated separately for each field in the SSC using Eqn. III.14, and the results are listed in each field header in units of 100 times the area in square degrees. Use of the equivalent width values listed in Table III.D assumes that the reference and confirming grids register perfectly. If the input grid pairs have large scan angle differences, $\Delta\theta$, these values may be slightly underestimated. In such fields, there may also be a deficiency of confirmed sources in the corners unrelated to sensitivity, but simply due to the non-overlap of the grids in these areas. This effect would produce a roll-off in the number of sources found at the edges of both the in-scan and cross-scan distributions. Because of the relatively uniform cross-scan distributions of sources found in all macro classes this effect has not been included in these calculations.

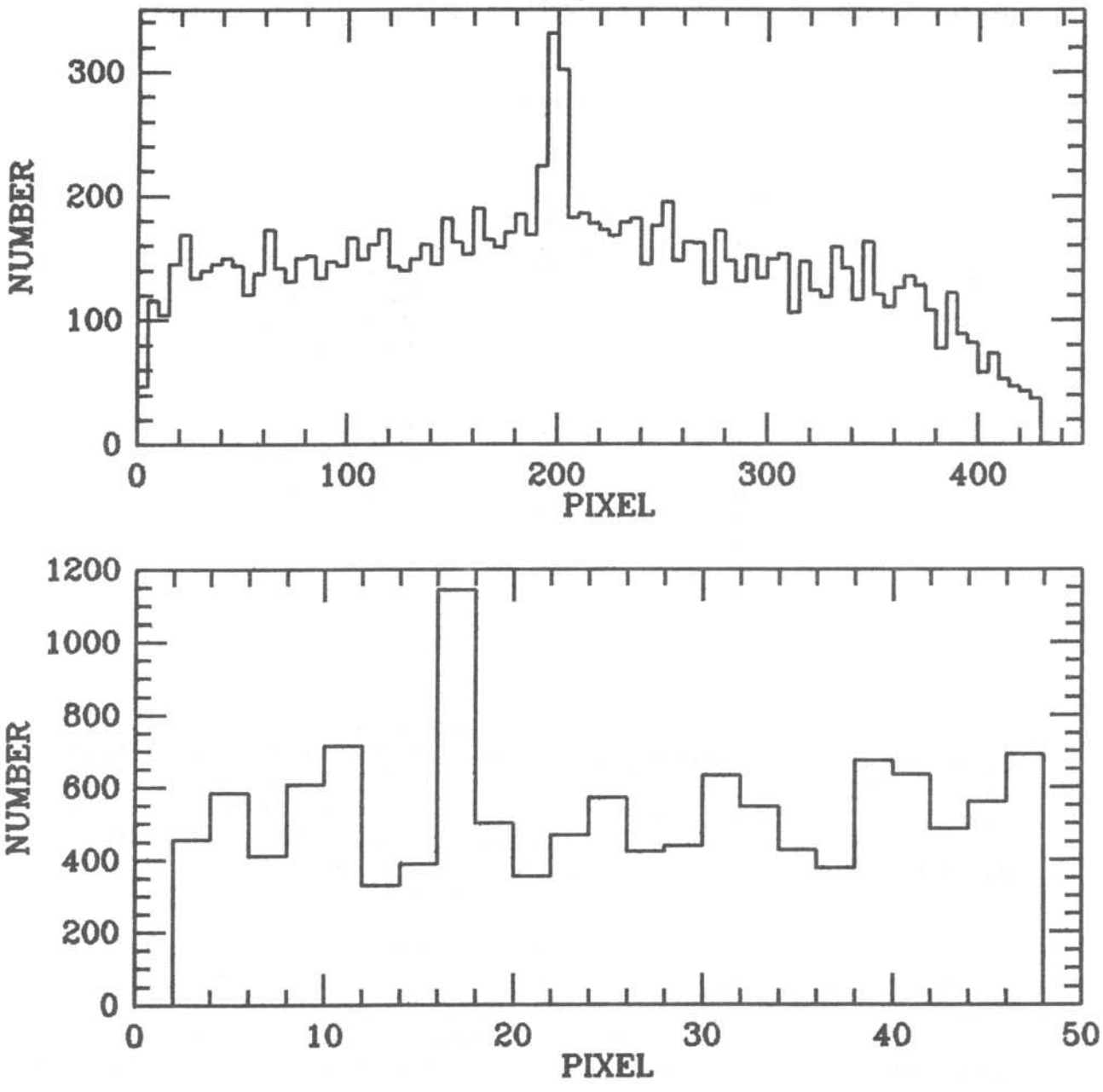

Figure III.C Distribution of sources as a function of in-scan pixel position (upper plot) and cross-scan pixel position (lower plot) for all DPS02B, 52B, 62D and 63D macro observations.

The effective areas given in the field headers are useful for statistical calculations concerning the effective sky coverage of the SSC at a given limiting flux density. In all references to area coverage and source density in this document these areas were used. When the geometric overlap areas of an SSC field are required, the effective areas should be divided by the factors given in Table III.D.

Table III.D. Effective Grid Area Parameters

Macro Code	Nominal Grid Area (Degree^2)	W(y)	W(z)
A	0.822	0.81	1.00
B	2.754	0.85	1.00
C	0.822	0.81	1.00
D	2.754	0.85	1.00
E	0.575	0.82	1.00
K	0.562	0.82	1.00
F	0.575	0.74	1.00
M	0.406	0.82	1.00
G	0.575	0.82	1.00
H	0.575	0.74	1.00
I	0.822	0.81	1.00
J	0.822	0.81	1.00
L	0.822	0.81	1.00

G. Identification of Overlapping Fields

The targeted fields in the Pointed Observation program occasionally overlapped one another. In particular, the region near NGC 6543 (the primary reference source for IRAS calibrations), the Large Magellanic Cloud, and the Small Magellanic Cloud were observed many times during the course of the mission. To identify cases where grids overlapped, pixel positions of nearby grids were mapped onto the grid coordinate system of each grid used in the catalog. All fields where more than 5% of the area of the reference grid overlapped the reference grid of another field are listed in Appendix A. The amount of overlap (calculated on the basis of integer pixels) is given in units of square arc minutes.

The NGC 6543 fields are treated as a special case by this catalog. Over the course of the mission, more than 100 Pointed Observations of that object were made. These observations have been coadded and analyzed by Hacking and Houck (1986). Since their study of this region goes to much fainter levels than this catalog, we have chosen to delete these fields from the Serendipitous Survey.

H. Associations With Other Astronomical Catalogs

Positional associations of SSC sources were made with objects in other astronomical catalogs; the processing was carried out at the IPAC. Associations for the SSC used the same catalogs and search boxes as the PSC (cf. Main IRAS Supplement, Chapter V.H.9 for details of catalogs, search radius and catalog information), with the following exceptions:

1. Positional associations are made with the PSC when SSC and PSC positions agree to within 60 ". The PSC catalog is assigned catalog number 41.
2. The search box for associations with high precision stellar catalogs, 13 (SAO), 15 (Bright Star catalog), and 24 (Two Micron Sky Survey with Improved Positions) is 28" x 180" rather than the 16" x 90" search box used for associations in the PSC.
3. The search radius for associations with the Dearborn catalog is increased to 120".

IV. ANALYSIS OF THE SSC

The field-by-field organization of the SSC reflects the great diversity in the Pointed Observation program on which it is based. Because of the range of observational properties represented in the SSC fields, it is difficult to quantify broad statistical characteristics of the catalog as a whole. Therefore, for the purpose of this analysis it proved necessary to define a high latitude subset of relatively uncrowded, non- overlapping fields. Most of the analysis which follows was confined to this subset of the SSC although many of the results do pertain to the catalog as a whole. The subset of fields was selected as follows:

(a) field centers were located at $|b| > 30°$,

(b) only one field was included from each group of overlapping fields, and that field was selected by starting with a right ascension ordered list of fields and selecting the first field from each group of overlapping fields as listed in Appendix A,

(c) only those fields were included with surface densities of 60 μm sources less than 20 sources/deg.^{2}.

Although there are 721 fields which satisfy condition (a), the high latitude subset is comprised of only 450 fields containing 5100 individual sources. According to condition (b) there were 133 overlapping fields included and 206 excluded; condition (c) excluded 70 fields to avoid further undesirable confusion effects. Seventy-seven fields are located in the Magellanic clouds and were excluded from the high latitude subset either by condition (b) or (c). The subset contains 1245, 614, 2765 and 2427 sources at 12, 25, 60, and 100 μm, respectively, and the combined effective area of the fields is 271 deg.^{2}.

A. Confirmation, Reliability and Sensitivity Limits

The confirmation strategy, on which reliability and accuracy rests, was finely tuned before the final processing was begun. In addition, the character of the raw data and the final results of the data processing determine the "confirmation rate" measured in each band. This parameter indicates the degree of difficulty encountered in separating reliable astronomical sources from the various sources of noise and interference. The question of reliability in the SSC refers both to the reliability of the confirmed sources within each of the four bands, and to the accuracy of band merging in producing merged sources.

The completeness level in the SSC varies widely from field to field because of the large dispersion in the median noise levels, as illustrated in Figures IV.A.1-4. Rather than attempting a global estimate of completeness, which would be of little value, the limiting flux densities in each band are determined for the high latitude subset of fields. Figures IV.A.1-4 show the relatively narrow distribution of median noise levels for these fields.

A.1 Confirmation Tuning and Confirmation Rates

The goal of the entire confirmation procedure was to produce lists of highly reliable point sources. Therefore, confirmation itself, which requires that a source must appear at nearly the same location and have a similar flux level in two independent observations of each field, is the first level of reliability assurance for sources in individual bands.

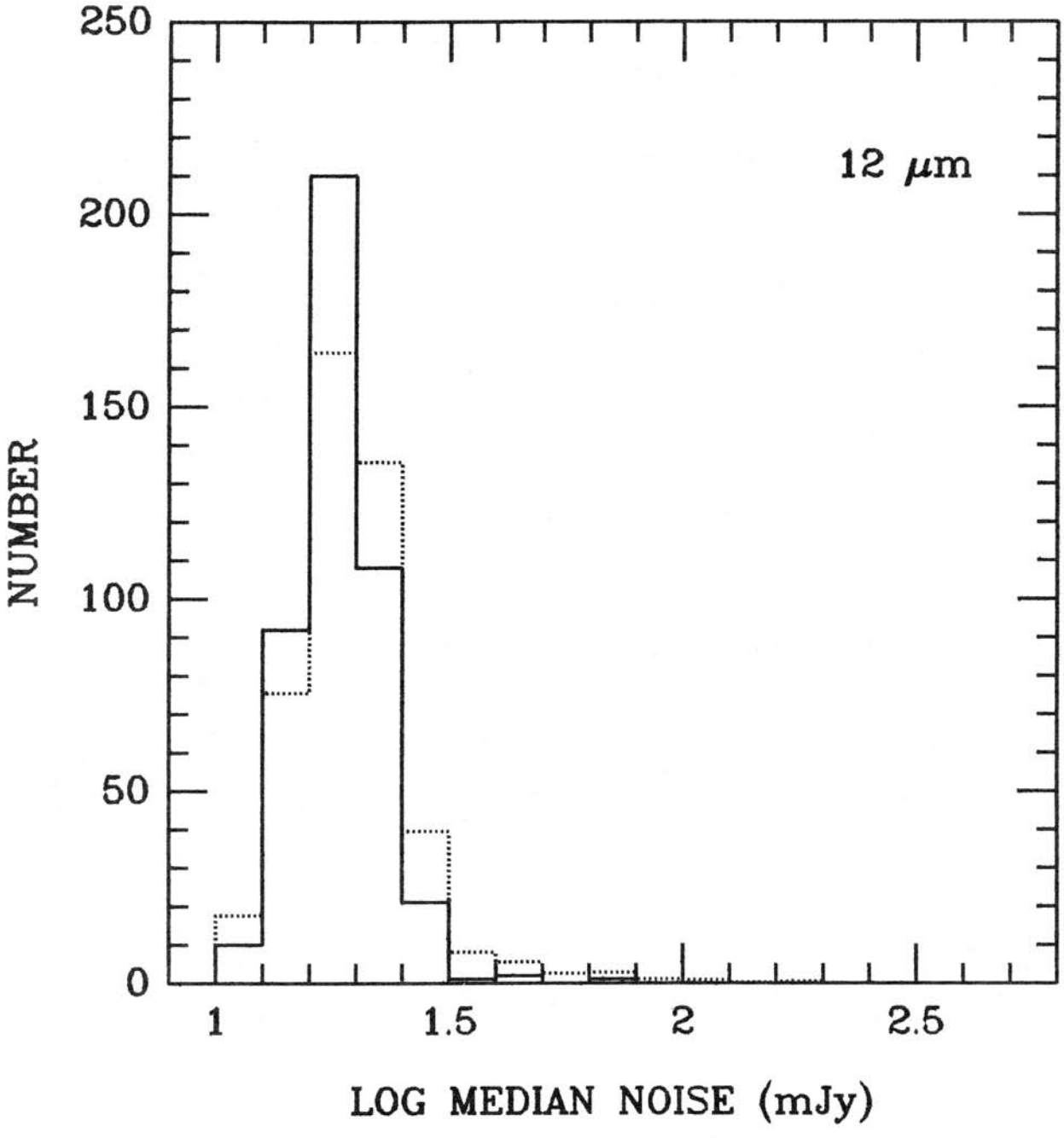

Figure IV.A.1 Number of fields versus median noise; solid line represents the high latitude subset of fields, the dotted line represents the complete set of fields with the verticle scale divided by 4.

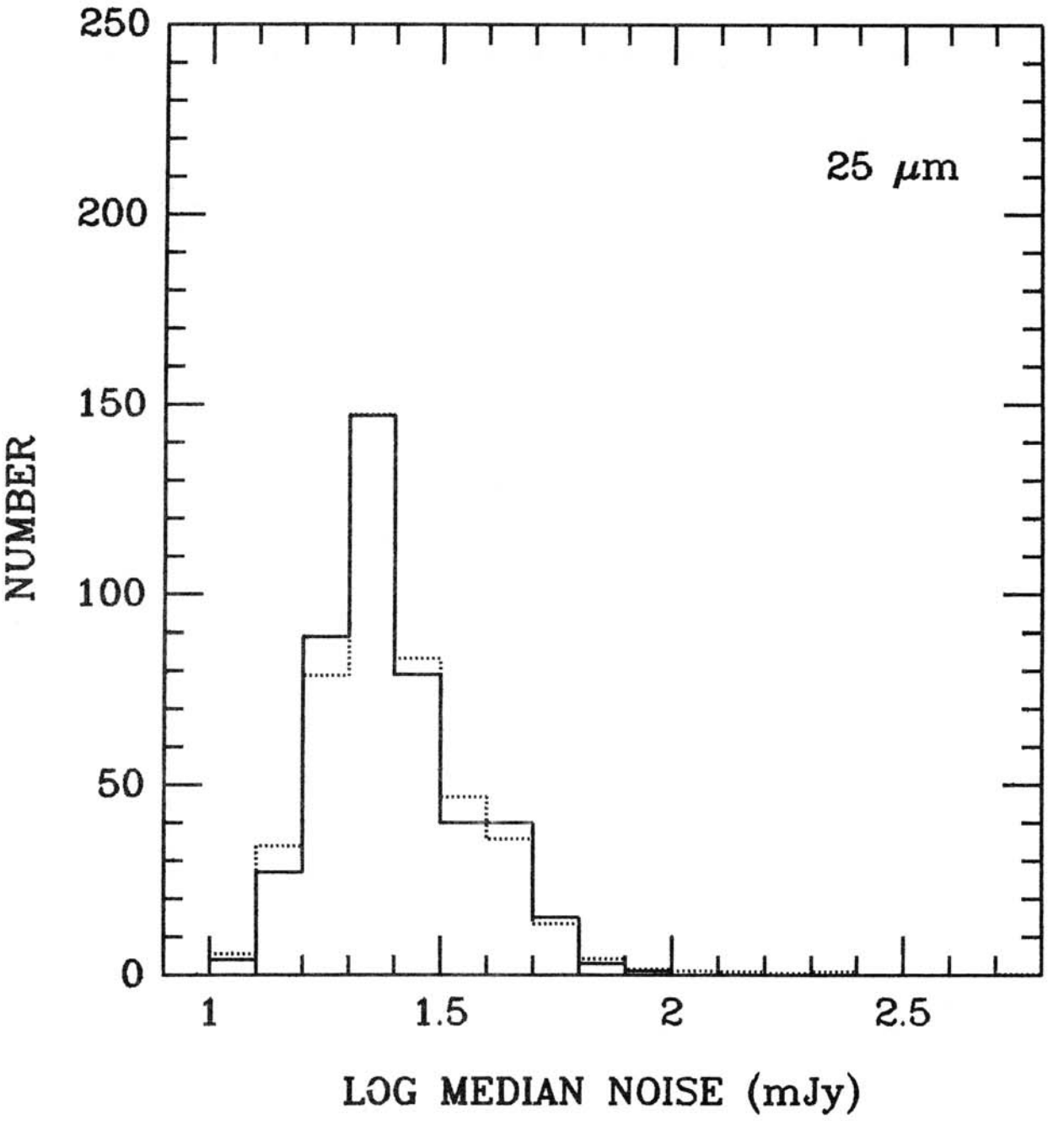

Figure IV.A.2 Number of fields versus median noise; solid line represents the high latitude subset of fields, the dotted line represents the complete set of fields with the verticle scale divided by 4.

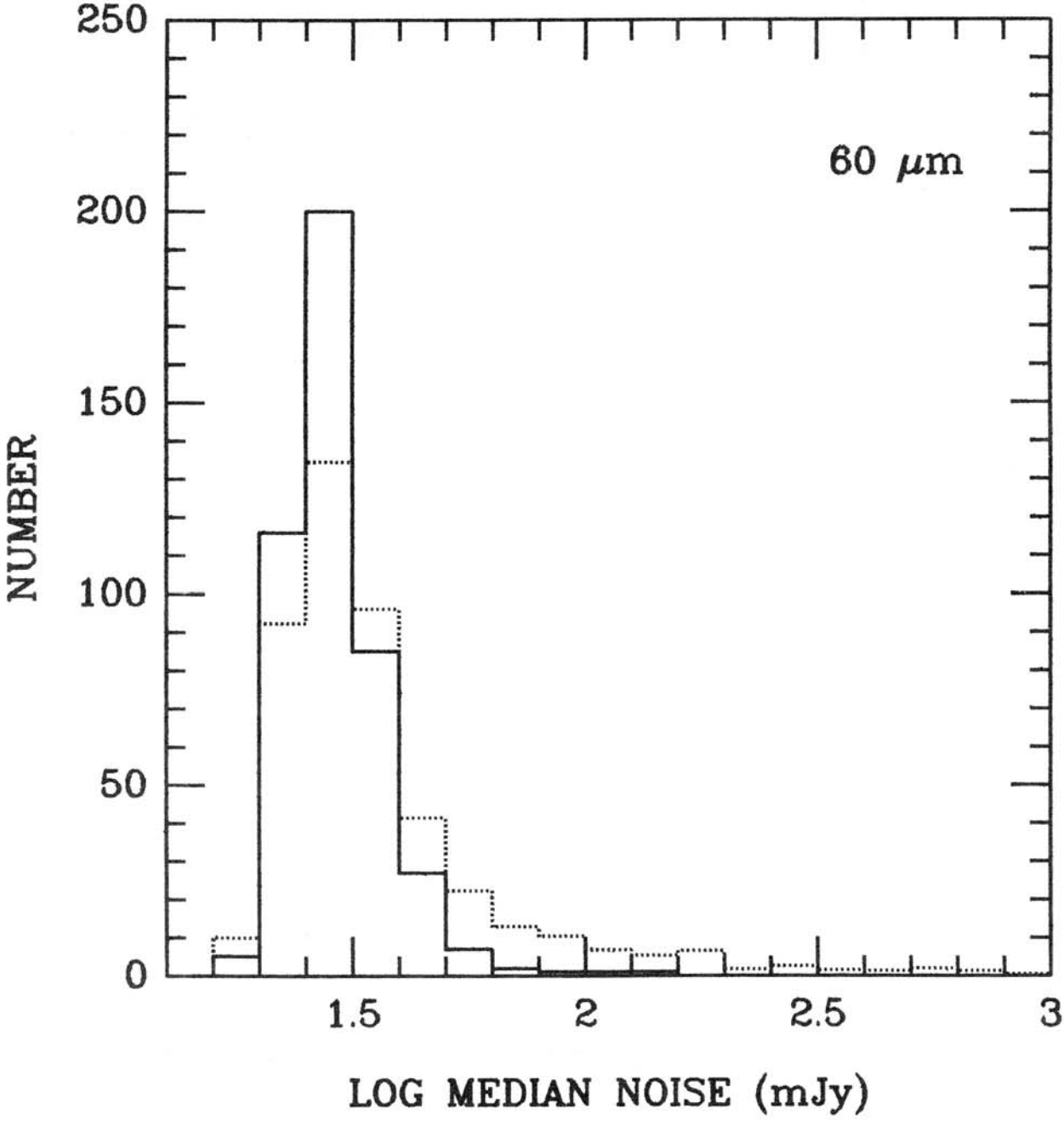

Figure IV.A.3 Number of fields versus median noise; solid line represents the high latitude subset of fields, the dotted line represents the complete set of fields with the verticle scale divided by 4.

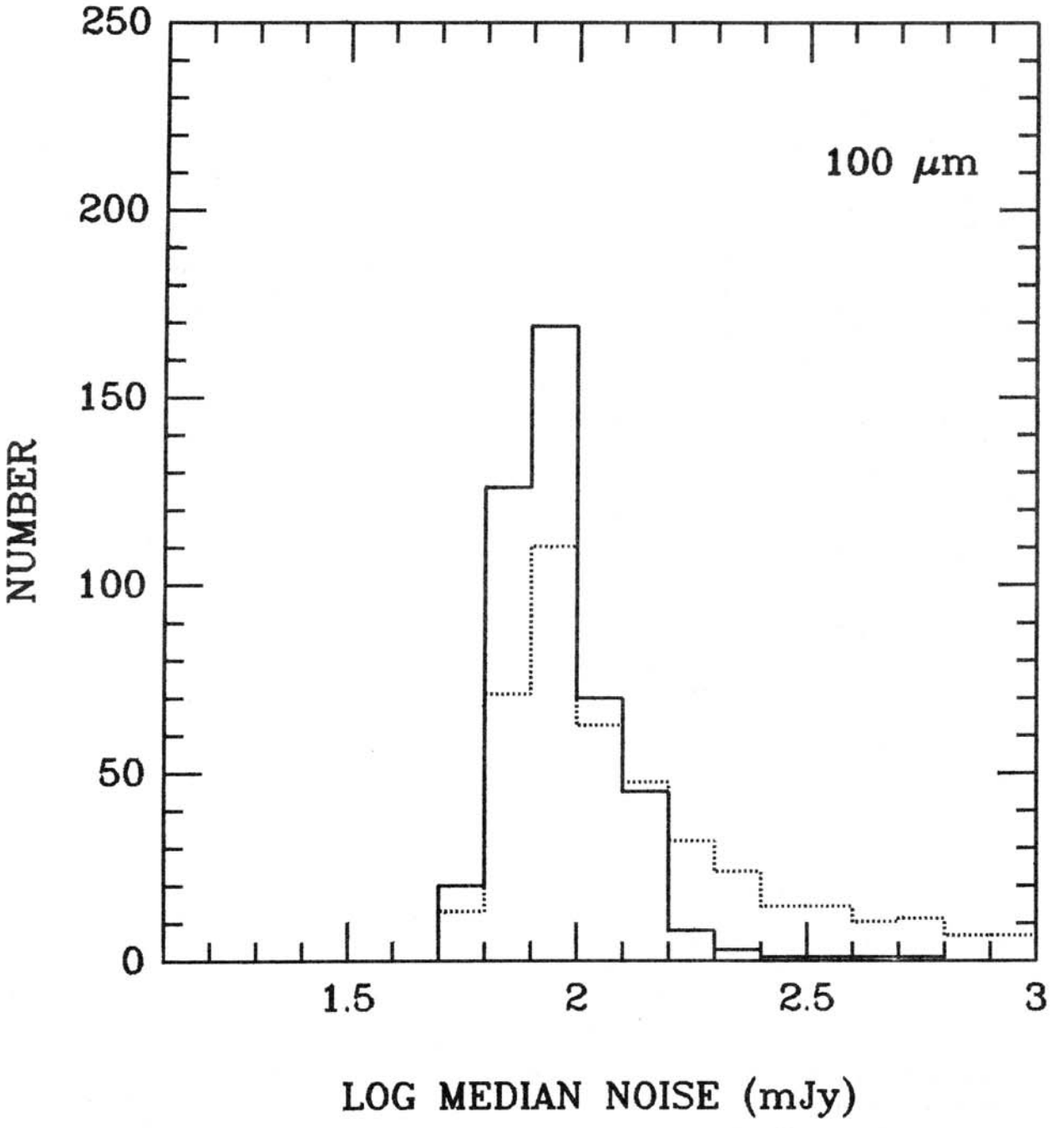

Figure IV.A.4 Number of fields versus median noise; solid line represents the high latitude subset of fields, the dotted line represents the complete set of fields with the verticle scale divided by 4.

The process used to optimize or "tune" the confirmation parameters (Section III.B) is in essence a process to make the natural trade-off between reliability and sensitivity. Data from 10 randomly selected fields, which were observed a minimum of three times during the Pointed Observation program, were co-added to yield a higher net sensitivity than was achieved for the SSC. Lists of sources from these fields were taken to constitute "truth-tables" against which the sources produced by the SSC processing of these fields could be compared. It is quite important to note that, although the co-addition of independent observations decreases the effective detector noise in a field allowing the detection of fainter sources, crowded co-added fields can still contain fixed-pattern noise caused by source confusion.

During the tuning procedure several confirmation parameters, including the positional windows, the flux ratio limits, minimum local signal-to-noise, and minimum correlation coefficients were varied. The sources confirmed using selected values of these parameters were compared to those in the deeply co-added fields. A source which was identified in both the SSC processing and the co-added field was considered verified. Sources which appeared in the SSC lists but failed to be detected in the co-adds were taken to be spurious. Those sources which were included in the deep co-adds and not the SSC were noted, and follow-up investigation was carried out to ascertain why they were not confirmed for the SSC.

Figures IV.B and IV.C illustrate the results of two such co- additions of fields corresponding to the SSC fields with reference grid numbers 13783 and 8595. Field 13783 covers a mid- latitude region of low source density. Nine individual observations were co-added to produce the contour maps which show the positions of 12 and 60 μm sources for this field. Three observations were co-added to produce the 12 μm map of field 8595; this very crowded field lies only a few degrees from the galactic plane. Single contours on the 12 μm maps represent sources with flux densities of 20 and 32 mJy for 13783 and 8595 respectively, and the single contours on the 60 μm map of 13783 indicate 90 mJy sources. Each additional contour represents an isophote a factor of three higher. Superimposed on the source contours are the locations of SSC source identifications.

The parameters were tuned until all spurious sources were eliminated, that is, until the reliability level of the test fields was nearly 100%. The final adopted parameters (cf. Section III.B) were conservative in the sense that some sacrifice of sensitivity was made, but they were consistent with the goal of emphasizing reliability.

The confirmation rate for an SSC field may be defined as the ratio of the number of confirmed sources in the field to the number of extractions in the reference grid. Based on results using the final confirmation parameters, the confirmation rates for fields in the high latitude subset are 0.12 at 12 μm, 0.09 at 25 μm, 0.39 at 60 μm and 0.41 at 100 μm. These rates vary with wavelength in a manner roughly consistent with the simplified view that for a constant signal-to-noise ratio the confirmation rate should increase with an increase in the surface density of sources until confusion dominates. As expected, using the observed source densities from Table IV.G, the ratios of confirmation rates to the source densities are, in order of increasing wavelength, 0.03, 0.04, 0.04 and 0.05. The relative constancy supports the foregoing interpretation despite the possible effects of confusion at 100 μm and the presence of highly non-random noise at 12 μm.

A.2 Reliability of Confirmed Sources

Final reliability testing was carried out by comparing the source lists of an additional 11 randomly selected deep co-added fields with the SSC source lists. These test fields spanned a representative range of source density and position on

the sky. In the combined 21 test fields, the SSC processing confirmed 572 sources: 139 at 12 μm, 91 at 25 μm, 198 at 60 μm and 144 at 100 μm. Of these, only 5 sources were found to be spurious. One 60 μm source in a low density, high galactic latitude field, with a reported flux density of 160 mJy had no counterpart in the deep co-adds. The remaining 4 spurious confirmations, 3 at 25 μm and 1 at 60 μm, were all found in a single high density field centered on a dense molecular cloud region.

For non-complex fields the reliability testing indicates that the confidence level for the SSC confirmations in all bands is >98%. In high density regions, the reliability is compromised, as evidenced by the 4 spurious confirmations. It is due to the effects of confusion operating on both the source extractions and the confirmation processing.

A.3 Band Merging Reliability

Because band merging windows are based on positional uncertainties which were refined during the confirmation procedure, the band merge process is quite conservative in the sense that merges are more likely to be missed rather than to be performed incorrectly. Preliminary analysis of the reliability level of the band merging was carried out graphically during the examination of the deep coadded field outputs. Among the 572 single band sources in the 21 test fields there are 133 reported merged sources in the SSC processing. Based on their positional proximity, there were four instances where sources in one or two bands failed to merge with the proper source in another band, and in one instance what should have been a single source detected in four bands was reported as two sources, each detected in two bands. *On no occasion were spurious band merges found.*

The positional testing for band merge accuracy does not take into account whether a particular merge is physically reasonable. The flux-flux plots shown in Figures IV.D, IV.E and IV.F clearly illustrate that for mid- to high latitude fields, no grossly nonphysical matches were made during the processing. This is further supported by the color-color plots shown in Figures IV.G.1-2. None of the sources detected in at least 3 bands examined in the analysis fields appear to lie outside the color regions consistent with known astronomical sources.

The very high quality of the band merge processing in the SSC is a consequence of the goal of reliability. It was accepted that some fraction of the true band merges would be missed in order to avoid spurious ones. The user is encouraged to examine nearby sources within the field of interest to search for additional band merge candidates. All information necessary to reconstruct source positions in the individual input grids, or to construct new band merges with less conservative windowing has been retained in the SSC source listings.

A.4 Sensitivity Limits

The analysis of the deep co-added fields was also used to form the first of two sensitivity estimates for the SSC. All sources which were found in the "truth-table" source lists, but were not reported in the SSC fields were summarized. The flux density of the brightest true source missed in each band should then define the sensitivity limit for that field. The brightest sources which failed to be confirmed in the test fields had flux densities of 94, 185, 110 and 400 mJy at 12, 25, 60 and 100 μm, respectively and, for the four bands in the same order, the faintest sources confirmed were at flux densities of 65, 70, 80, and 250 mJy.

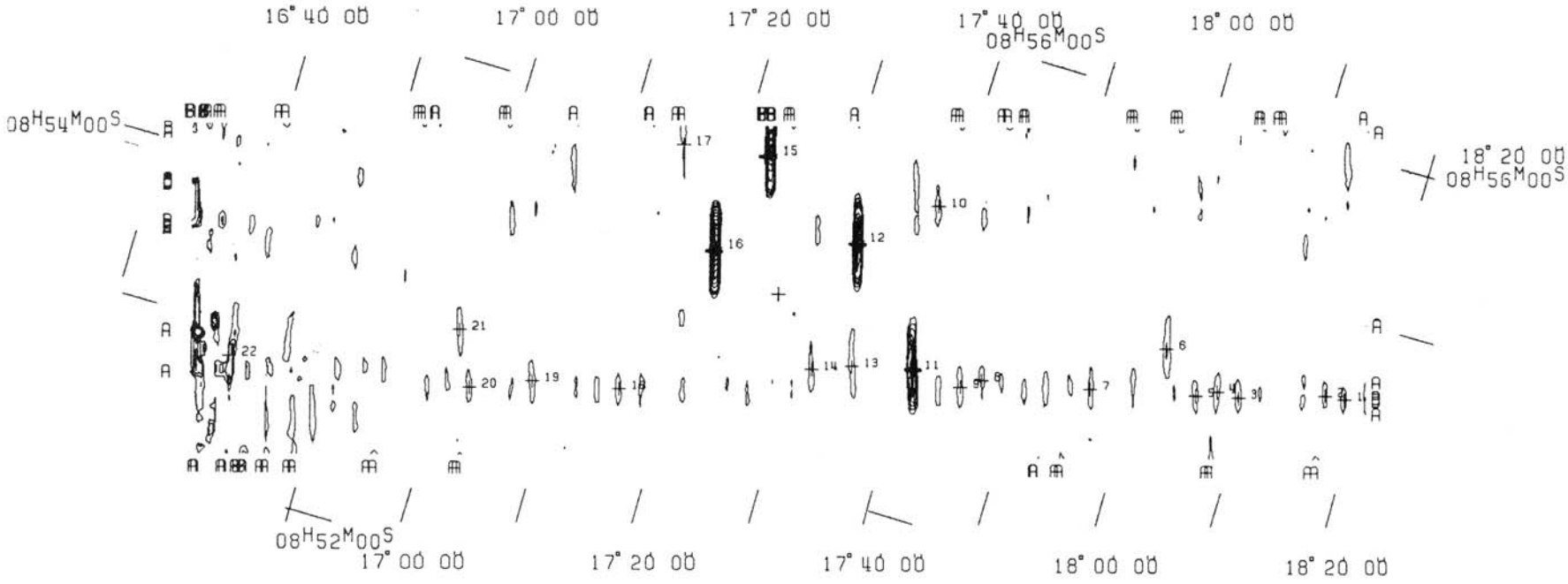

Figure IV.B.1 12 μm FLUX filtered map of a low source density region. Confirmed 12 μm sources indicated by heavy crosses; light crosses with numbers indicate source extractions prior to confirmation processing.

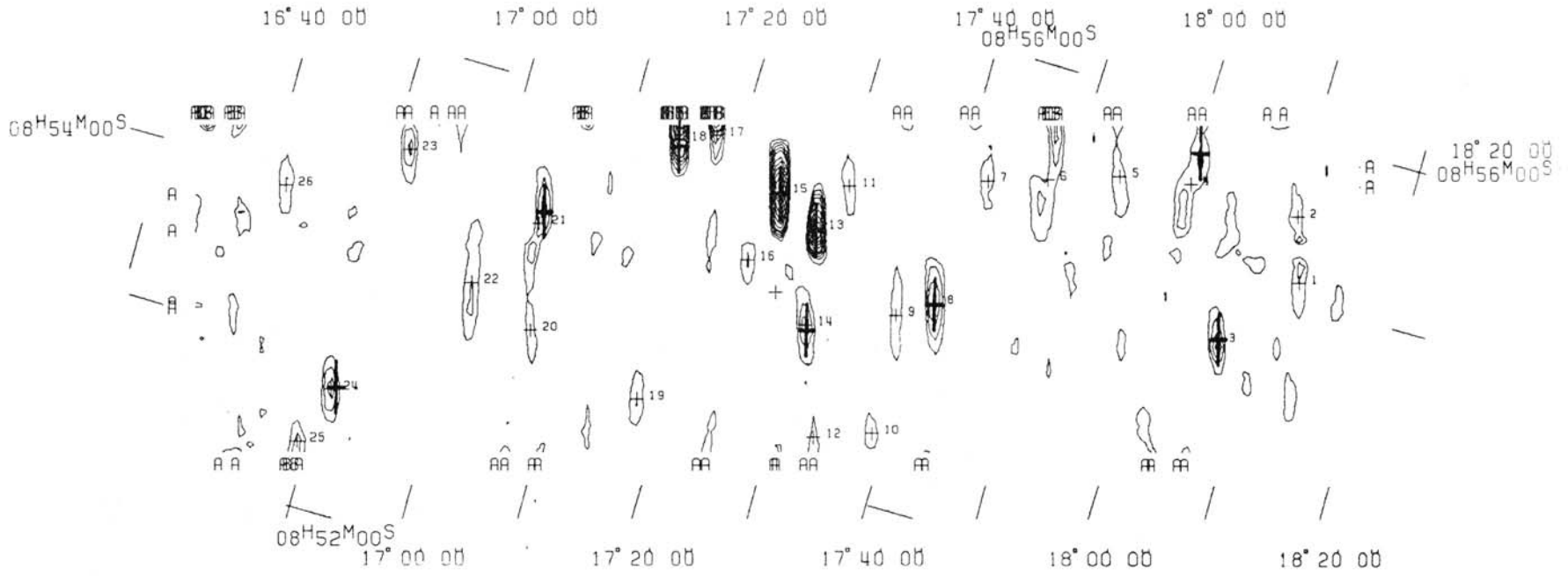

Figure IV.B.2 60 μm FLUX filtered map of a low source density region. Confirmed 60 μm sources indicated by heavy crosses; light crosses with numbers indicate source extractions prior to confirmation processing.

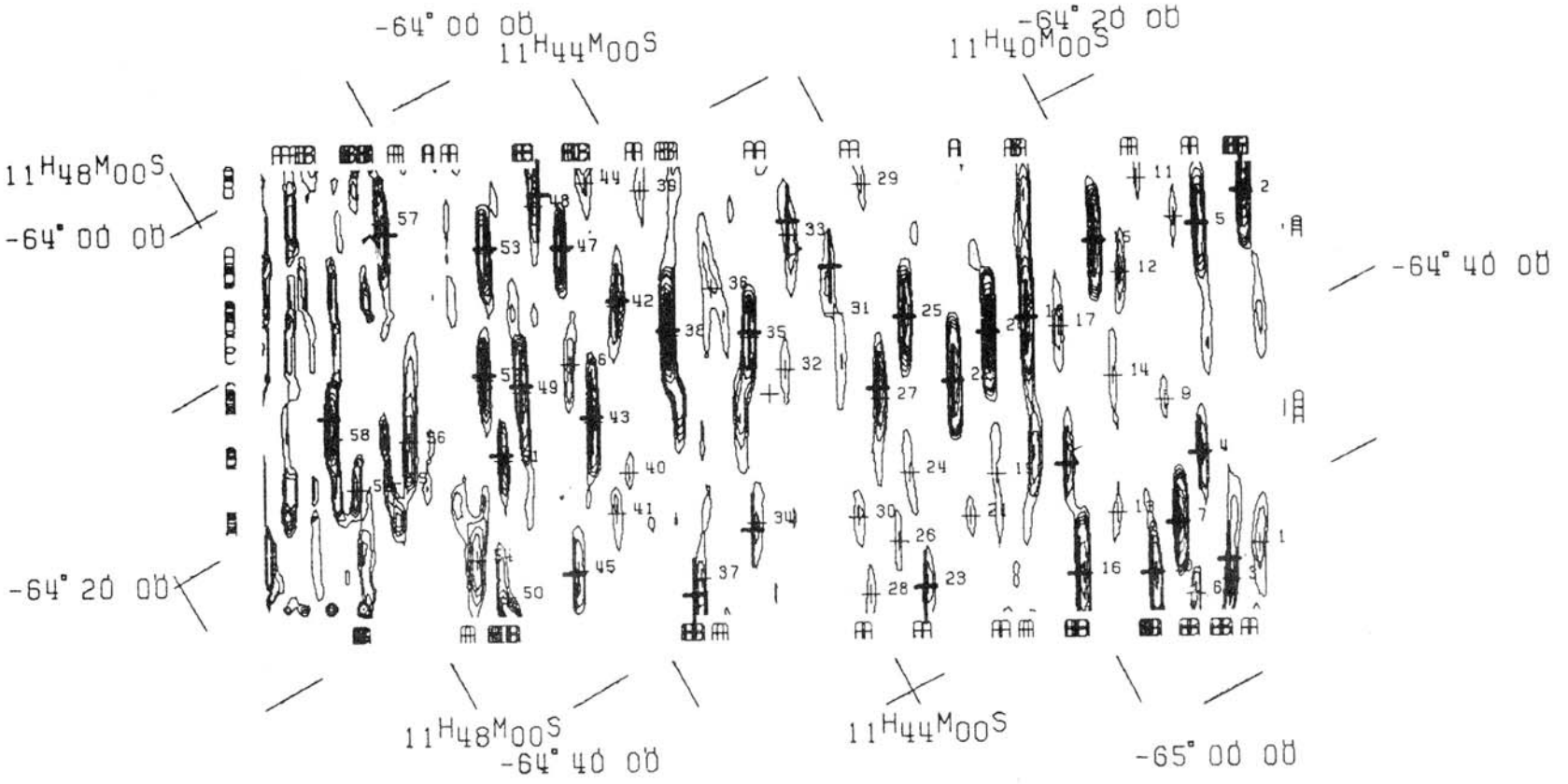

Figure IV.C 12 μm FLUX filtered map of a high source density region. Confirmed 12 μm sources indicated by heavy crosses; light crosses with numbers indicate source extractions prior to confirmation processing.

Figures IV.H.1-4 represent the differential Log N vs Log F relationships at 12, 25, 60 and 100 μm for all sources in the high latitude subset. A second estimate for the sensitivity limit of the highest quality fields in the SSC may be deduced from the turnover point at which the observed Log N vs Log F curves deviate from simple power laws. From these figures the formal 90% completeness limits occur at approximately 120 ± 10 mJy for 12 μm sources, 150 ± 15 mJy at 25 um, 120 ± 10 mJy at 60 μm and 440 ± 50 mJy at 100 μm, values which are reasonably consistent with the estimates made from the examination of the deep co-added fields. Furthermore, the detection threshhold, defined here as the faintest sources confirmed, is the same for both the deep co-added fields and the larger subset of high latitude fields.

The Log N vs Log F plots of Figure IV.H illustrate several complications introduced by the selection effects and biases of the SSC. The structure seen in these plots is not necessarily a true representation of the average infrared sky at these flux levels since corrections have not been applied for a number of known observational effects including: targeted sources, variation in the sensitivity levels and source confusion.

B. Association Statistics

Table IV.A contains a summary of the number of sources in the SSC which have been positionally associated with objects in various celestial catalogs. The catalog identification numbers are as listed in Table X.B.4 of the Main IRAS Supplement and in Section III.H of this document.

A total of 16,599 SSC sources are associated with objects in one or more of the reference catalogs. Of the associated sources in the SSC, only 11,129 are associated with the PSC. Therefore, ~75% of the detections in the SSC are "new" infrared sources, in the sense that they are not found in the PSC. The actual number of unique new sources is somewhat smaller due to the presence of redundant sources from overlapping fields.

Table IV.A. Associations with Various Catalogs

Catalog	Number in SSC	Catalog	Number in SSC
1	687	19	35
2	1003	20	109
3	297	21	24
4	312	22	238
5	516	23	2150
6	537	24	117
7	286	25	18
8	30	26	55
9	545	27	117
10	1215	28	61
11	60	29	261
12	860	30	59
13	2906	31	61
14	821	32	1106
15	482	39	1770
16	538	40	869
17	155	41	11129
18	154		

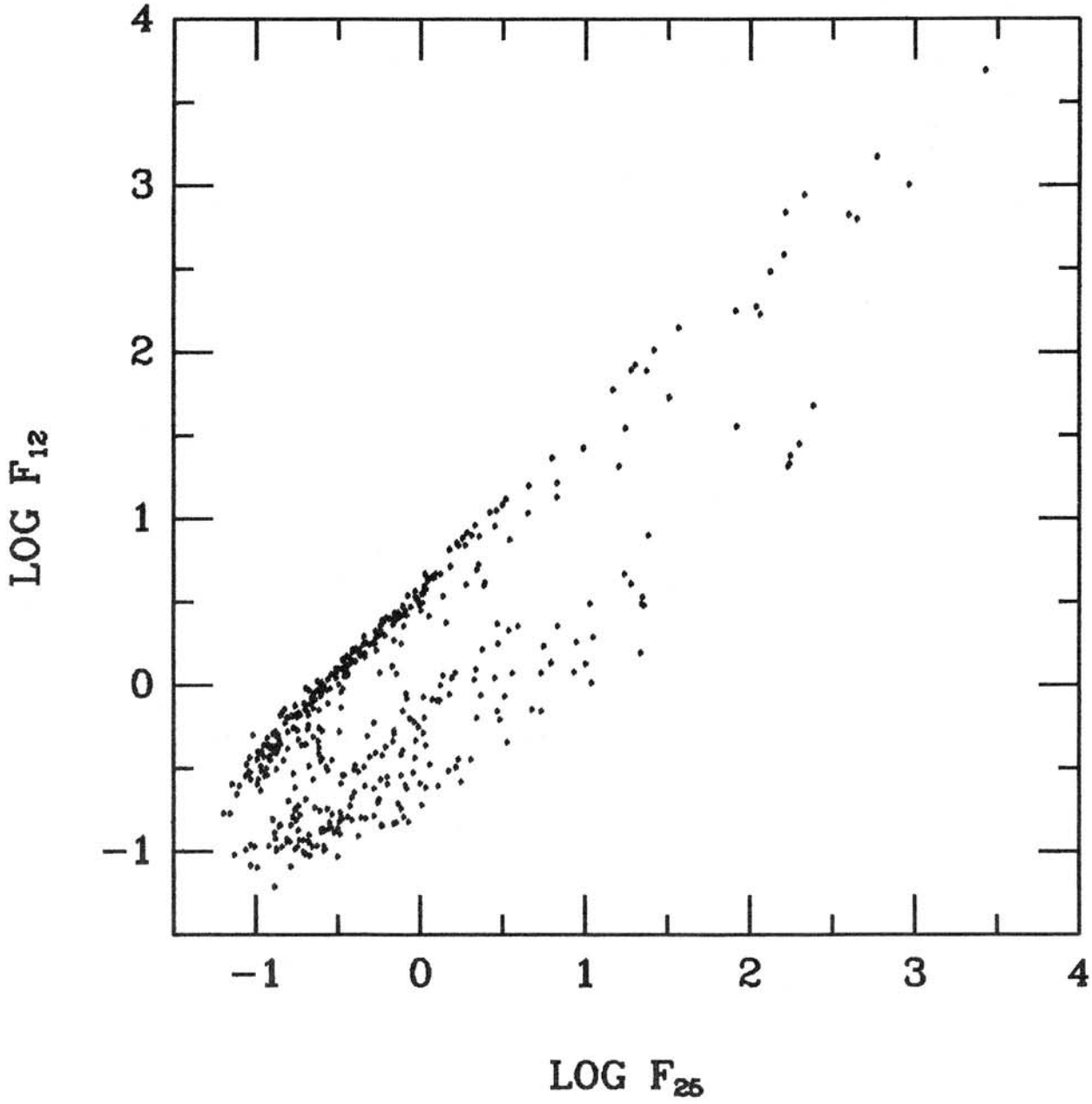

Figure IV.D Flux density, in Jy, at 12 μm versus 25 μm for sources at |b| > 30°.

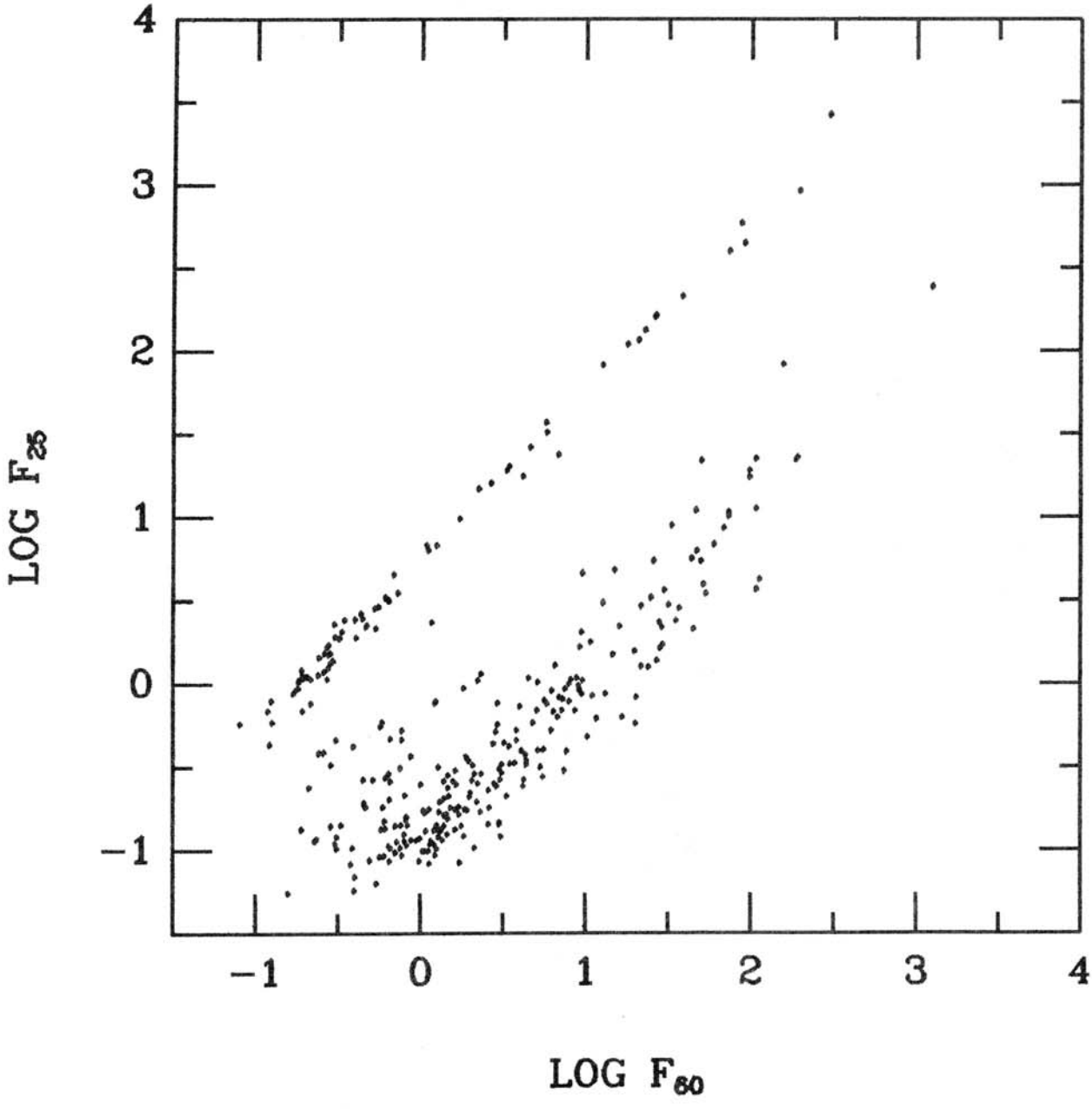

Figure IV.E Flux density, in Jy, at 25 μm versus 60 μm for sources at |b| > 30°.

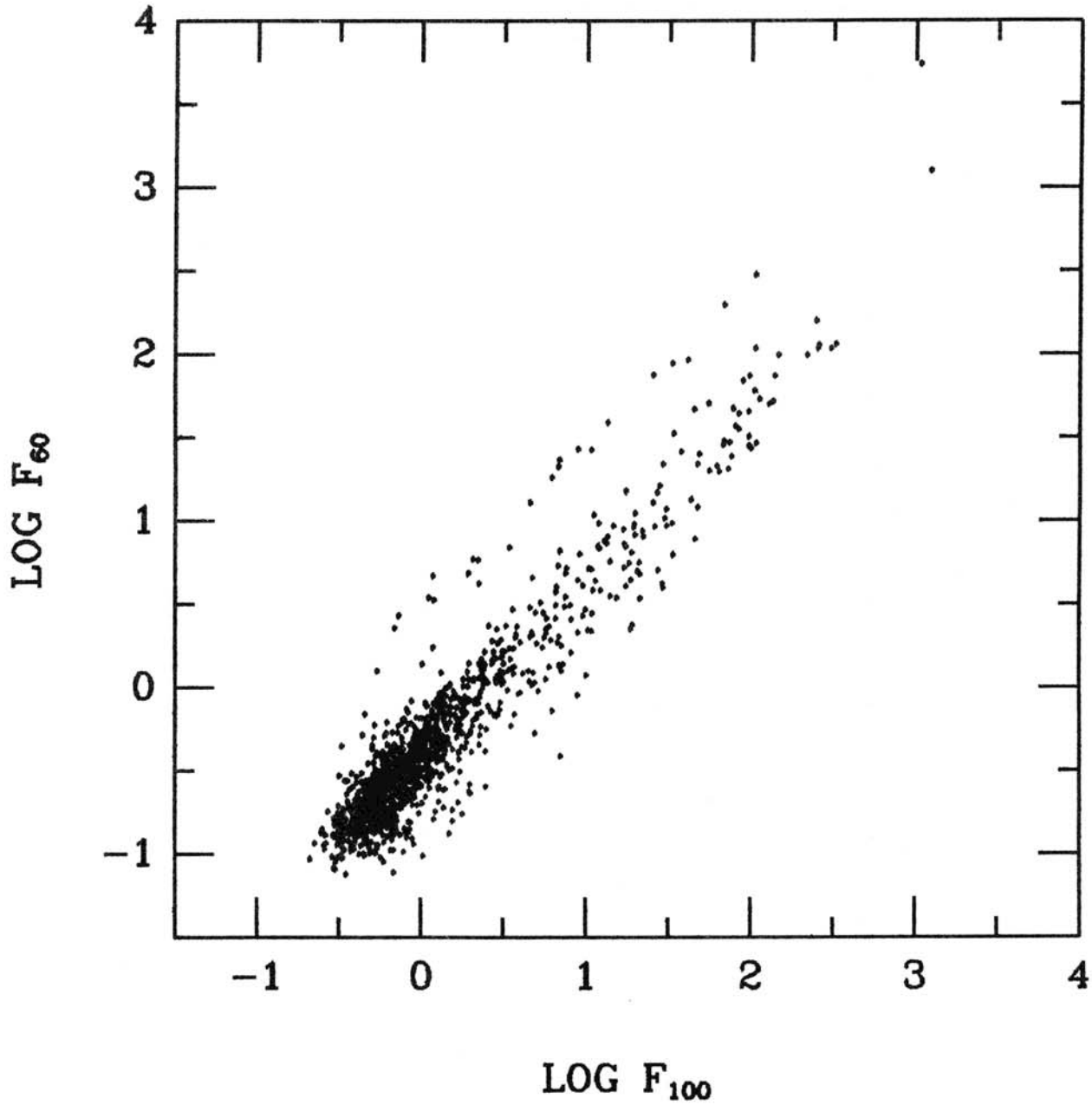

Figure IV.F Flux density, in Jy, at 60 μm versus 100 μm for sources at |b| > 30°.

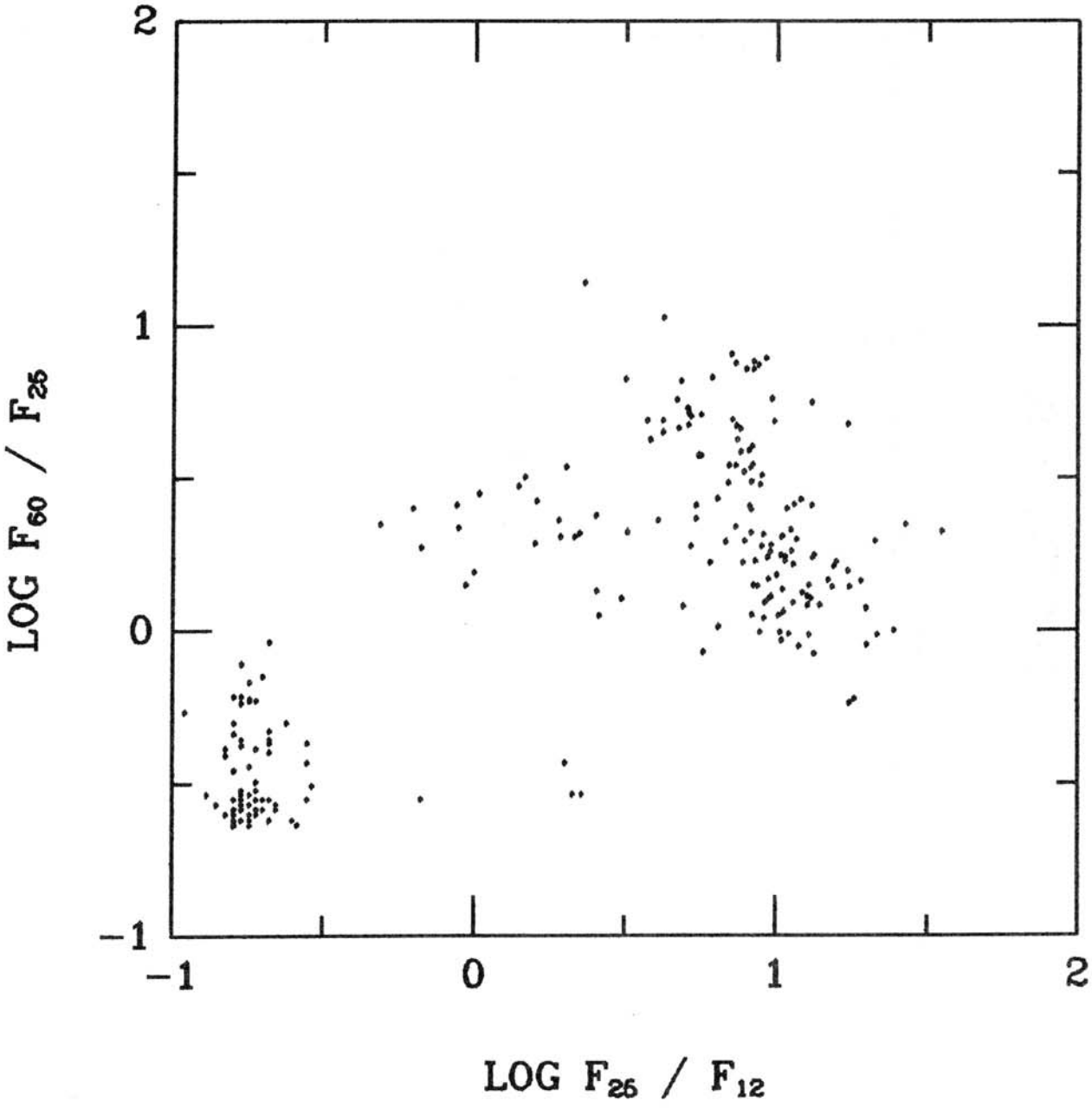

Figure IV.G.1 Color-color plot for high latitude subset sources.

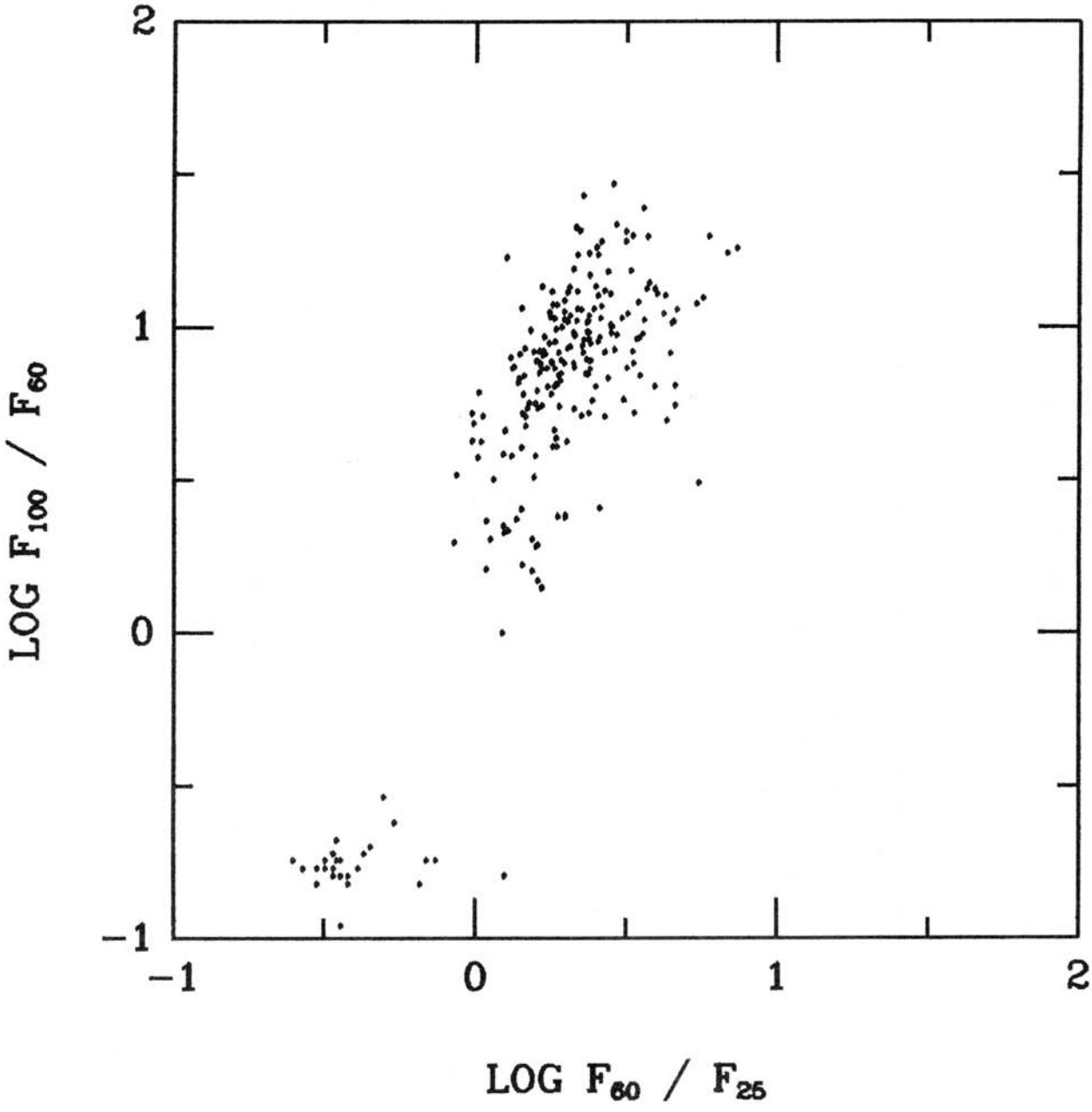

Figure IV.G.2 Color-color plot for high latitude subset sources.

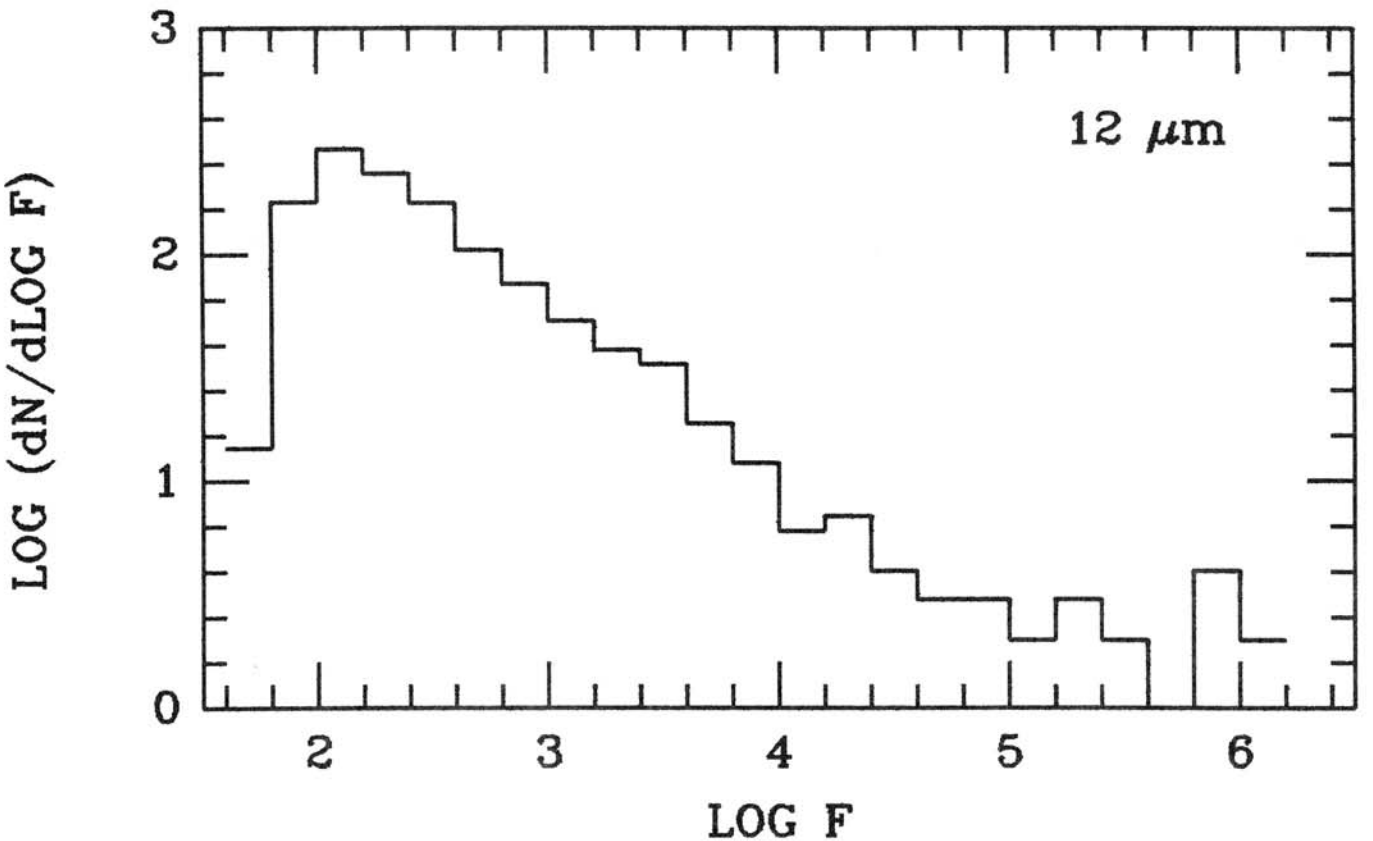

Figure IV.H.1 Differential Log N versus Log F relation for high latitude subset sources; flux density in mJy.

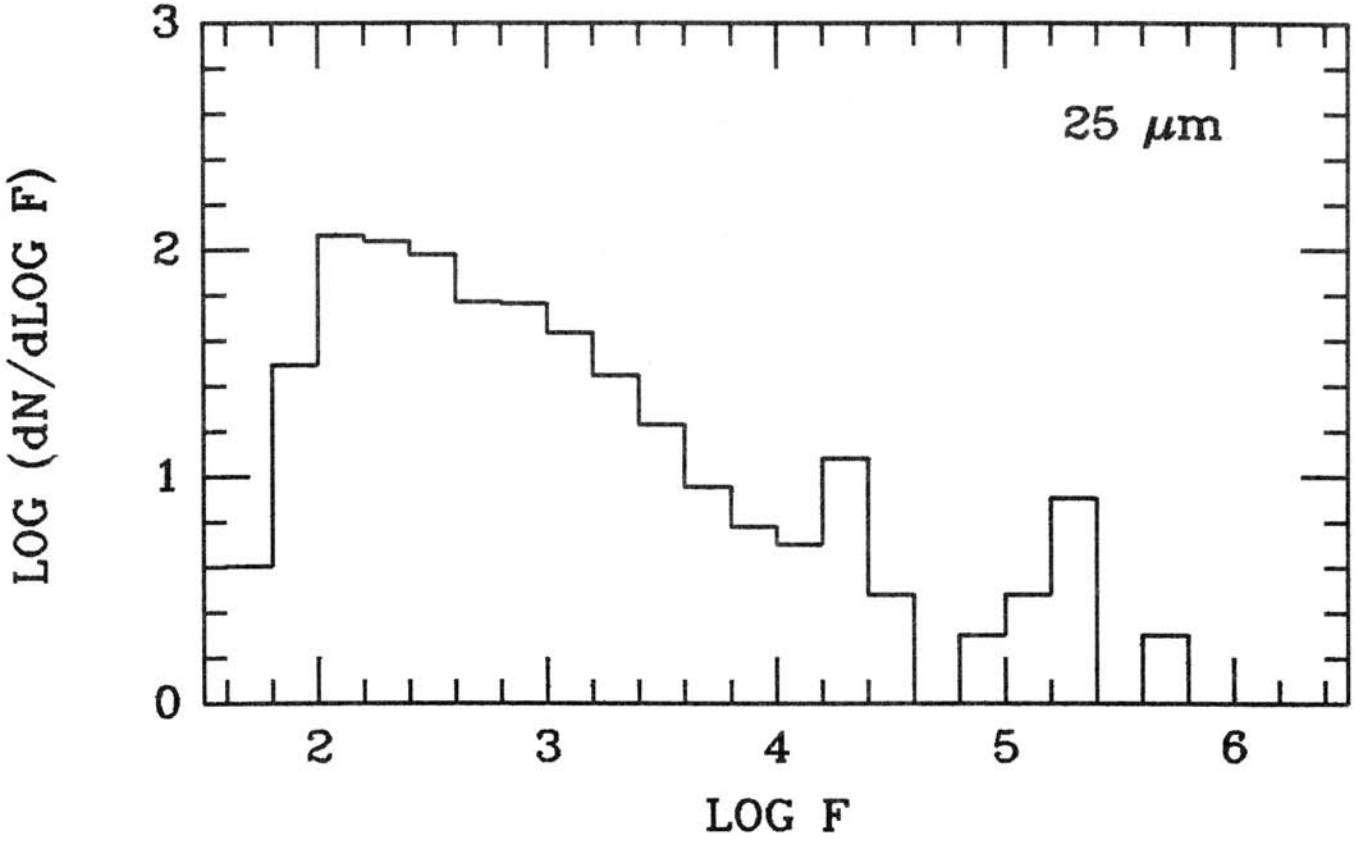

Figure IV.H.2 Differential Log N versus Log F relation for high latitude subset sources; flux density in mJy.

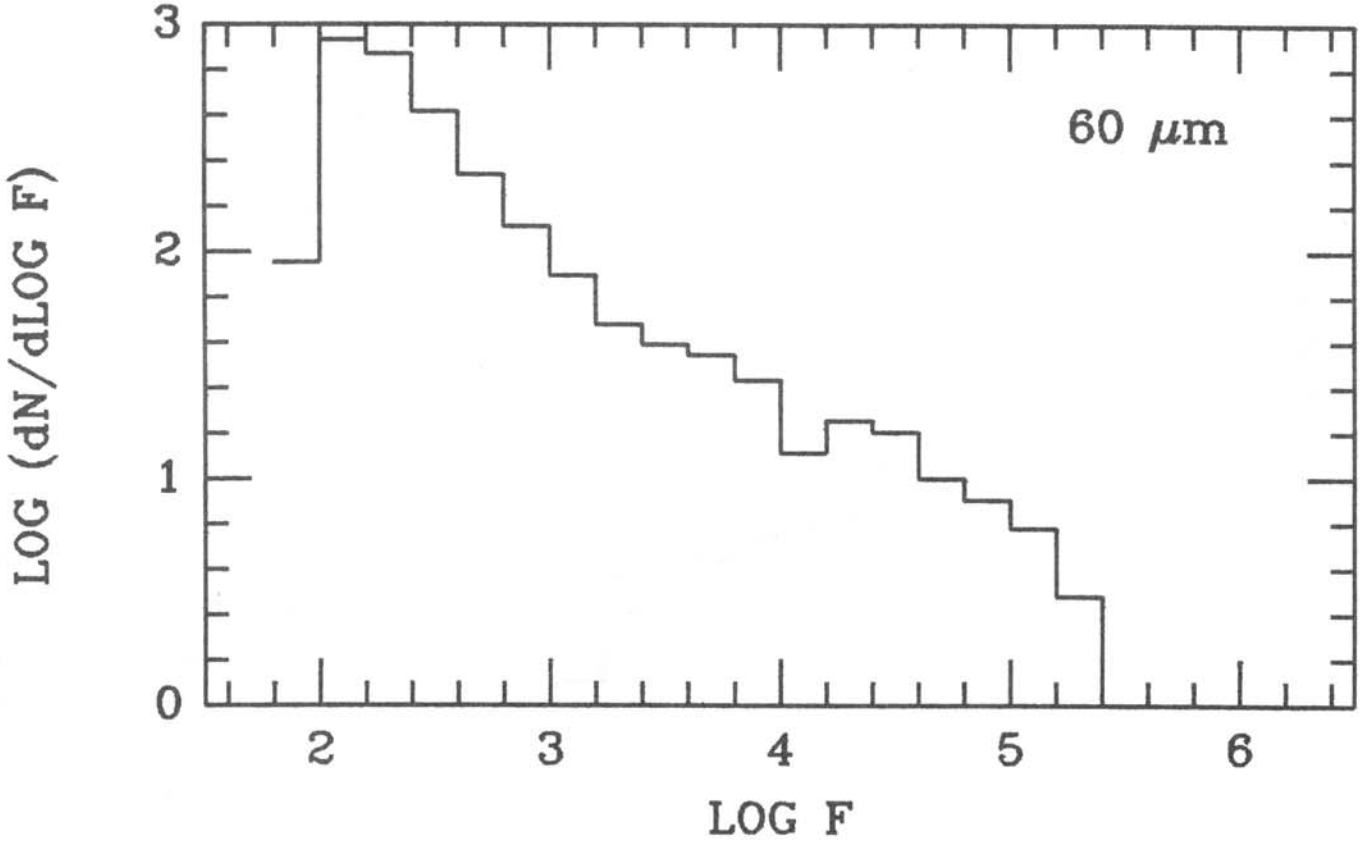

Figure IV.H.3 Differential Log N versus Log F relation for high latitude subset sources; flux density in mJy.

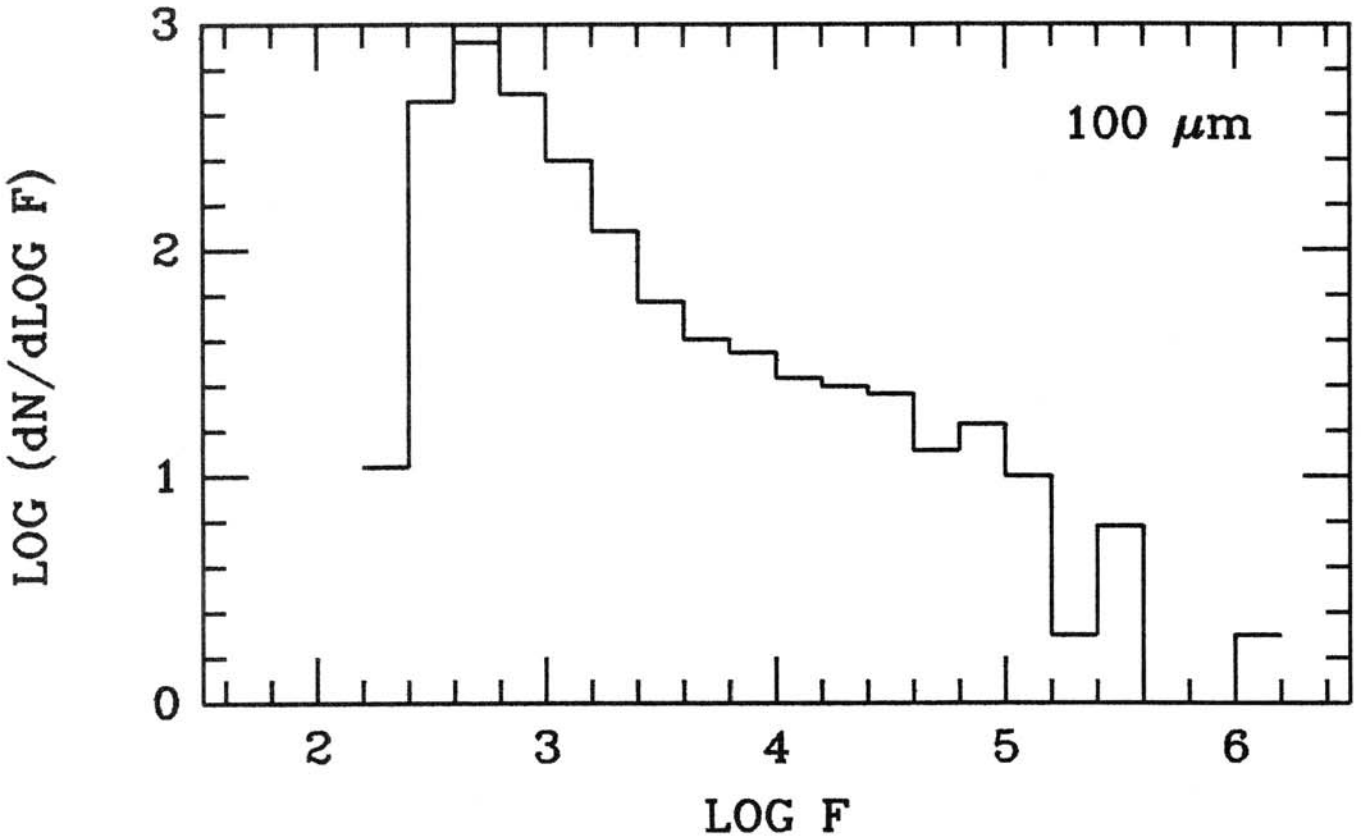

Figure IV.H.4 Differential Log N versus Log F relation for high latitude subset sources; flux density in mJy.

C. Absolute Positional Accuracy

The Pointed Observation Users Guide (Young et al. 1985) reports that individual Pointed Observations yield 12 μm positions of SAO stars which have an absolute accuracy of 1 sigma ~7 arcsec in the in-scan direction and ~35 arcsec cross-scan. Since the SSC effectively averages two independent observations during the confirmation process, positional accuracy should improve by a factor of $\sqrt{2}$. In practice, however, systematic effects can degrade this improvement. Such effects include errors in pointing repeatability, and the influence of other bands during positional updating for band merged sources.

To test the actual absolute accuracy of the source positions in the SSC, the reported positions of all sources at |b| > 30 deg. which were associated with objects in the SAO Star Catalog and the subset of the UGC which have accurate positions (Dressel and Condon 1976) were compared with the positions from the respective catalogs. The positions of band-merged SSC sources were evaluated as weighted means of the positions of the source in each individual band, such that the final position was most strongly influenced by the band with the highest signal-to-noise ratio. Therefore, the precision of the coordinates of SSC sources associated with SAO catalog stars is indicative of all 12 μm dominant sources. Equivalently, those sources associated with UGC galaxies will represent most 60 μm dominant sources. The positional differences between SSC and individual catalog sources were computed for the in-scan and cross-scan directions. Figures IV.I and IV.J show histograms of the positional differences for the SAO stars and UGC galaxies, respectively.

The distribution of in-scan and cross-scan position differences are well-approximated by Gaussian functions. To characterize these distributions, recursive fits were made using combinations of a Gaussian function and a constant "background" term. The background term accounts for the possible occurrences of chance associations of SSC sources with catalog objects, sources with uncharacteristically bad positions, or the rare spurious source. Table IV.B contains a listing of the best-fit parameters for the in-scan and cross-scan position distributions for the SAO and UGC sources. Sigma represents the half-width of the Gaussian and thus the absolute positional accuracy relative to the catalog positions. The level of the background term in sources per separation bin is denoted NB. For the associations with SAO stars, these bins were 2" in the in-scan direction and 3" in the cross-scan direction. In the case of the UGC galaxies, they were 3" in-scan and 5" cross-scan. For comparison, the table also shows the positional accuracy according to the Main IRAS Supplement for PSC sources fainter than 1.2 Jy at 12 μm and fainter than 1.9 Jy at 60 μm.

The positional uncertainties listed in Table IV.B should be taken as the 1 sigma dimensions of the uncertainty ellipses of 12 and 60 μm SSC sources. Inspection of Figures IV.I and IV.J indicates that there are significant numbers of sources with positional discrepancies out to several sigma, especially in the cross-scan direction. A small number of these (<10%) are due to bad associations. The remainder may result from poor position reconstruction in the confirmation and band merging processing because of significant scan angle differences between the two input grids. Because of the large tails of the distributions, the user is recommended to use greater than 3 sigma positional uncertainties when making tests of source locations in the SSC. Specifically, at 12 μm the search box should be 30" x 180" and at 60 μm it should be 60" x 140", with the orientation as indicated in the appropriate field header.

Table IV.B. Absolute Positional Accuracy of SSC Sources

	Sigma (SSC) (Arcsec)	NB	Sigma (PSC) (Arcsec)
SAO Stars			
In-scan	6.5	0	2.8
Cross-scan	25.5	4	15.6
UGC Galaxies[1]			
In-scan	8.8	5	5.7
Cross-scan	23.5	3	15.2

NOTE: [1] This group includes only those whose accurate positions were measured by Dressel and Condon (1976).

D. Photometric Accuracy

D.1. Accuracy of Relative Flux Densities

A measure of the relative flux accuracy of the SSC can be obtained by comparing the fluxes of merged sources in different bands. Figures IV.D - V.F show these relationships for 12 - 25 um, 25 - 60 μm and 60 - 100 μm band combinations for the high latitude subset of SSC sources. These results should be compared to the corresponding plots in the Main IRAS Supplement, Figures VII.D.1,2,3. Over the full range of SSC flux densities, there are no obvious departures from the expected flux ratios. Furthermore, the confinement of most points below the boundary corresponding to an infinitely hot blackbody provides confidence in the accuracy of the absolute calibrations used in the SSC processing.

D.2 Accuracy of Absolute Flux Densities

The absolute calibration of the SSC is based on the same calibration sources and procedures used in the PSC (cf. Section VI.C of the Main IRAS Supplement). In this section a comparison is made between the photometry of a specially selected and processed set of stellar observations and the catalog values for these stars from the SSC and the PSC version 2.0. The method by which the magnitudes of these stars were obtained and the conversion from flux density to magnitude are described in the Main IRAS Supplement.

Table IV.C includes the magnitudes of eleven selected stars which were observed using the macro DPS61D. The observations were carefully hand-reduced from the raw data to provide an independent check of the entire processing chain. Nine of these stars are bright enough to be measured in all four bands and five are included in Table VI.C.1 in the Main IRAS Supplement. The differences between the hand calibrated magnitudes and those found in the SSC are tabulated along with the same results for the PSC version 2.0. As explained in the IRAS Circular (Nov. 1986) which accompanied version 2.0 of the PSC, systematic errors in the PSC at low flux densities were corrected in this version using the preliminary SSC results to "tune" the correction algorithm. This procedure did not affect the PSC flux densities above 2.0 Jy. The average magnitude differences, shown at the bottom of the table, indicate that both catalogs share the same calibration and the largest errors are at 100 μm. At 12 μm the difference of -0.053 magnitudes between the calibration stars and

Table IV.C Magnitudes of Calibration Stars

Star	Wavelength (μm)	m_{cal}	Δm_{ssc} [1]	Δm_{psc} [2]
IRC 10011	12	-3.635	-0.158	-0.011
	25	-5.125	-0.151	-0.104
	60	-5.26	-0.01	0.08
	100	-5.44	-0.02	0.03
ϵ Eri	12	1.616	-0.038	0.030
	25	1.406	0.012	0.025
	60	-0.096	0.045	-0.036
	100	-1.537	0.110	-0.023
β Pic	12	2.751	0.003	0.066
	25	0.068	0.016	0.017
	60	-2.729	-0.001	0.028
	100	-3.464	0.084	-0.010
α CMi	12	-0.742	-0.020	-0.030
	25	-0.715	-0.019	0.007
	60	-0.798	-0.054	-0.060
	100	-----	-----	-----
3 Pup	12	-2.016	-0.041	-0.020
	25	-2.915	-0.042	0.058
	60	-3.086	-0.029	-0.050
	100	-2.968	0.087	0.006
β Gem	12	-1.197	-0.023	0.009
	25	-1.179	-0.017	0.014
	60	-1.173	0.051	0.067
	100	-1.306	0.016	-0.072
α Boo	12	-3.151	-0.078	0.064
	25	-3.092	0.005	-0.004
	60	-3.127	-0.042	-0.091
	100	-3.183	0.033	-0.116
α Lyr	12	0.013	-0.015	0.027
	25	-0.203	0.005	-0.041
	60	-1.950	0.031	0.005
	100	-3.049	0.067	-0.002
R Lyr	12	-2.370	-0.023	0.020
	25	-2.517	0.006	0.019
	60	-2.710	-0.063	-0.059
	100	-3.303	-0.078	-0.133
α Aql	12	0.174	-0.029	-0.063
	25	0.191	0.011	0.014
	60	0.303	0.051	0.055
	100	-----	-----	-----
β Gru	12	-3.490	-0.156	-0.088
	25	-3.459	-0.077	0.038
	60	-3.526	-0.037	0.006
	100	-3.572	0.094	-0.051
Wavelength (μm)	12	25	60	100
$<\Delta m_{ssc}>$	-0.053 (-0.023)[3]	-0.025 (-0.007)[3]	-0.005 (+0.004)[3]	+0.021 (+0.048)[3]
Std.Dev.	0.017	0.015	0.013	0.026
$<\Delta m_{psc}>$	+0.000	+0.004	-0.005	-0.042
Std.Dev.	0.015	0.013	0.018	0.019
$<m_{ssc}-m_{psc}>$	+0.053	+0.025	+0.001	-0.085
Std.Dev.	0.017	0.014	0.014	0.020

NOTES:

[1] The difference between the calibrated magnitude and the SSC magnitude: $m_{cal} - m_{ssc}$.

[2] The difference between the calibrated magnitude and the PSC version 2.0 magnitude: $m_{cal} - m_{psc}$.

[3] $<\Delta m_{ssc}>$ excluding IRC 10011, α Boo, and β Gru.

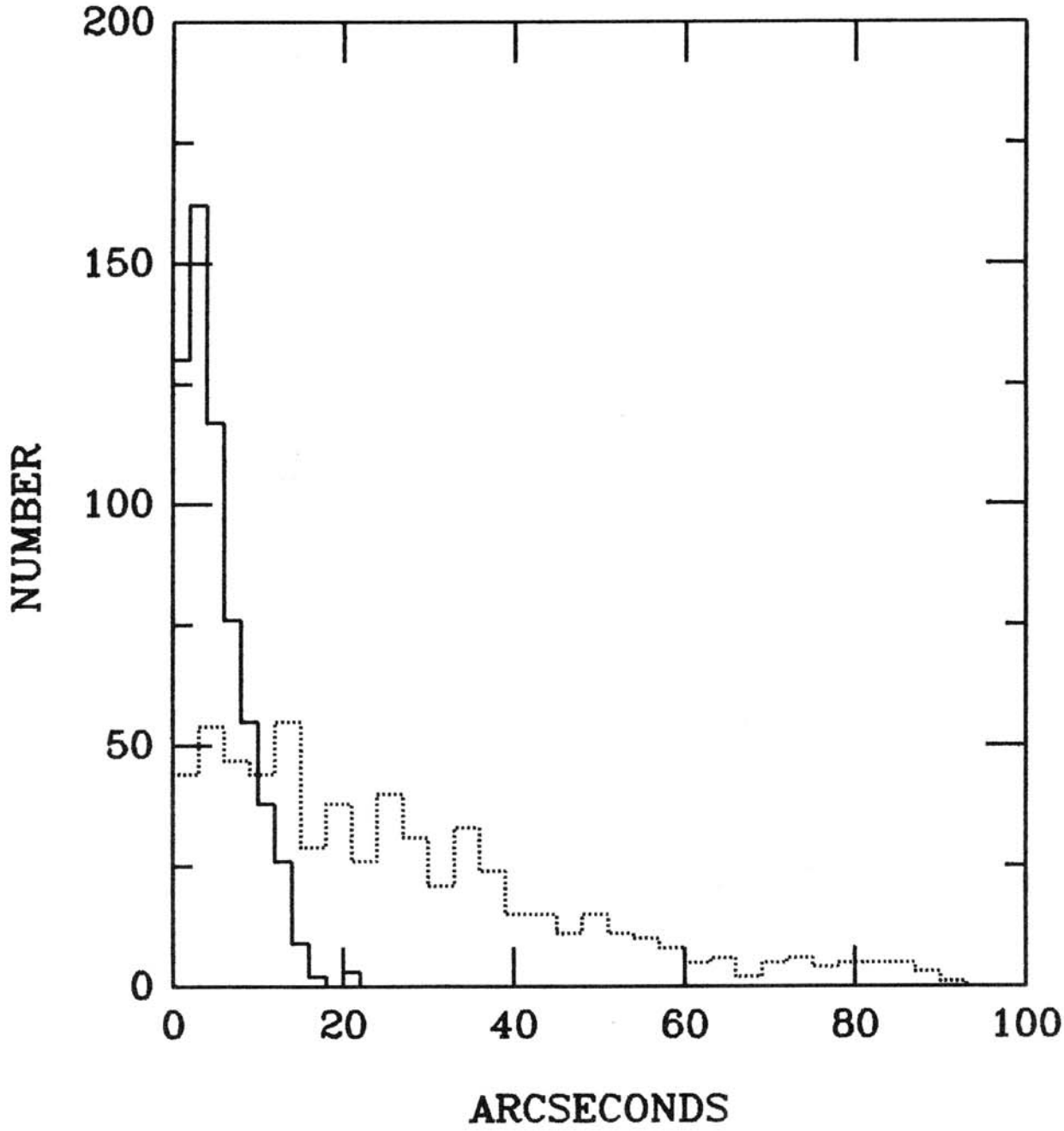

Figure IV.I Number of sources versus in-scan (solid line) and cross-scan (dotted line) separation between SSC position and SAO position for associated sources at |b| > 30°.

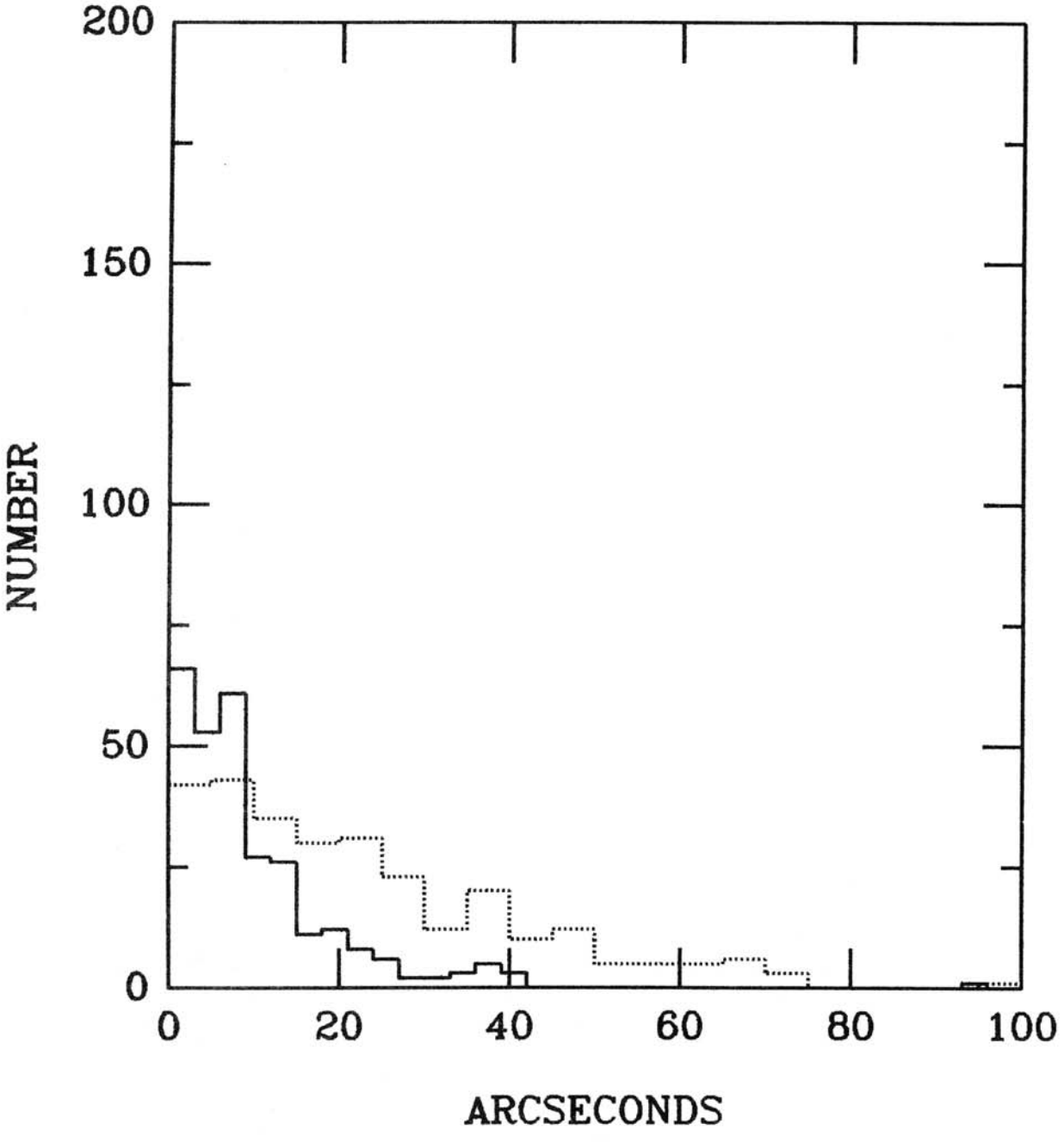

Figure IV.J Number of sources versus in-scan (solid line) and cross-scan (dotted line) separation between SSC position and selected UGC position for associated sources at |b| > 30°.

their SSC magnitudes is influenced significantly by the three brightest stars in the sample; if these three objects are removed the difference is reduced to -0.02 magnitudes, suggesting an uncorrected systematic error at 12 μm magnitudes brighter than -3. Since the SSC is to be used for much fainter sources and the magnitudes of virtually all such bright objects are found in the PSC, this potential errors has not been corrected.

A second comparison between the two catalogs is illustrated in Figures IV.K.1-4. Here the flux densities of a large sample of objects common to both catalogs are ratioed, displaying the dispersion withint each sample and providing another measure of the systematic errors between the two catalogs. Again, the overall agreement is quite good with percentage differences in the mean of -5.2%, 1.1%, 4.2% and 9.6% at 12, 25, 60 and 100 μm, respectively.

D.3 Flux Density Uncertainties

Three measures of the flux density uncertainty for each band in which a detection is reported are included in each SSC source listing: the relative flux density uncertainty, <n>/<F>, the local signal-to-noise ratio, LSNR, and the flux density ratio, F_c/F_r (Section III.C.2). Each of these parameters offers an independent indication of the uncertainty in the flux densities.

The relative flux density uncertainty in each band is the most accurate assessment of the noise level relative to that of the signal because it is determined from the median noises of the two input fields. As discussed in Section II.C, the median noise represents the average noise for the entire field and is therefore less susceptible to isolated events such as residual radiation hits. Figures IV.L.1-4 show the relative flux density uncertainty as a function of flux density in the four IRAS bands for the high latitude subset of fields. In the 12 and 25 μm bands and for most sources at 60 μm the relative flux density uncertainty scales roughly as the inverse square root of the flux density, as expected when the uncertainty is primarily driven by detector noise. At 100 μm, the uncertainty follows an 1/F relationship because other sources of noise affect the median noise measurement, in particular the presence of cirrus throughout the Pointed Observation fields and confusion noise in complex regions.

The local signal-to-noise ratio gives a similar estimate of statistical quality in most fields, but it is very sensitive to small-scale structure in high source density fields. As a consequence, the LSNR often overestimates the true flux density uncertainty.

The ratio of flux densities of a source from the two input grids provides a measure of both the intrinsic uncertainty in the flux density and the potential error produced by systematic differences between the two individual scans. In some cases the source brightness may have changed during the time between the two observations. Figures IV.M.1,2 show histograms of the flux density ratios for sources in the high latitude subset. Sources brighter than 0.5 Jy at 12, 25, and 60 μm and than 1.0 Jy at 100 μm are presented in Figure IV.M.1, while fainter sources are presented in Figures IV.M.2. These figures illustrate that systematic differences between the fluxes reported from the two input grids of each pair are minimal. The full width at half maximum (FWHM) of the distributions offer a measure of the characteristic flux density uncertainties for the two brightness regimes. In Table IV.D are listed the relative uncertainties calculated by measuring $10^{FWHM/2}$- 1 for the bright and faint flux ratio distributions. While the actual flux density uncertainty is a continuous function of the flux level, these values represent additional guidelines by which the general photometric quality of arbitrary SSC sources may be estimated.

Table IV.D. Relative Flux Uncertainty Estimated From Flux-Ratio Distributions

Source Brightness	$\sigma(F_r/F_c)$			
	12 μm	25 μm	60 μm	100 μm
High[1]	0.06	0.06	0.08	0.12
Low[2]	0.13	0.15	0.18	0.19

NOTES:

[1] $F_\nu > 0.5$ Jy at 12, 25 and 60 μm and > 1.0 Jy at 100 μm.

[2] $F_\nu < 0.5$ Jy at 12, 25 and 60 μm and < 1.0 Jy at 100 μm.

E. Sky Coverage and Source Densities

The IRAS Serendipitous Survey utilizes the results from 1813 Pointed Observation fields. The grid pairs which comprise these fields were selected by the guidelines stated in Section III.A. In Table IV.E are listed the number of fields as a function of macro type and galactic latitude. The distribution of fields on the sky is shown in Figure II.A.

Table IV.E Distribution of Fields with Macro Type and Galactic Latitude

Macro Code	N(|b|) <10°	10-30°	30-50°	>50°	Total
A	174	258	213	143	788
B	3	2	21	2	28
C	54	48	15	10	127
D	16	9	0	0	25
E	13	23	20	9	65
F	56	37	29	12	134
M	1	0	0	0	1
H	62	100	69	17	248
I	33	160	113	24	330
J	9	29	19	5	62
L	2	3	0	0	5
Total	423	669	499	222	1813
Effective Area (Degree^2)	255.8	401.4	318.0	132.6	1107.7

The effective sky coverage, also listed in Table IV.E, is the area sampled at a uniform sensitivity near the maximum of the survey (cf. Section III.F. An effective area of 1108 deg^2 on the sky is sampled by the SSC. The nominal sampling area of the SSC, that is, the purely geometric coverage of the fields, is approximately 1400 deg^2.

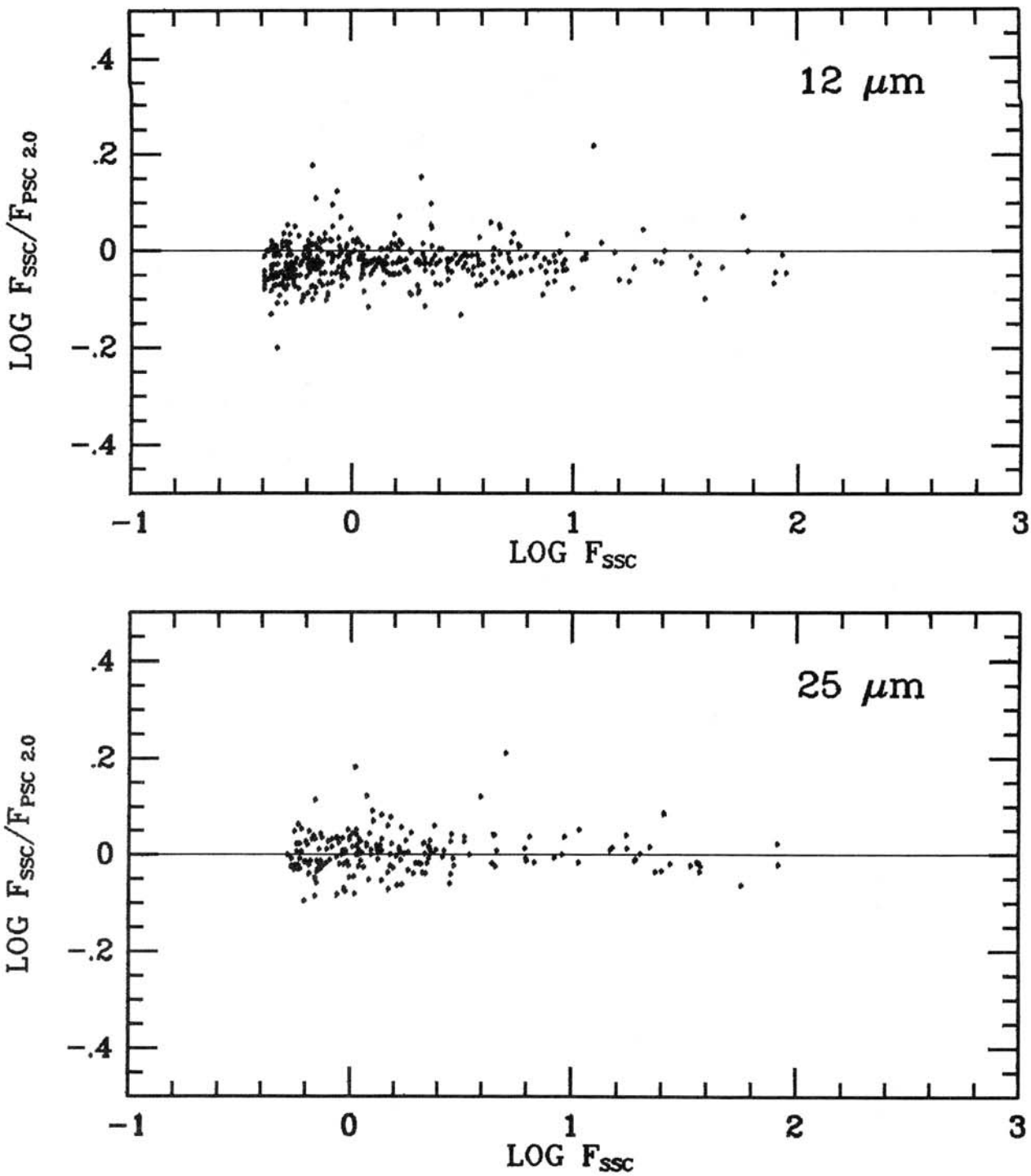

Figure IV.K.1-2 Ratio of SSC to PSC version 2.0 flux densities versus SSC flux density at 12 and 25 μm for sources selected from both catalogs. Expressed as a percentage difference from unity, the mean at 12 and 25 μm are -5.2% and 1.1%, respectively.

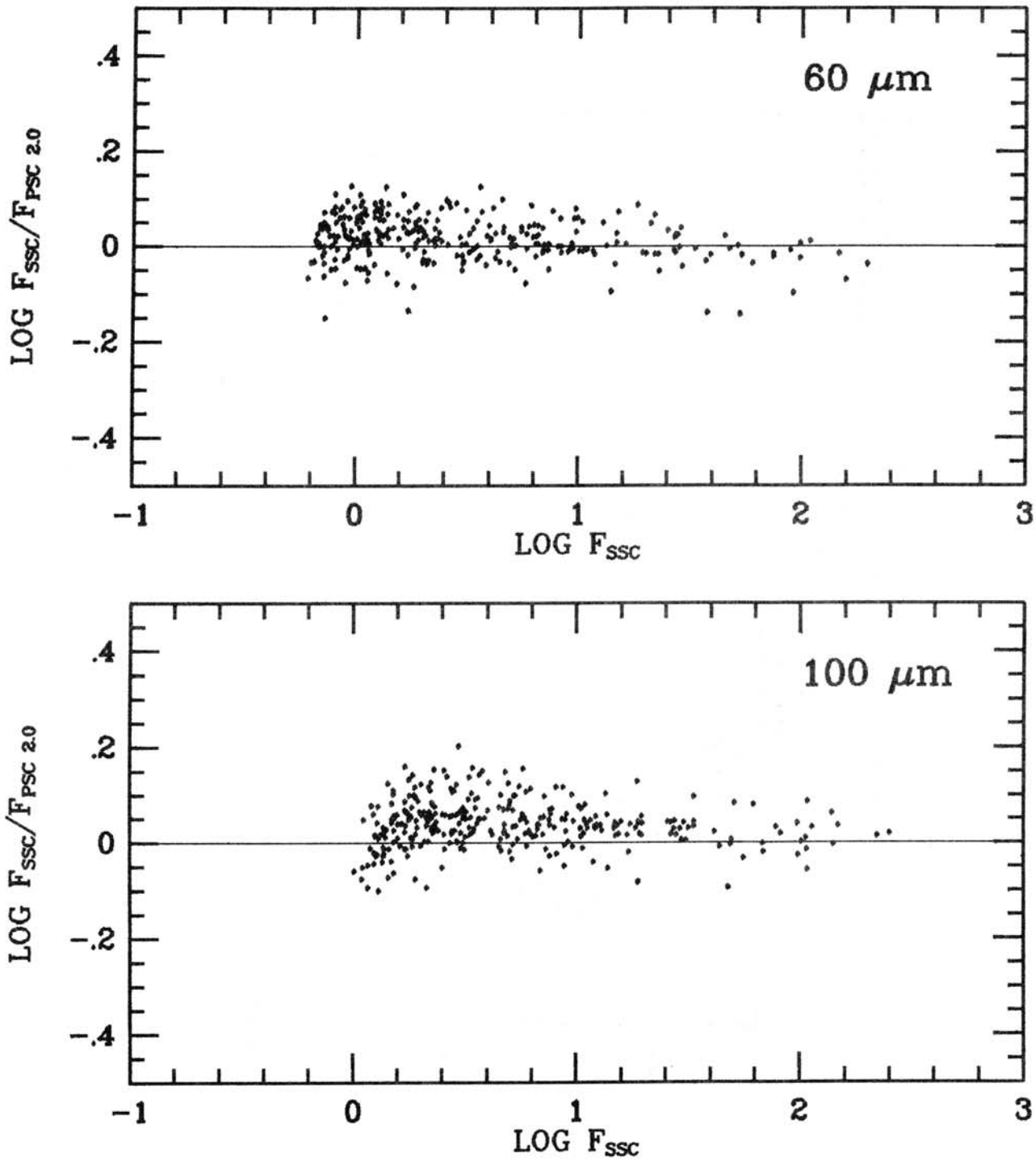

Figure IV.K.3-4 Ratio of SSC to PSC version 2.0 flux densities versus SSC flux densities at 60 and 100 μm for sources selected from both catalogs. Expressed as a percentage difference from unity, the mean at 60 and 100 μm are 4.2% and 9.6%, respectively.

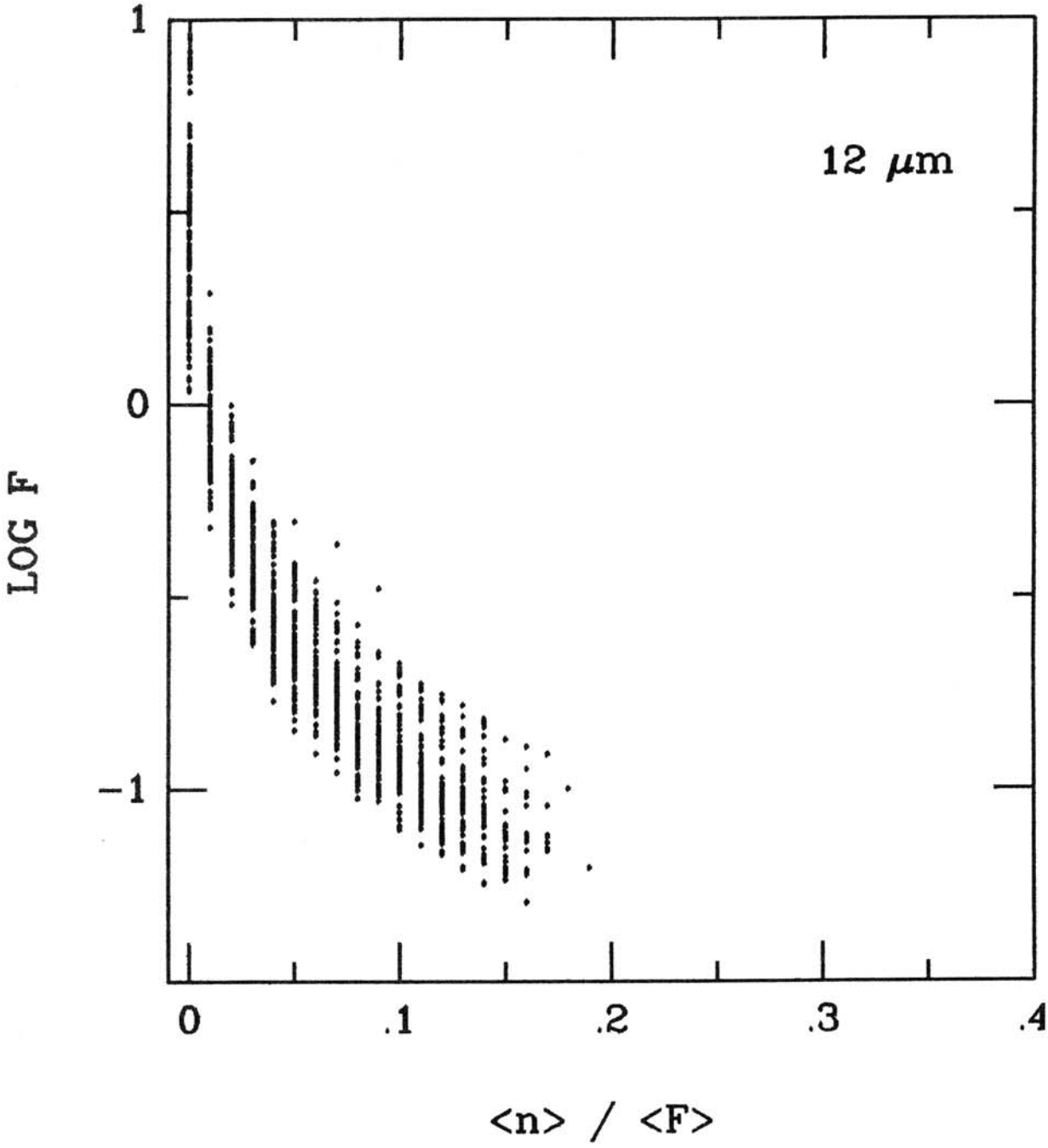

Figure IV.L.1 Flux density versus <n>/F, a measure of median noise divided by the flux density.

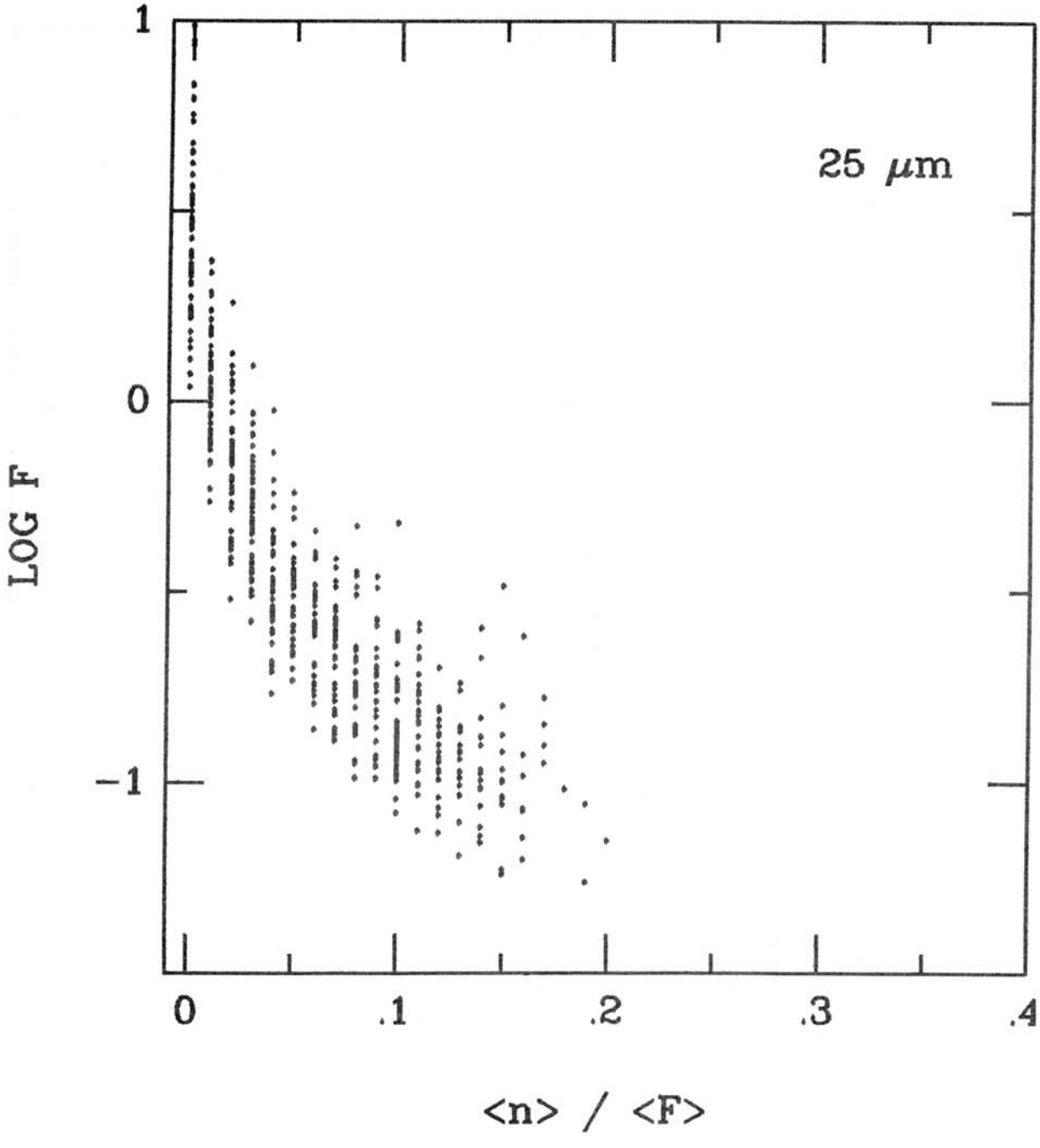

Figure IV.L.2 Flux density versus <n>/F, a measure of median noise divided by the flux density.

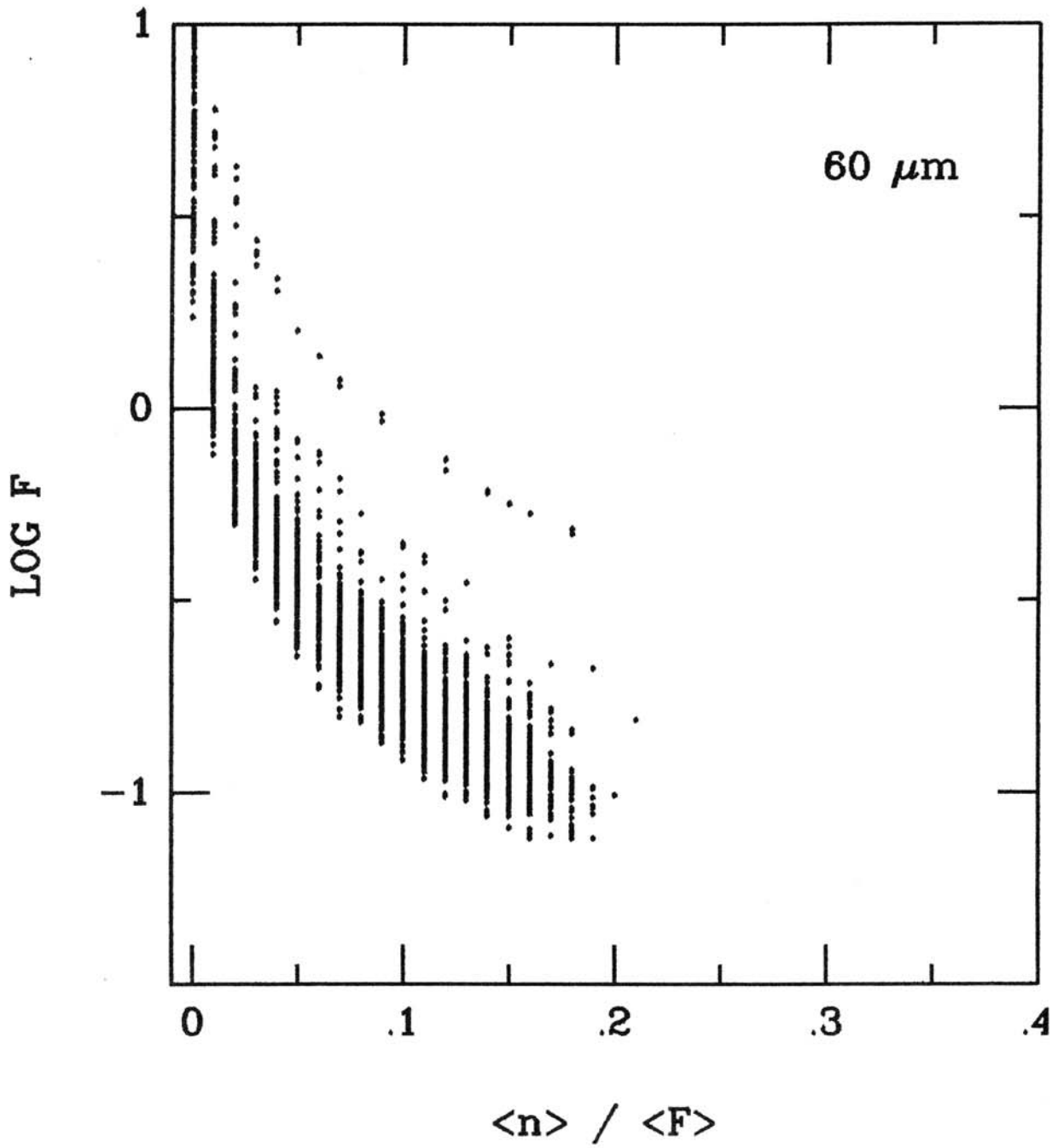

Figure IV.L.3 Flux density versus <n>/F, a measure of median noise divided by the flux density.

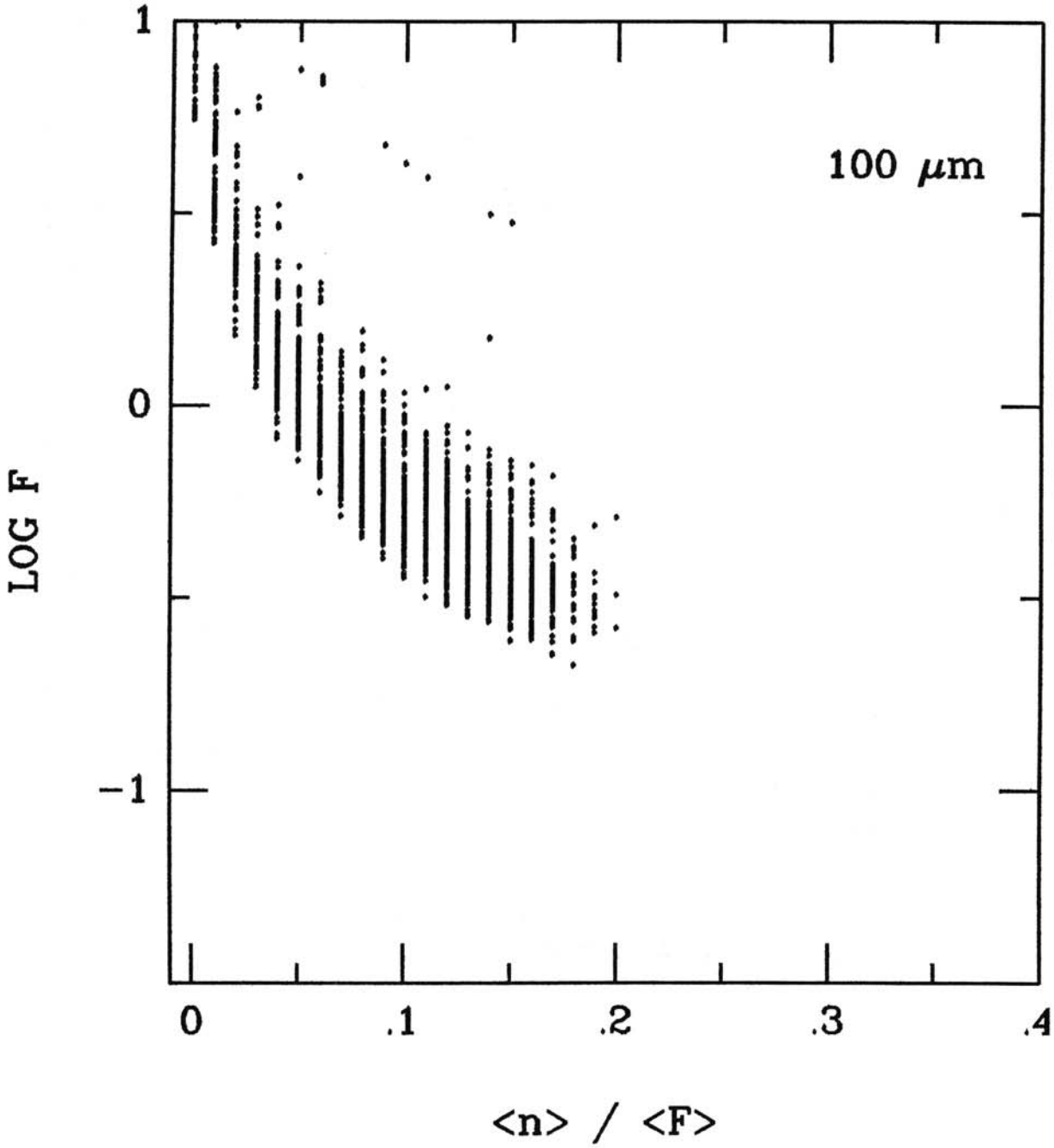

Figure IV.L.4 Flux density versus <n>/F, a measure of median noise divided by the flux density.

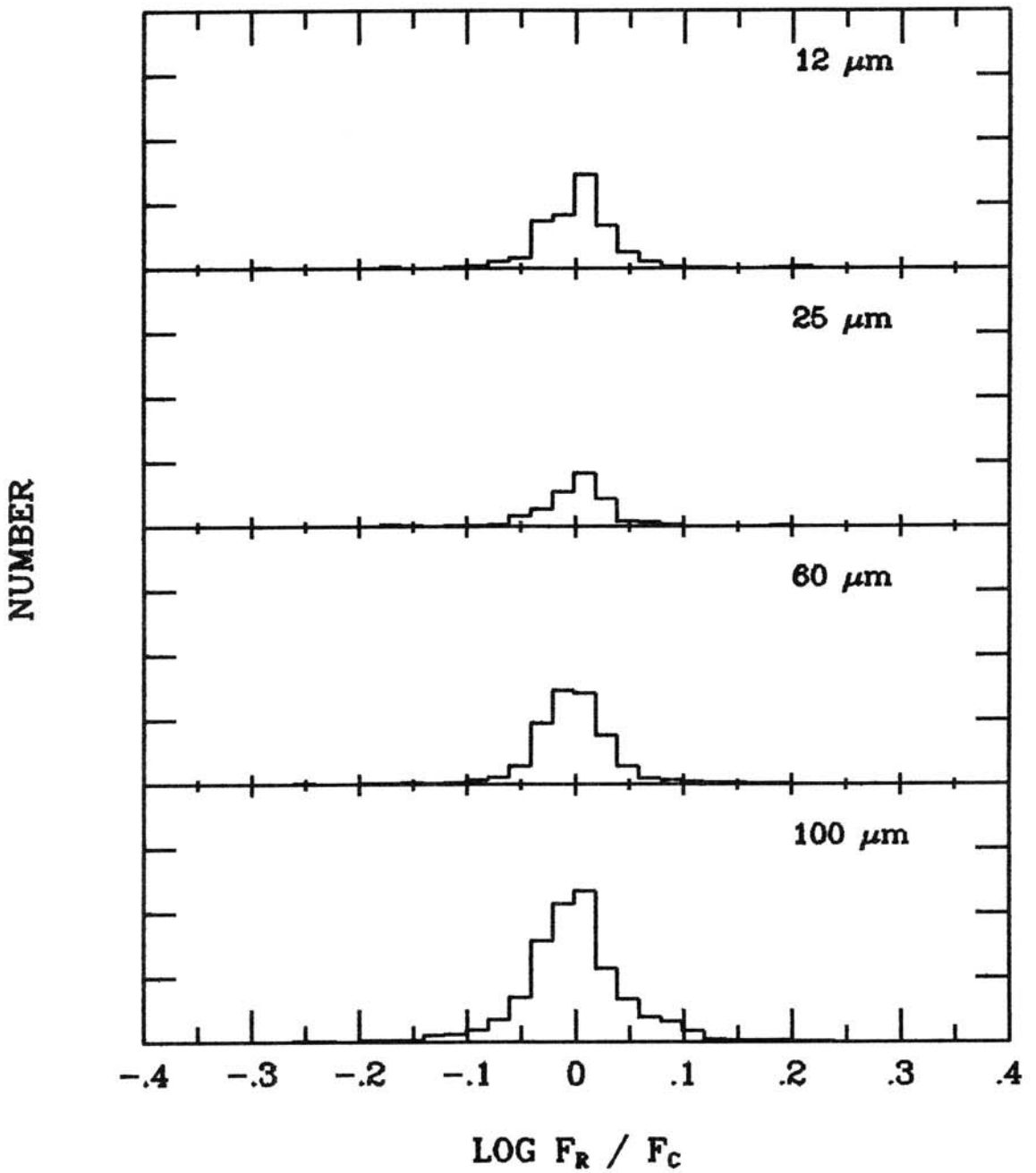

Figure IV.M.1 Number of high latitude subset sources versus the ratio of confirming source to reference source flux densities; high flux density, high latitude subset. 400 sources full scale in each band.

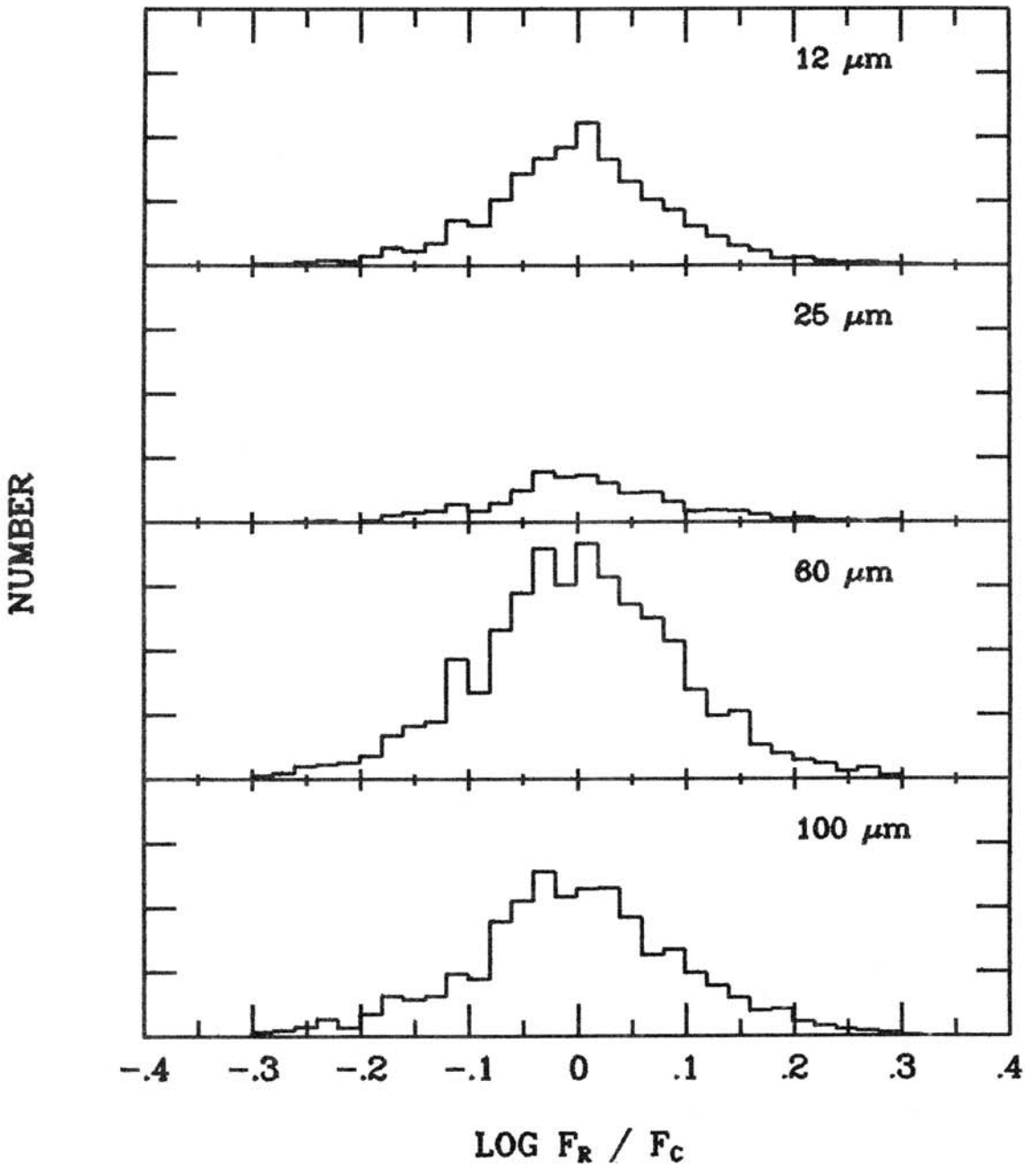

Figure IV.M.2 Number of high latitude subset sources versus the ratio of confirming source to reference source flux densities; low flux density, high latitude subset. 400 sources full scale in each band.

F. General Catalog Statistics

The IRAS SSC contains 43,886 infrared sources. The number of high quality point sources detected in each of the four IRAS bandpasses, and the resultant source densities are summarized in Table IV.F. Mean source densities in each band as a function of galactic latitude are listed in Table IV.G.

Table IV.F. Number of Point Source Detections in Each Band

	Band (μm)			
	12	25	60	100
No. of Sources	17,697	10,895	18,805	13,007
Mean Surface Density	16.0	9.8	17.0	11.7
No. of Merged Sources				43,886

Table IV.G. Distribution of Sources with Galactic Latitude

|b|	Surface Density (No./Degree^2)				Sky Coverage (Degree^2)
	12 μm	25 μm	60 μm	100 μm	
<10°	39.6	25.6	26.8	14.5	255.8
10-30°	10.3	4.9	14.7	12.0	401.4
30-50°	9.2	6.6	14.5	10.5	317.9
>50°	3.8	2.1	10.6	8.4	132.6

For comparison, the PSC contains approximately 0.6 point sources/deg^2 brighter than 0.5 Jy at 12, 25, and 60 μm at high galactic latitudes. At the flux densities greater than the sensitivity limits of the SSC (cf. Section IV.A.3), the Log N vs. Log F relationship determined for the PSC, as reported in the Main IRAS Supplement, predicts that approximately 3, 2, and 6 sources/deg^2 should be observed at 12, 25, and 60 μm, respectively. Some number of excess detections can be understood in terms of the selection biases introduced by targeting of Pointed Observation fields.

The relatively high density of infrared sources found between Galactic latitude 30 deg. and 50 deg. is due primarily to the inclusion of Pointed Observations of the **Large and Small Magellanic Clouds. Source densities in fields centered on the Magellanic Clouds exceed those found in other regions at similar Galactic latitudes** by more than a factor of ten.

A summary of the spectral information contained in the SSC is given in Table IV.H. In a fashion similar to that in the Main IRAS Supplement, this table lists the numbers of sources with moderate to high quality detections in various band combinations. The four-digit row headings specify the band-detection combination, where "1" signifies that a detection is present in a given band and "0" denotes an upper limit. For example, the row labeled "1000" pertains to 12 μm only sources, and "1100" to sources with moderate or high quality detections at 12 and 25 μm. For

comparison, the ratios of the number of various band- detection combinations to the total number of sources are listed for the SSC, and for the PSC.

Table IV.H. Spectral Information Content of the SSC

Combination	Total Number	Percent of Total	
		SSC	PSC
1000	9120	.208	.274
1100	5351	.122	.273
1110	1542	.035	.054
1111	878	.020	.026
0100	2215	.051	.016
0110	789	.018	.015
0111	400	.009	.016
0010	10799	.246	.078
0011	4252	.097	.092
0001	7332	.167	.135
1101	136	.003	.008
1010	557	.013	.005
1011	192	.004	.002
1001	209	.005	.005
0101	114	.003	.002

There are significant differences between the spectral statistics of the SSC and the PSC; one case is the larger percentage of 60 μm only sources in the SSC. This difference can be understood in terms of the relative increase in sensitivity at 60 and 100 μm. The sensitivity of the measurements in the SSC exceeds that in the PSC by nearly a factor of 5 at 60 μm, but only by ~2.5 at 100 μm. If most of the 60 μm sources in the SSC are associated with objects having galaxy-like spectra, which is the case in the PSC, and these objects follow the Log N vs. Log F relationship reported for the PSC, then the SSC should contain roughly a factor of 3 times more 60 μm only sources. Given these rather simple assumptions, the fractional increase in 60 μm only sources agrees well with expectation.

V. THE FORMATS OF THE IRAS SERENDIPITOUS SURVEY CATALOG

A. Introduction

This chapter describes the formats of the IRAS Serendipitous Survey Catalog in its printed and machine-readable forms. A brief description is given of each entry in the catalog; tables describe each column of the catalog in more detail and give, for the machine readable versions, the logical type of each variable and its length in bytes. The catalog consists of three basic parts; a) field headers, b) source listings, and c) redundant fields (a printed list of the redundant fields is also available in Appendix A). The field header includes information on the global properties of each pair of reference/confirming grids. The source listing documents the properties of the individual confirmed sources found in each field. The redundant field listing identifies those grid pairs with more than 5% overlapping coverage on the sky.

Because the Serendipitous Survey fields are non-uniformly distributed on the sky, the catalog has been arranged by fields, with the fields ordered by the right ascension of the field center. The field header is located at the beginning of the source listing for that field. Within a field the sources are also arranged in order of right ascension. The redundant field listing is separate and follows the rest of the catalog. As much as possible, the conventions established for the IRAS/PSC have been adopted for the Serendipitous Survey.

B. The Machine Readable Version

The tape version of the SSC is written with 80-character (ASCII) logical records and blocked with 256 logical records per physical record so that one can regard the tape as a sequence of card images. The entries are arranged so that the source data fit into two records. Association information requires an additional 40 characters per association and appears in subsequent records, two associations per record.

Like other IRAS catalogs, the tape contains a header file containing the date and version number of the data on the Tape (Table V.A)

Table V.A. Format of Header Files

Start Byte	Name	Description	Length
00	Name	Name of IRAS data product	30A1
30	Date	Date of Production	12A1
42	Vers	Version Number	5A1
47	Comment	32 bytes of comment	32A1

Table V.B describes each entry in the tape field header. Each catalog field header entry requires 160 bytes. Those columns that are also included in the printed version of the Serendipitous Survey are marked.

Table V.C describes each entry in the catalog tape source listing. Each catalog source entry requires 160 + NID * 40 bytes where NID is the number of catalog associations, including the IRAS/PSC, for each source. In the tables, the Column "format" refers to the length and type of the (FORTRAN) character field used to read or write each entry.

Table V.B. Format of Field Headers[1] (SSC Tape Version)

Start Byte	Name	Description	Units	Format
00	FNAME[2]	Field Name		13A1
13	RGRID[2]	Reference Grid No.		I5
18	RDATE[2]	Obs. Date, Ref. Grid	Days JD 2445000 +	I3
21	CGRID[2]	Confirming Grid No.		I5
26	CDATE[2]	Obs. Date, Conf. Grid	Days JD 2445000 +	I3
29	MACRO[2]	Macro Type		1A1
30	GLON[2]	Galactic Longitude	Degree	I3
33	GLAT[2]	Galactic Latitude	Degree	I3
36	PDRAS	Sign of R.A. Difference Between Grid centers	+/-	1A1
37	PDRA	Amplitude of R.A. Difference Between Grid Centers	Arcsec	I3
40	PDDECS	Sign of Dec. Difference Between Grid Centers	+/-	1A1
41	PDDEC	Amplitude of Dec. Difference Between Grid Centers	Arcsec	I3
44	RANGLE	Reference Grid Scan Direction (E of N)	Degree	I4
48	CANGLE	Confirming Grid Scan Direction (E of N)	Degree	I4
52	EFFAREA[2]	100x Effective Area of Grid Overlap	Degree^2	I3
55	RUNDF[2]	No. of Fields with Overlap > 5%	NN	I2
57	SPARES	23 spare bytes		23A1
-----	-----	-------New Record-------	-----	
80	RNOISE	Median Noise of Ref. Grid (1 value per band)	mJy	4I5
100	CNOISE	Median Noise of Conf. Grid (1 value per band)	mJy	4I5
120	NSOURC	Number of Confirmed Sources (1 value per band)	NNN	4I3
132	NCONF[2]	Number of Confused Confirmations (1 value per band)	NNN	4I3
144	CIRRUS[2]	Number of 100 μm only Confirmed Sources	NN	I3
147	NMERGE	Number of Merged Sources	NNN	I3
150	SPARES	10 spare bytes		10A1

NOTES:

[1] Fields are listed in order of increasing Right Ascension of the Reference Grid center. Field header records are located at the beginning of the source listing for each field.

[2] This quantity is listed in the printed version of the catalog.

The following is a brief description of the individual entries in the Field Headers of the tape version of the SSC.

Field Name: FNAME
The IRAS/SSC field name is the position of the center of the reference grid, given in the form hhmmssSddmmss.

Grid Number: RGRID, CGRID
The identifying number (see Section III.A) for the reference (R) and confirming (C) grids for the field. The reference grid has the lower 60 μm median noise.

Observation Date: RDATE, CDATE
The observation dates for the reference (R) and confirming (C) grids in Julian Days -2445000.

Macro Type: MACRO
The macro identifying code is given in Table II.1.

Galactic Coordinates: GLON, GLAT
Galactic coordinates rounded to nearest degree

Position Differences: PDRAS, PDRA, PDDECS, PDDEC
The sign and magnitude of the position difference between reference and confirming grid centers, in the sense of (confirming - reference), in right ascension and declination.

Grid Orientation: RANGLE, CANGLE
The orientation of the in-scan direction of the reference and confirming grids on the sky, measured in degrees East of North.

Effective area: EFFAREA
The effective area of the sky covered by both the reference and confirming grids.

Redundant Fields: RUNDF
The number of additional grid pairs in the Serendipitous Survey, i.e. with different OBSID's, which overlap this field by more than 5%.

Grid Noise: RNOISE, CNOISE
The median noise of the reference and confirming grids.

Confirmed Sources: NSOURC
The number of confirmed sources in this field, in the 12, 25, 60 and 100 μm bands, respectively.

Confused Sources: NCONF
The number of confused confirmations in this field, in the 12, 25, 60 and 100 μm bands, respectively.

100 μm Only Sources: CIRRUS
The number of 100 μm confirmed sources in the field that are not band merged. The density of such sources is taken to be a measure of the infrared "cirrus" in the field.

Band-Merged Sources: NMERGE
The number of band-merged sources in the field, i.e., the number of source records following the field header.

Table V.C. Format of Source Listings[1] (SSC Tape Version)

Start Byte	Name	Description	Units	Format
00	NAME[2]	Source Name		11A1
11	HOUR	Right Ascension 1950	Hours	I2
13	MINUTE	Right Ascension 1950	Minutes	I2
15	SECOND	Right Ascension 1950	Deci-seconds	I3
18	DSIGN	Declination Sign	+/-	1A1
19	DECDEG	Declination 1950	Degree	I2
21	DECMIN	Declination 1950	Arcmin	I2
23	DECSEC	Declination 1950	Arcsec	I2
25	SPARE	1 spare byte		1A1
26	ANGLE	Position Angle of Source Error Box		I3
29	SPARE	1 spare byte		1A1
30	FLUX[2]	Averaged Non-color Corrected Flux Densities (1 value per band)	Jansky (10^{-26} W/m^2/Hz)	4E9.3
66	FQUAL[2]	Flux Density Quality (1 value per band)		4I1
70	RGRID	Reference Grid Number		I5
76	SPARE	9 spare bytes		9A1
	-----	-------New Record-------	-----	
80	RELUNC[2]	Percent Relative Flux Density Uncertainties (1 value per band)		4I3
92	TLSNR	10x Local Signal-to-Noise Ratio (1 value per band)		4I4
108	CC[2]	Point Source Correlation Coefficient (1 value per band)		4A1
112	TRFLUX	10x F_c/F_r		4I2
120	POSDRS12	Right Ascension Delta Sign	+/-	1A1
121	POSDR12	Right Ascension Delta	Arcsec	I3
124	POSDDS12	Declination Delta Sign	+/-	1A1
125	POSDD12	Declination Delta	Arcsec	I3
128		Repeat for 25 μm Band	+/-	1A1
-135			Arcsec	I3
136		Repeat for 60 μm Band	+/-	1A1
-143			Arcsec	I3
144		Repeat for 100 μm Band	+/-	1A1
-151			Arcsec	I3
152	PNEARC[2]	Number of Sources in Confusion Window (1 value per band)		4I1 I2
156	NID[2]	Number of Positional Associations		I2
158	IDTYPE[2]	Type of Object		I1

159	SPARE	1 spare bytes		1A1
	-----	-------New Record-------	-----	
160	CATNO	Catalog Number[4]		I2
162	SOURCE	Source ID		15A1
177	IDTYPE	Source Type/Spectral Class[5]		5A1
182	RADIUS	Radius Vector from SSC Position to Association	Arcsec	I3
185	POS	Position Angle from SSC Position to Association (E of N)	Degree	I3
188	FIELD1	Object Field #1	Catalog Dependent[6]	I4
192	FIELD2	Object Field #2	Catalog Dependent[7]	I4
196	FIELD3	Object Field #3	Catalog Dependent[8]	I4
200 -240		Continuation of Associations in Blocks of 40 Bytes etc.		
	.			
	.			
	.			

NOTES:

[1] Sources are listed in order of increasing Right Ascension within each field.

[2] This quantity is listed in the printed version of the SSC.

[3] For associations with the IRAS/PSC, this value is 41.

[4] For associations with the IRAS/PSC, this value is 3.

[5] For associations with the IRAS/PSC, this field is left blank.

[6] For associations with the IRAS/PSC, this value is a flag indicating the bands in which the source was detected with medium or high quality; it is encoded as indicated in the PSC Supplement Table X.B.2.

[7] For associations with the IRAS/PSC, this value is the PSC 2.0 Flux Density in the shortest (first) wavelength band in which it was detected. Flux Densities higher than 10 Jy are encoded 9999.

[8] For associations with the IRAS/PSC, this value is the PSC 2.0 Flux Density in the second wavelength band in which it was detected. Flux Densities higher than 10 Jy are encoded 9999.

The following is a brief description of the individual entries in the Source Listings of the tape version of the SSC.

Source Name: NAME, APPNAME
The IRAS/SSC source name is constructed as for IRAS/PSC sources and is derived from its position by combining the hours, minutes and tenths of minutes of right ascension and the sign, degrees and minutes of the declination. In obtaining the minutes of right ascension and declination for the name, the positions were truncated. If sources within a field have duplicate positional names, they are distinguished by an appended letter (APPNAME), starting with the letter A.

Position: (HOUR,MINUTE,SECOND,DSIGN,DECDEG,DECMIN,DECSEC)
Positions are, as in the IRAS/PSC, given for the equinox 1950.0 and epoch 1983.5. Hours (HOUR) and minutes (MINUTE) of right ascension are given as integers while seconds (SECOND) are rounded to integer deciseconds. The declination is given as a character sign (DSIGN) followed by integer values of degrees (DECDEG), minutes (DECMIN) and seconds (DECSEC).

Position Angle: ANGLE
The position angle of the major axis of the SSC source error box expressed in degrees East of North.

Flux Density: FLUX(4)
Each of the four wavelengths has a NON-COLOR-CORRECTED flux density in units of Janskys, (1 Jy = 10^{-26} W $m^{-2}Hz^{-1}$). The quoted value is the noise weighted average as defined in Section III.C.2.

Flux Quality: FQUAL(4)
Each flux density measurement is designated high quality, moderate quality or upper limit (FQUAL = 3, 2, or 1, respectively) based on the prescription discussed in Section III.C.

Flux Density Uncertainty: RELUNC(4), TLSNR(4)
Each flux density measurement other than an upper limit has an associated uncertainty expressed in two ways; RELUNC is the uncertainty expressed as a 1 sigma value in units of 100x<n>/<F> (see Section III.C.2). TLSNR is ten times the local signal to noise ratio (see Section II.C) as determined from the reference or confirming grid, whichever is least.

Point Source Correlation Coefficient: CC(4)
As discussed in Section III.B, SSC sources can have point source correlation coefficients between 70-100%. These are encoded as alphabetic characters with A=100, B=99.....Z=75-70, one value per band. The quoted correlation coefficients come from the reference or confirming grids, whichever is higher, for high quality sources.

Flux Density Ratio: TRFLUX(4)
As discussed in Section III.B, SSC sources can have flux density

ratios $0.5 < F_{(c)}/F_{(r)} < 2.0$. TRFLUX is the flux density ratio for high quality sources expressed as $10 \times F_c/F_r$.

Position differences: POSDRS12, POSDR12, POSDDS12, POSDD12.....
The quoted positions of SSC sources are determined from a weighted average of the positions of the confirmed sources in each band with a high quality flux density(see Section III.C.1). POSDRS12, POSDR12, POSDDS12 and POSDD12 give the sign and amplitude (in arcsec), of the difference in right ascension and declination respectively, between the final band-merged position and the 12 μm confirmed source position. The following 12 entries repeat the above format for 25, 60 and 100 μm confirmed source components.

Confusion: PNEARC(4)
In regions of high source density, the Pointed Observation source extraction process, as well as the Serendipitous Survey Confirmation and Band Merging processing, can result in degraded positions and incorrectly band merged sources. PNEARC is 1-(number of confirmed sources in the confusion and band merge window)(See Section III.D) Any value greater than zero is indicative of potential confusion in the processing and the resulting source information should be examined carefully, e.g. by inspection of the grids in question.

Positional Associations: NID, IDTYPE, CATNO, SOURCE, TYPE, RADIUS, POS, FIELD 1-3
The positional associations formats and definitions are done as per the IRAS/PSC (Chapter X, Supplement), with the exceptions noted in Section III.F.

Table V.D Format of Overlapping Fields File (SSC Tape Version)

Start Byte	Name	Description	Units	Format
00	GRID0	Prime Ref. Grid		I5
05	SPARE	1 spare byte		1A1
06	GRID1	Overlapping Field #1, Ref. Grid		I5
11	SPARE	1 spare byte		1A1
12	AOVLP1	Overlapping Sky Coverage	Arcmin^2	I4
16-26		Repeat of 5-15 for Overlapping Field # 2		
27-37		Repeat of 5-15 for Overlapping Field # 3		
.				
.				
60-70		Repeat of 5-15 for Overlapping Field # 5		
71-79	SPARE	9 spare bytes		9A1
	-----	-------New Record-------	-----	
80-85	SPARE	6 spare bytes		6A1
86-96		Repeat of 5-15 for Overlapping Field # 6		
.				
.				

The quantities in the Overlapping Fields List are as follows:

Prime Reference Grid: GRID0
The grid against which other reference grids are checked for overlapping sky coverage.

First Overlapping Grid: GRID1
The number of the first reference grid with more than 5% overlap with GRID0.

Overlap Area: AOVLP1
Area of overlapping sky coverage between GRID0 and GRID1 in square arcminutes.

The format is repeated for each additional grid overlapping with GRID0. If more than 5 grids overlap with GRID0, they are listed in succeeding records, as necessary; the first six bytes of each of these additional records begins with a string of 6 spaces.

C. The Printed Version of the IRAS/SSC

The printed version of the IRAS/SSC is organized in the same fashion as the machine readable version, with the catalog sources listed in order of increasing right ascension within a given field and with the fields listed in order of increasing right ascension of the field center. Both the field header and the source listings of the printed version contain subsets of the information found in the machine readable version.

Table V.E. Format of Field Headers (SSC Printed Version)

Column	Title	Format	Machine-Readable Quantity
1-13	FIELD NAME	HHMMSS±DDMMSS	FNAME
14	Space		
15-20	LLL±BB	NNN±NN	GLON,GLAT
21-29	MN(12)	NNNNN.NNN	RNOISE(12)[1]
30-39	MN(25)	NNNNN.NNN	RNOISE(25)[1]
40-49	MN(60)	NNNNN.NNN	RNOISE(60)[1]
50-59	MN(100)	NNNNN.NNN	RNOISE(100)[1]
60	Space		
61-64	POS	±NNN	RANGLE
65	Space		
66-68	N12	NNN	NSOURC(12)
69-71	N25	NNN	NSOURC(25)
72-74	N60	NNN	NSOURC(60)
75-77	N100	NNN	NSOURC(100)
78	Space		
79-80	C	NN	CIRRUS
81	Space		
82-92	GRIDS	NNNNN NNNNN	RGRID CGRID
93	Space		
94-100	OBS-DATES	NNN NNN	RDATE CDATE

101	Space		
102	M	A	MACRO
103	Space		
104-106	AR	NNN	EFFAREA
107	Space		
108-110	OVP	NN	RUNDF

NOTES:

[1] The median noise listed is $1/(1/n_r^2 + 1/n_c^2)^{0.5}$ where n_r and n_c are the median noise levels of the reference and confirming grids, respectively.

Table V.F. Format of Source Listings (SSC Printed Version)

Column	Title	Format	Machine-Readable Quantity
1-11	SRC NAME	HHMMM-DDMMA	NAME
12	Space		
13-16	S	SS.S	SECOND[1]
17	Space		
18-19	D	SS	DECSEC
20-21	Spaces		
21-30	FLUX(JY)12	FFFFF.FFFL	FLUX(12)[2]
31-40	25	FFFFF.FFFL	FLUX(25)[2]
41-50	60	FFFFF.FFFL	FLUX(60)[2]
51-60	100	FFFFF.FFFL	FLUX(100)[2]
61	Space		
62-65	CC	AAAA	CC(12),CC(25),CC(60),CC(100)
66	Space		
67-68	R12	NNN	TRFLUX(12)
69	Space		
70-71	R25	NNN	TRFLUX(25)
72	Space		
73-74	R60	NNN	TRFLUX(60)
75	Space		
76-77	R100	NNN	TRFLUX(100)
78-79	Spaces		
80-83	CONF	NNNN	PNEARC(12),PNEARC(25) PNEARC(60),PNEARC(100)
84	Space		
85-86	PSC	NN	FIELD1[3]
87	Space		
88-89	NID	NNN	NID
90	Space		
91-92	C#	NN	CATNO
93	Space		
94-113	NAME & TYPE		SOURCE, IDTYPE[4]
114-116	RAD	NNN	RADIUS

NOTES:

[1] Right Ascension decimal seconds of time.

[2] Flux densities are given in units of 1 Jy. Moderate quality flux densities are indicated with a colon(:) and upper limits are indicated with the letter L.

[3] The flag indicating the wavelength bands in which the IRAS/PSC lists a high or moderate quality flux density, encoded as in the PSC Supplement, Table X.B.2.

[4] Formatted as in the IRAS/PSC (PSC Supplement Section X.B).

An erroneous 6-digit value of the CIRRUS indicator "C" was printed in the headers of 11 fields in the SSC Printed Version *only*. The subsequent entries in the field headers are correct, but are offset 5 columns to the right. Below is a list of the Printed Version fields in which this occurred, along with the reference grid number of the field and the proper value of the CIRRUS indicator.

Table V.G. Fields With Incorrect CIRRUS Counts

Field Name	RGRID	C
053226-051906	1222	3
053828-020030	10951	1
102225-572609	6693	1
104148-591213	7082	3
104326-591832	5973	5
130916-621123	8850	3
163716-475203	10392	3
173114-323259	11387	3
180035-242137	12149	1
184238-031728	2450	2
203735+421259	3239	2

VI. ADDITIONAL CONSIDERATIONS

A. High Source Density Considerations

A significant fraction of the fields included in the SSC are in regions of high source density. In particular, the fields near the plane of the galaxy, in the Large and Small Magellanic Clouds, and in large molecular clouds all suffer from the effects of source confusion. These fields are included in the SSC because the large majority of the sources at 12 and 25 um are genuine, even in grids of very high density. THE USER IS CAUTIONED, HOWEVER, THAT THE LEVELS OF RELIABILITY, SENSITIVITY AND ACCURACY THAT APPLY TO LOW SOURCE DENSITY REGIONS ARE NOT SATISFIED IN THESE FIELDS. At the longer wavelengths, the observations are generally so heavily confused that only the brightest sources have any validity. This section documents a number of the known anomalies that can occur in high source density regions.

The FLUX filtering was designed to provide the highest sensitivity for the detection of weak point sources. As illustrated in the simulation shown in Section II.D, the large negative sidelobes complicate the effects of confusion. Additionally, the FLUX filter passes all spatial components of the background at the point source frequency. In regions of high, complicated backgrounds, "sources" may be present that are only point-like modulations of the extended background. These effects are particularly noticeable at 60 and 100 μm in molecular clouds and at 100 μm over large parts of the sky influenced by infrared cirrus. Figure VI.A shows the FLUX filtered 60 μm map of a region of complicated background. Many of the 60 μm "sources" are, in fact, components of infrared cirrus.

Figure VI.B is a portion of the 12 μm FLUX filtered map for Grid 12871. This grid is representative of the highest 12 μm source density in the SSC.

If sources are partially overlapping, they may appear as only a single entry in the SSC. Although the source extractor uses an algorithm to separate regions, it is reliable only in the simplest cases. The quoted position from the source extractor is a flux weighted centroid of all contiguous pixels above threshold. Therefore, the error in position will depend on the ratio of fluxes from the two sources. If one source is significantly brighter than the other, the quoted position will be close to the position of the brighter source, and the weaker source will be lost. This effect is shown in example "A" of Figure VI.B. If the sources are of roughly the same flux, the quoted position will not be correct for either source, as shown in example "B". Because of the shape of the IRAS beam, the source overlap problem is most severe in the cross scan direction.

The loss of photometric accuracy in crowded fields is illustrated in example "C", shown in Figure VI.B. Here the negative sidelobe of source "A" has reduced the flux density of the nearby source.

B. Asteroids

The confirmation strategy used in the SSC required that each source be observed on two separate occasions. Unlike the Point Source Catalog, which used confirming observations separated by weeks or even months, the SSC has no explicit requirements for the time interval between confirming observations. For many pointed observations, the confirming observation was scheduled for the next orbit, giving a time delay of only 103 minutes. While effective for discriminating against dust particles and earth satellites, many asteroids may appear fixed at the IRAS resolution. The observation times for the reference and confirming grid are given

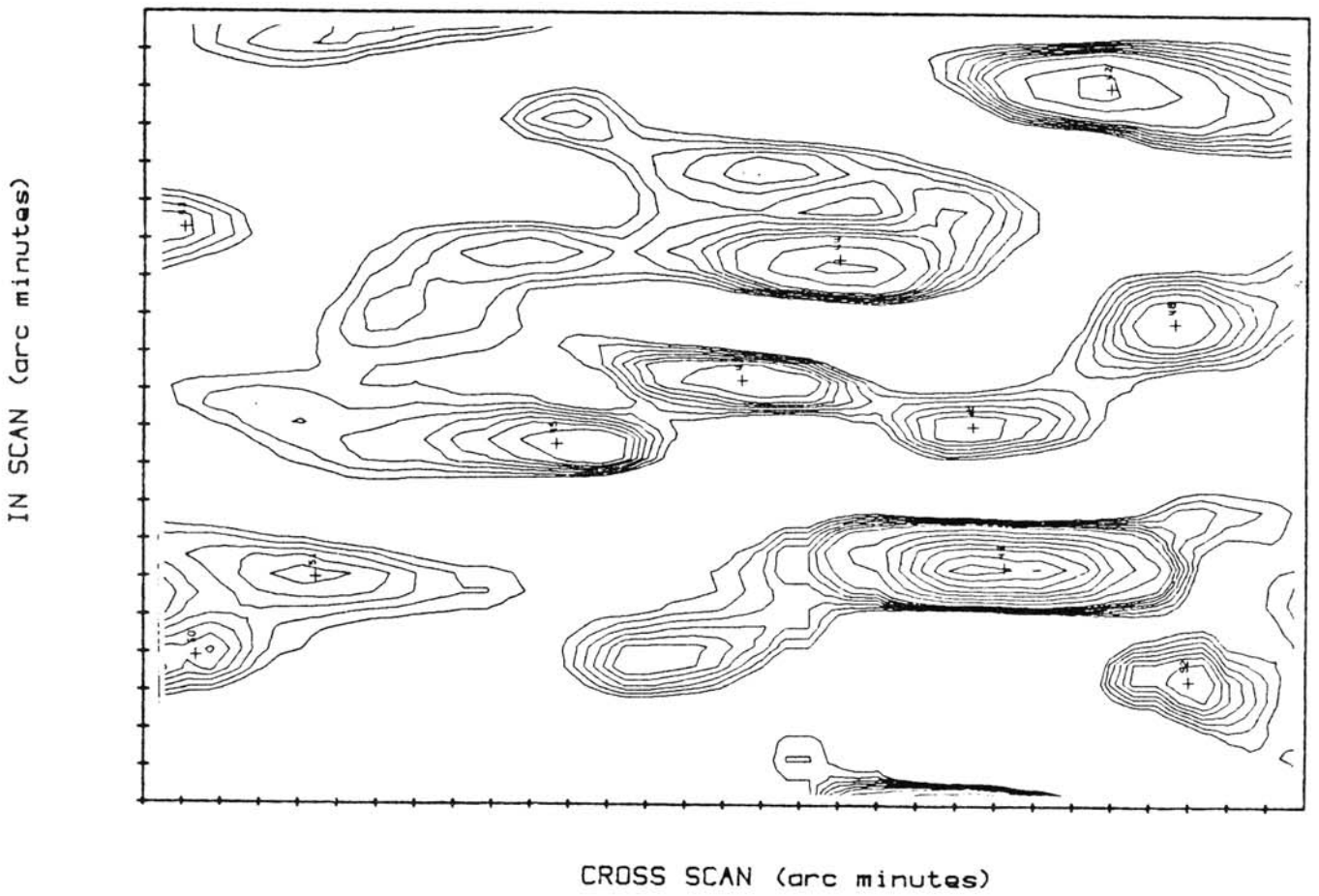

Figure VI.A FLUX filtered map at 60 μm of a molecular cloud region. Many "sources" are actually modulations in the extended background at the point source spatial frequency.

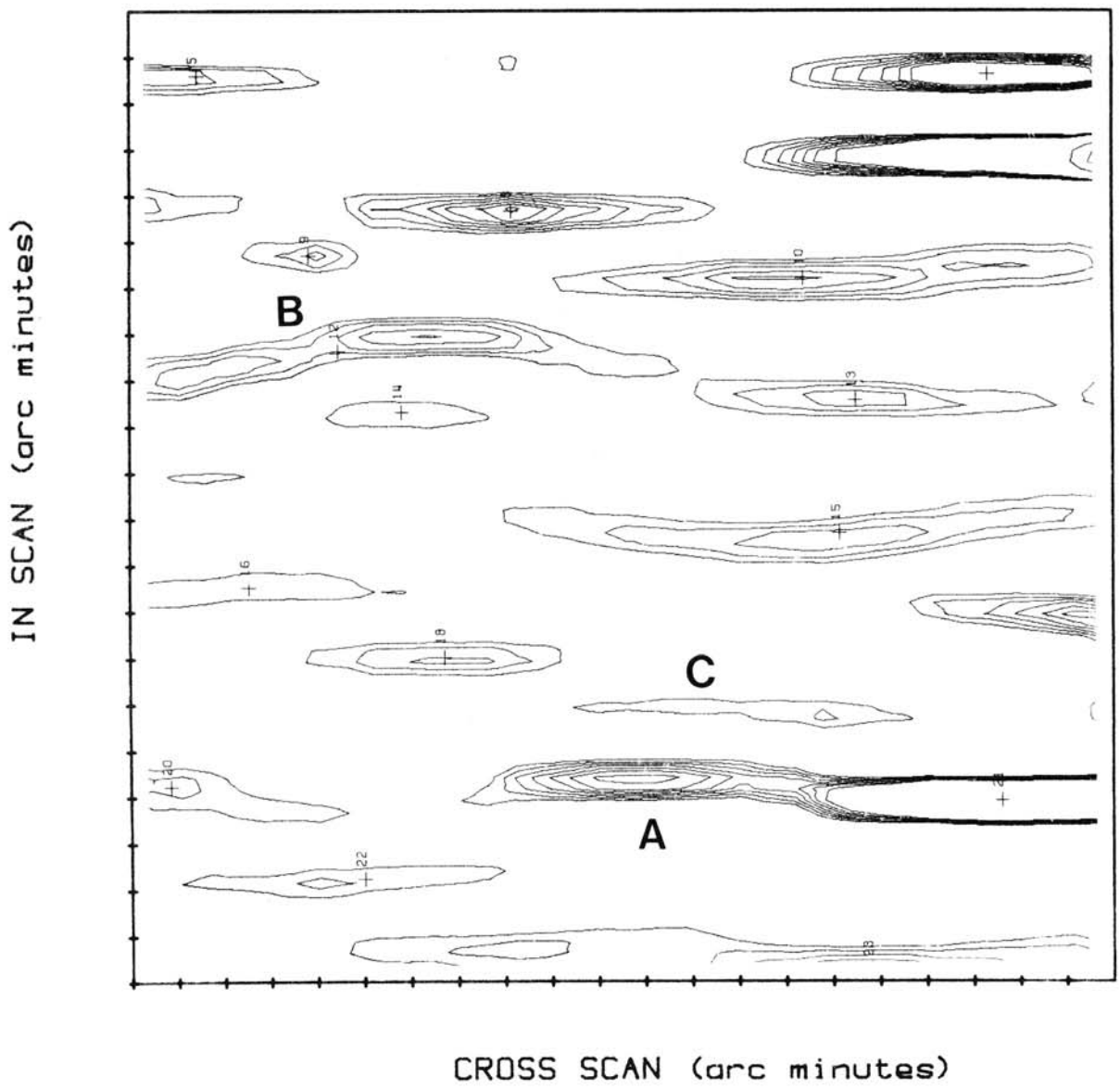

Figure VI.B FLUX filtered map at 12 μm of a high source density region. "A" indicates a missed source not separated from a nearby brighter source. "B" indicates a single source listed at a position between two partially overlapping sources. "C" indicates a source whose flux is reduced by the negative sidelobe of source "A".

in the field header and may be used to judge the validity of a given source, particularly those within 5 degrees of the ecliptic plane. Typical catalog flux densities (i.e. not color corrected) of a 200 K asteroid, normalized to the peak at 25 μm, are 0.3, 1.0, 0.6, and 0.25 at 12, 25, 60, and 100 μm, respectively. Refer to Matson (1986) for a discussion of asteroids detected in the IRAS survey mode.

C. Redundant Sources

The SSC is ordered on a field by field basis to maintain the organization of the Pointed Observation program. In regions covered by more than one SSC field, sources in the overlapping areas are included in both fields. Generally, these redundant sources have slightly different positions and flux densities but may, in a few cases, have identical names. It is recommended that the reference grid number be used as an additional identifier for these redundant sources. Location of areas where redundant sources occur is facilitated by the compilation of overlapping fields in Appendix A.

REFERENCES

Beichman, C. A., et al. "IRAS Catalog & Atlases Explanatory Supplement." 1984, Washington, D.C.: U. S. Government Printing Office.

Dressel, L. L. and Condon, J. J. 1976, Ap. J. Suppl., **31**, 187.

Hacking, P. and Houck, J. 1986, "*Very Deep IRAS Survey at* $l^{II} = 97°$, $b^{II} = +30°$" to appear in Proceedings of Star Formation in Galaxies Conference.

IRAS Circular (Nov. 6, 1986).

Low, F. J., et al. 1984, Ap. J. (Lett.), **278**, L19.

Matson, D. L. 1986, JPL D-3698, "IRAS Asteroid and Comet Survey" 1986, Pasadena, CA: Jet Propulsion Laboratory.

Young, E. T., et al. 1985, JPL PRE-008 "User's Guide to IRAS Pointed Observations."

ACKNOWLEDGEMENTS

This catalog was produced and supported by the NASA IRAS Extended Mission at the Infrared Processing and Analysis Center, by the Jet Propulsion Laboratory of the California Institute of Technology and by the National Science Foundation through the National Optical Astronomy Observatories operated by the Association of Universities for Research in Astronomy, Inc.. We extend our thanks to members of the IPAC staff who provided both support and technical assistance: Gael Squibb, Tom Soifer and Chas Beichman skillfully administered this support.

The Pointed Observations used in the SSC were reduced at IPAC by Gene Kopan and co-workers and formed the fundamental data base. The source extractions, also carried out at IPAC, were the contribution of Dave Gregorich and again were a basic step in the production of the SSC. Iffat Khan contributed to the catalog association processing. In addition to the scientific advice of the U. S. Science Team as a whole, we acknowledge the following individual members who made direct contributions to this work: Chas Beichman, Tom Chester, and Gerry Neugebauer.

The National Optical Astronomy Observatories generously provided support, including extensive use of their computing facilities throughout this project, making it possible for the work to be carried out in Tucson. The University of Arizona Steward Observatory also provided support and facilities. Tom Green, a Steward Observatory graduate student, deserves special thanks for his contributions to the analysis of the catalog. Special thanks also go to Pat Lambotte and Patsy Van Buren, who contributed generously to the typing and editing of this manuscript.

Most of the figures were generated using the program MONGO, developed by John L. Tonry.

APPENDIX A: OVERLAPPING FIELD TABLE

GRID0	GRID1	OVLP	GRID2	OVLP	GRID3	OVLP	GRID4	OVLP	GRID5	OVLP	GRID6	OVLP
17	2591	792	290	2447								
58	72	846	3076	783	925	1599	98	665	914	1286	112	1874
	927	296	409	912	663	670						
65	9428	1011										
72	3076	788	925	852	98	2014	914	472	112	836	325	871
	58	786	95	792	927	1614						
90	12205	619	92	723	11906	1067	814	245				
92	95	723	90	784	12205	1303	3076	280	325	169	11906	1104
	814	1492										
95	72	731	12205	1102	3076	781	98	691	325	1545	92	784
	927	1357	11906	227	814	1012						
98	914	180	112	983	325	1213	925	523	3076	794	12205	398
	72	2034	58	620	95	738	927	1576				
112	914	1107	98	1050	925	1769	3076	795	72	879	58	1839
	927	553										
121	164	765	8292	931	8223	1249	8693	1391	6744	1568	6579	879
	8274	998	8236	705								
135	5074	328										
137	5074	1838										
141	5074	398										
147	206	400										
153	206	464										
155	169	832	208	781	275	304	303	1766	10708	955	6948	1727
	6579	379	6650	1220	8464	978	230	2422	216	1584		
164	169	765	121	832	10631	1039	6744	1253	6579	1444	6650	887
	8274	758	8236	293								
167	365	388	225	457								
169	164	832	155	765	10708	923	10631	833	6948	719	6744	301
	6579	1232	6650	1444	8464	887	230	641				
177	495	485										
195	314	440	9693	937								
206	147	461	153	402								
208	155	847	275	2273	303	1819	6948	1298	6650	404	230	857
	216	1280										
216	230	1904	8464	609	6650	991	6579	163	6948	1615	10708	565
	303	2005	275	850	208	1246	155	1651				
225	167	519	359	357								
230	8464	961	6650	1214	6579	395	6948	1651	10708	920	303	1708
	275	338	208	808	155	2459	169	702	216	1829		
260	8123	397										
262	10580	1273										
275	208	2358	155	365	303	1336	6948	1027	6650	218	230	393
	216	889										
283	7700	1237										
290	17	2461	2591	832								
303	275	1264	208	1741	155	1845	10708	435	6948	1637	6650	872
	8464	479	230	1745	216	2028						
314	195	485										

GRIDO	GRID1	OVLP	GRID2	OVLP	GRID3	OVLP	GRID4	OVLP	GRID5	OVLP	GRID6	OVLP
325	98	1148	3076	470	12205	1013	72	821	95	1570	92	211
	927	941	814	626								
359	225	418										
365	167	329										
388	7002	1304										
409	691	149	871	755	618	207	58	956	925	150	914	283
	663	2314										
482	8895	2478	9235	2782								
495	177	485	11701	532								
543	9144	1753	8550	1990								
548	6501	1162										
580	1925	1078	12804	895	9714	475	9092	381	3420	801	601	926
589	1979	353	3798	769								
601	580	974	1925	752	12804	151	3420	805				
618	871	2194	691	1592	409	235	663	328				
636	1626	991	1835	1626	12822	271	2433	535				
641	857	2281	1277	1798	832	2116	766	2027	1316	1296	776	904
648	744	1819										
654	1512	1608	674	2065	680	438						
663	409	2319	871	899	618	284	58	713				
674	1512	1649	654	2146	680	663						
680	674	676	1512	876	654	461	851	270	1456	1315	15458	298
	3589	792	3607	791	3577	796	3617	769				
691	871	1013	618	1658	409	178						
700	3607	805	3589	806	1489	1714	866	2023	3577	809	3617	803
	2952	747										
744	648	1898										
763	10956	382										
766	641	2049	857	1644	1277	1312	832	1436	2454	1083	2543	1039
	1316	925	776	1066	1626	151						
774	10848	199										
776	1316	530	766	1112	641	964	857	553	1277	358	832	436
	2454	1088	1626	875								
781	2916	341	847	1353								
814	11906	671	92	1516	95	985	90	274	12205	1633	3076	154
	325	601										
826	2009	374	1586	1060	2952	919						
832	1277	2191	857	2529	641	2067	766	1373	1316	1451	776	389
847	781	1362										
851	2433	230	1494	1851	14223	709	2749	809	2756	1006	15450	1016
	680	233	1456	331	15458	1008	3589	422				
855	859	379										
857	1277	2267	832	2613	641	2237	766	1579	1316	1456	776	500
859	855	346										
866	1489	1729	700	2056	3607	827	3589	829	3577	835	3617	828
	2952	489										
871	618	2128	691	955	409	785	663	933				
891	2567	328										
899	902	1096										
902	899	1045										
914	112	1146	98	206	925	1748	3076	1076	72	487	58	1294
	409	257										
925	98	566	914	1691	112	1801	3076	951	72	880	58	1583

GRIDO	GRID1	OVLP	GRID2	OVLP	GRID3	OVLP	GRID4	OVLP	GRID5	OVLP	GRID6	OVLP
927	95	1407	58	266	72	1582	3076	952	98	1571	112	529
	325	996										
930	6306	824										
939	1027	2737										
957	2343	2045										
969	1285	1907										
979	1432	1367										
983	995	465	1000	384								
995	983	413										
1000	983	437										
1024	1339	2459	1061	807								
1027	939	2737										
1033	1283	2306										
1061	1024	827	1339	951	2543	1334	2454	1062	3420	931		
1067	10951	1229	12167	632								
1073	11547	991	11718	839								
1136	2081	1882	3571	941								
1183	7603	1009	8860	1317	8876	1343	14239	1259				
1187	12454	1629										
1197	9615	1029										
1204	13358	1253										
1257	1679	2510	11241	316								
1268	11816	530										
1277	832	2212	857	2252	641	1770	766	1256	1316	1640	776	323
	1835	250										
1283	1033	2313										
1285	969	2113										
1294	1449	311	12246	542								
1301	13659	1286										
1316	766	899	641	1297	857	1468	1277	1658	832	1474	776	490
	1835	901	2433	751	2749	400						
1339	1024	2462	1061	934								
1367	11919	890										
1414	10884	1312	12113	1214								
1430	1925	404	9714	704	9092	797	4043	805				
1432	1458	178	979	1307								
1449	1294	332	12246	1789								
1456	680	1296	15450	415	851	368	14223	190	15458	1196	3589	818
	3607	245										
1458	1432	209										
1469	10365	1278										
1489	700	1738	3607	985	3589	550	866	1755	3577	1021	3617	994
	2952	940										
1494	14223	923	851	1849	2749	359	2756	881	15450	1338	15458	1500
	3589	446										
1512	654	1623	674	1645	680	886						
1530	2011	2627										
1551	13053	1768										
1564	2414	2442	11355	173								
1568	3030	1684										
1582	3589	698										
1586	2952	1239	3617	1010	3577	779	3607	332	2009	686	826	1054
1626	1835	416	776	881	1316	156	766	161	636	1025	2433	1949

GRID0	GRID1	OVLP	GRID2	OVLP	GRID3	OVLP	GRID4	OVLP	GRID5	OVLP	GRID6	OVLP
	2749	1372	2756	853	15450	326						
1670	14447	392										
1679	11241	331	1257	2471								
1713	2971	426	14857	355	13743	956	9274	916				
1749	1785	2774	3885	1093								
1775	3147	1640	2104	855								
1785	3885	1114	1749	2782								
1835	1316	912	1277	242	1626	375	636	1621	12822	583		
1852	12808	1003										
1866	4043	929	2583	1789	1870	2119						
1870	2583	1879	1866	2200	4043	855						
1872	2270	2694	13147	967	3428	360						
1878	2028	456	2203	1763	2635	501						
1885	2205	2692										
1925	12804	1132	9714	1075	9092	979	1430	362	580	1095	601	742
1979	589	323										
2009	1586	743	3617	182	826	404						
2011	1530	2623										
2028	1878	507										
2035	10427	1193	15308	1181								
2049	3036	154										
2072	2912	2449	13230	1240								
2081	3571	1416	1136	1877								
2091	2231	2717										
2104	3147	730	1775	854								
2120	11587	1282										
2150	12609	1535	13320	1418								
2170	3175	1862	2845	460								
2188	14469	421										
2203	1878	1726										
2205	1885	2692										
2214	11800	1186										
2231	2091	2635										
2270	13147	976	3428	393	1872	2684						
2308	12094	1793										
2343	957	2042										
2362	15065	1431	13762	1393	3734	1957						
2366	13990	1280	13325	1304	13080	228						
2378	13011	1493	14283	1396								
2402	3548	2136	3693	1837	4049	1795	14875	1806				
2408	11409	1137	14316	1453								
2414	1564	2443	11355	299	11580	188						
2433	636	569	1626	1958	1316	800	2749	3892	2756	1770	15450	503
2454	2543	5348	1061	1096	3420	1993	766	1083	776	1089		
2492	4276	308										
2512	13462	1442										
2528	3349	229										
2543	1061	1334	2454	5144	3420	2101	766	1039				
2567	891	328										
2569	2642	2807										
2583	1866	1813	4043	799	1870	1881						
2588	5571	919	5747	560	15376	365						
2591	17	791	290	831								

GRID0	GRID1	OVLP	GRID2	OVLP	GRID3	OVLP	GRID4	OVLP	GRID5	OVLP	GRID6	OVLP
2598	5436	877	15376	785								
2611	13592	1729										
2628	2633	2782										
2633	2628	2816										
2635	1878	487										
2642	2569	2792										
2702	13256	1509	3428	293								
2749	851	783	2433	4040	1626	1403	2756	5965	15450	2120		
2756	2749	6157	851	997	2433	1888	1494	839	1626	903	15450	5825
2764	3169	475										
2766	12710	1420	13682	1489								
2768	4075	1924										
2774	2793	252										
2778	13895	1148										
2793	2774	313										
2813	12362	1391										
2831	2861	284	3036	749								
2845	3175	797	2170	496								
2859	2861	355										
2861	2859	296	2831	344								
2881	2916	5305										
2908	11525	1291										
2912	2072	2444	13230	1353								
2914	3709	2709	14464	1818								
2916	2881	5107										
2918	9820	620										
2950	3500	5013	3485	1574								
2952	3617	3283	3577	2752	866	520	1489	973	700	770	3607	1208
	1586	1224	826	919								
2971	14857	1378	1713	452								
2984	5712	918										
3012	3891	725	3744	580	3092	186						
3019	3169	188										
3030	1568	1684										
3036	2831	706	2049	176								
3046	14475	1651										
3060	3066	2791	4193	1480	3804	2218	3644	1786	5153	1072	8389	761
	9100	775										
3066	3060	2807	4193	1469	3804	2197	3644	1775	5153	1063	8389	761
	9100	776										
3076	925	952	98	794	914	1072	112	796	325	497	72	788
	58	783	95	779	92	283	927	952	814	160		
3092	3012	192										
3111	3640	2442										
3139	4894	1563	11589	1024								
3147	2104	686	1775	1639								
3163	3278	4768										
3167	5144	1025	5113	1211	6705	828	6328	875	3381	4177	3373	6502
	6141	1018	5229	1165	3522	2003	6677	859	5751	935		
3169	3019	188	2764	466								
3175	2845	803	2170	1888								
3179	6984	801	7554	781	6679	829	7138	787	6455	844		
3201	15182	1825										

GRID0	GRID1	OVLP	GRID2	OVLP	GRID3	OVLP	GRID4	OVLP	GRID5	OVLP	GRID6	OVLP
3203	5629	1089	4973	1066	5227	972	6429	902				
3205	5773	410	5174	1118	5170	1150	5903	844	6334	911	7000	832
3257	15212	1768										
3278	3163	4567										
3310	6229	1012	5953	332	4731	1366	4129	1601				
3318	3356	1144										
3326	15108	902										
3334	3877	1570										
3349	2528	197										
3356	3318	1109										
3373	3381	6581	3167	6627	5144	1087	5113	1311	6705	848	3528	1002
	6328	921	6141	1076	5229	1254	3522	2537	6677	883	5751	890
3381	3167	4346	5144	1058	5113	1265	6705	838	3528	1785	6328	904
	3373	6762	6141	1051	5229	1214	3522	2350	6677	789	5751	667
3420	2454	1993	2543	2121	1061	931	580	801	601	805		
3428	2702	268	13256	938	13147	708	2270	375	1872	346		
3455	13852	1010										
3485	3500	5399	2950	1697								
3494	5254	1285										
3496	14568	1816										
3500	3485	5173	2950	5219								
3502	4276	2122										
3514	4525	304	4468	1544	4458	214	3812	976				
3522	5229	1210	6141	633	3373	2596	3381	2287	3167	2066	5144	1056
	5113	1247	6705	836	3528	1234	6328	903	6677	794	5751	817
3528	6328	974	6705	899	5113	1544	5144	1067	3167	542	3381	1853
	3373	1066	6141	234	5229	1349	3522	1305	6677	349	5751	331
3534	3864	2125										
3544	15512	2509	4105	2371								
3548	2402	2138	3693	2503	4049	2459	14875	1832				
3552	3563	2591										
3563	3552	2555										
3571	2081	1419	1136	941								
3577	866	835	1489	1020	700	809	3607	4973	680	796	3617	4504
	2952	2704	1586	752								
3589	15458	1430	1456	841	680	792	14223	882	3607	3732	700	806
	1489	519	866	829	1582	730						
3607	3589	3935	680	791	700	805	1489	977	866	827	3577	4780
	2952	1156										
3617	3577	4700	866	823	1489	998	700	802	680	779	2952	3284
	1586	1010										
3640	3111	2438										
3644	3804	1935	4193	1664	3060	1786	3066	1776	5153	1274	8389	768
	9100	773										
3646	3668	1776										
3668	3646	1854										
3678	5389	1495	5442	1339								
3687	4361	1720										
3693	3548	2512	15157	161	2402	1840	4049	2788	14875	1825		
3709	2914	2742	14464	1813								
3724	13384	1141	12477	968								
3730	15165	1445										
3734	2362	1993	15065	1817	13762	1779						

GRIDO	GRID1	OVLP	GRID2	OVLP	GRID3	OVLP	GRID4	OVLP	GRID5	OVLP	GRID6	OVLP
3744	3891	2376	3012	575								
3748	4585	2117										
3784	4232	2524	5098	1095								
3798	589	769										
3804	4193	1751	3060	2209	3066	2186	3644	1947	5153	1444	8389	776
	9100	760										
3808	14655	1690										
3812	4458	1291	4468	2094	3514	1025						
3837	15552	2417	4595	2111								
3855	4011	2600										
3864	3534	2122										
3877	3334	1643										
3885	12878	500	10026	181	1785	1113	1749	1093				
3891	3744	2348	3012	711								
3901	4067	2531	4764	1408	4956	742	4993	989	4881	499		
3925	4831	2156										
3958	14998	1441										
3983	4414	2649										
4008	4788	2710										
4011	3855	2602										
4018	4051	2816										
4043	1430	803	9714	260	9092	251	1866	928	2583	784	1870	853
4049	3693	2758	3548	2464	15157	167	2402	1795	14875	1857		
4051	4018	2782										
4055	4721	461	4446	443								
4067	4764	1472	4956	709	3901	2529	4993	826	4881	343		
4075	2768	1928										
4100	13904	1352	12950	1060								
4105	3544	2374	15512	2075								
4129	4731	1060	6229	1253	3310	1613						
4193	3060	1483	3066	1472	3804	1754	3644	1666	5153	1582	8389	828
	9100	789										
4195	4238	2732	5037	858								
4212	15300	250										
4232	3784	2506	5098	1132								
4236	4656	1924	5794	1720								
4238	5037	840	4195	2727								
4276	3502	2138	2492	295								
4294	8757	873	9502	813	15536	2386						
4361	3687	1720										
4401	5569	1602	6045	486	5548	403	5555	1032				
4414	3983	2642										
4446	4721	2502	4055	399								
4458	4468	983	3514	246	3812	1355						
4462	4672	2579										
4468	3514	1615	4525	308	4458	919	3812	2078				
4476	4490	1786										
4490	4476	1712										
4510	4613	2769										
4521	6095	1818										
4525	3514	310	4468	313								
4585	3748	2110										
4595	3837	2113	15552	1747								

GRIDO	GRID1	OVLP	GRID2	OVLP	GRID3	OVLP	GRID4	OVLP	GRID5	OVLP	GRID6	OVLP
4603	5380	285										
4613	4510	2747										
4617	5039	1107										
4627	4646	2845										
4646	4627	2755										
4656	4236	1944	5794	1815								
4672	4462	2579										
4696	4770	2732	5067	533	15556	1232						
4700	4796	1478										
4705	5009	284										
4707	5561	751	5542	1978								
4711	5852	1691										
4721	4055	430	4446	2498								
4731	5953	801	6229	1555	3310	1328	4129	991				
4764	4956	1886	4067	1544	3901	1479						
4770	4696	2794	5067	479	15556	1170						
4778	5675	1909										
4788	4008	2696										
4796	5166	258	4700	1457								
4831	3925	2153										
4848	4856	1270										
4856	4848	1202										
4881	4993	2089	3901	455	4067	303						
4894	3139	1567	11589	784								
4930	5912	2185										
4956	4764	1968	4067	764	3901	793						
4973	3203	1066	6429	188								
4993	3901	964	4067	782	4881	2168						
5005	6215	1731										
5009	4705	317										
5019	5123	1954										
5037	4238	832	4195	850								
5039	4617	1152										
5067	4696	495	4770	442	15556	1553						
5074	141	407	137	1839	135	320						
5098	4232	1202	3784	1162								
5113	6705	1559	3528	1545	6328	1381	5144	3323	3167	1210	3381	1265
	3373	1310	5229	2323	3522	1250	5751	818				
5123	5019	2000										
5144	5113	3248	6705	556	3528	1062	6328	2303	3167	1025	3381	1058
	3373	1087	6141	2040	5229	1031	3522	1056	6677	654	5751	2023
5153	3644	1279	3804	1441	4193	1588	3060	1071	3066	1063	8389	1032
	9100	926										
5166	4796	257										
5170	5903	2700	5174	1744	3205	1153	6334	1054	7000	1088		
5174	5170	1567	5773	2183	3205	1119	6334	1970	7000	1704		
5217	5508	400	5391	188								
5227	3203	979	5629	1528	6429	1312						
5229	3373	1256	3381	1214	3167	1164	5144	1085	5113	2258	6705	1505
	3528	1330	6328	785	3522	1210	5751	1208				
5254	3494	1285										
5380	4603	332										
5389	5442	1819	3678	1495								

GRIDO	GRID1	OVLP	GRID2	OVLP	GRID3	OVLP	GRID4	OVLP	GRID5	OVLP	GRID6	OVLP
5391	5508	2203	5217	225								
5407	5420	2533										
5420	5407	2534										
5436	2598	878	15376	1103								
5442	5389	1898	3678	1346								
5479	5577	2387										
5489	6061	1145										
5508	5217	446	5391	2177								
5520	14250	847	6263	2228								
5522	5862	170										
5542	4707	1912	5561	224								
5548	5561	602	6045	2605	4401	365						
5555	5569	1859	4401	1084								
5561	5548	536	6045	542	4707	797	5542	248				
5569	5555	1874	4401	1669								
5571	5963	222	2588	919								
5577	5479	2305										
5599	6545	1547	5945	1558								
5619	5741	1163	6468	1387								
5629	6677	168	3203	1092	4973	175	5227	1505	6429	1370		
5638	5945	1815	5903	2762								
5675	4778	1905										
5712	2984	919										
5741	5745	1165	6468	1654	5619	1369						
5745	5908	1724	5741	1373								
5747	5963	897	9317	931	2588	580						
5751	3522	794	5229	1150	3373	872	3381	634	3167	926	5144	2087
	5113	759	6705	1087	3528	299	6328	394				
5773	5174	2054	5908	1471								
5794	4656	1817	4236	1715								
5818	5923	877	5914	1271								
5849	6338	2484	9261	313	7048	2094						
5852	4711	1693										
5862	5522	212										
5903	5638	2644	5170	2806	3205	848						
5908	5773	1264	5745	1864								
5912	4930	2183										
5914	5818	1268	5923	446								
5923	5818	812	5914	418								
5931	6439	1068										
5935	6024	800										
5945	5599	1354	5638	1937								
5953	6229	807	3310	299	4731	746						
5963	5747	857	9317	1097	5571	250						
5973	6039	783	7082	979	6278	590						
5978	6368	2338										
6024	5935	839										
6039	5973	829	7082	1499								
6045	5548	2600	5561	608	4401	455						
6055	6304	1319										
6061	5489	1091										
6095	4521	1790										
6113	7029	2272										

GRID0	GRID1	OVLP	GRID2	OVLP	GRID3	OVLP	GRID4	OVLP	GRID5	OVLP	GRID6	OVLP
6119	6423	1995										
6127	6269	488										
6141	3373	1076	3381	1049	3167	1018	5144	1840	3522	630	6677	2224
6152	12752	295	6166	760								
6162	7074	383										
6166	6152	795										
6170	6956	323										
6190	6362	2740										
6208	10220	991	6405	688	6300	685						
6215	5005	1709										
6229	3310	1012	5953	857	4731	1573	4129	1247				
6263	5520	2217	14250	818								
6269	6127	449										
6278	5973	549	7301	302								
6300	6405	1688	6208	640	10220	857						
6304	6055	1315										
6306	930	826										
6328	3528	977	5113	1326	5144	2323	3167	880	3381	904	3373	920
	6141	473	5229	753	3522	903	6677	739	5751	385		
6334	3205	911	5174	2014	5170	991	7000	2402				
6338	9261	278	5849	2499	7048	2341						
6362	6190	2714										
6368	5978	2310										
6382	7249	319										
6405	6208	641	10220	862	6300	1706						
6407	6423	1323	6537	1456								
6423	6119	1870	6407	1528								
6429	5227	1246	4973	210	3203	895	5629	1342				
6439	5931	1119										
6455	7138	808	6679	721	7554	455	6984	343	3179	845		
6468	5745	173	5741	1603	5619	1442						
6475	7366	2288										
6501	548	1154										
6525	8434	2267										
6537	6407	1264	6545	1949								
6545	6537	1834	5599	1702								
6565	7777	333										
6579	6744	1126	10631	1000	8693	185	8292	285	10708	434	155	387
	164	1441	169	1237	121	867	6650	1229	8464	485	230	405
	216	169	8274	211								
6631	6669	1663										
6650	6579	1162	6948	1097	10631	838	10708	905	303	882	275	224
	208	414	155	1234	164	877	169	1442	8464	1146	230	1220
	216	999										
6669	6631	1629										
6677	3522	793	6141	2220	3373	877	3381	769	3167	859	5144	601
	3528	320	6328	691	5629	194						
6679	7554	2274	6984	2375	3179	829	7138	2439	6455	668		
6691	8138	1783										
6705	3528	897	6746	223	5113	1570	5144	601	3167	821	3381	838
	3373	848	5229	1529	3522	836	5751	1139				
6715	7266	772										
6744	10631	524	8693	1120	8223	1069	8292	980	164	1264	169	308

GRID0	GRID1	OVLP	GRID2	OVLP	GRID3	OVLP	GRID4	OVLP	GRID5	OVLP	GRID6	OVLP
	121	1566	6579	1193	8274	1028	8236	301				
6746	6705	259										
6768	7494	2410	6986	2753								
6799	8413	1412										
6874	8106	1988	8316	1681	9955	1450	9466	1453	9630	1526	13706	781
	12785	829										
6882	9850	878										
6908	7070	539										
6922	8170	1903										
6948	10708	887	303	1645	275	1040	208	1309	155	1726	169	707
	6650	1030	8464	812	230	1641	216	1612				
6956	6170	293										
6984	3179	802	7554	2603	6679	2340	7138	2244	6455	308		
6986	7494	2460	6768	2764								
7000	6334	2383	3205	832	5174	1729	5170	1040				
7002	388	1293										
7029	6113	2281										
7048	5849	2081	6338	2311	9261	178						
7070	6908	595										
7074	6162	393										
7082	5973	1027	6039	1466								
7092	8513	1711										
7136	7418	2824										
7138	6679	2437	7554	2306	6984	2284	3179	789	6455	757		
7140	7668	1300										
7191	7718	1848										
7213	7587	1504										
7249	6382	323										
7252	7488	181										
7266	6715	730										
7282	7424	2423										
7301	6278	307										
7306	8092	839	7516	868								
7366	6475	2312										
7395	7894	193										
7418	7136	2748										
7420	7914	1806										
7424	7282	2482										
7447	7454	555										
7454	7447	595										
7488	7252	154										
7494	6986	2418	6768	2378								
7516	8092	2546	7306	890								
7554	6984	2597	3179	783	6679	2251	7138	2267	6455	424		
7587	7213	1539										
7603	1183	1007	8860	1685	8876	1663	14239	764				
7613	8188	2389	7960	392								
7632	7734	1871										
7668	7140	1334										
7700	283	1229										
7716	10087	1574										
7718	7191	1844										
7734	7632	1828										

GRIDO	GRID1	OVLP	GRID2	OVLP	GRID3	OVLP	GRID4	OVLP	GRID5	OVLP	GRID6	OVLP
7777	6565	334										
7826	8454	1829	9030	187								
7840	8318	2234										
7861	8364	1111										
7894	7395	167										
7914	7420	1784										
7944	9720	2276	13088	882								
7960	8188	562	7613	350								
8007	8198	2794										
8017	8618	2513										
8032	8741	2660										
8045	8651	154										
8057	8257	2521										
8059	8595	1263										
8090	8202	1218										
8092	7306	861	7516	2599								
8106	6874	1964	8316	1512	9955	1775	9271	473	9466	1761	9630	1810
	13706	857	12785	767								
8123	260	400										
8138	6691	1778										
8146	8503	1197										
8162	8364	879										
8170	6922	1864										
8188	7960	599	7613	2352								
8198	8007	2805										
8202	8090	1225										
8211	14160	788										
8223	8292	1203	121	1255	8693	2529	6744	1129	6579	164	8274	468
	8236	411										
8236	8274	1585	6744	316	8693	422	8223	380	164	295	121	705
8257	8057	2494										
8274	6579	224	6744	1043	10631	244	8693	437	8223	432	8292	307
	164	764	121	996	8236	1558						
8282	10723	1427	9283	1451								
8292	121	932	8223	1171	8693	1204	6744	998	6579	304	8274	335
8316	6874	1685	8106	1555	9955	1671	9271	221	9466	1673	9630	1712
	13706	865	12785	697								
8318	7840	2198										
8330	11251	1414	8420	1873	10508	1563	10471	1562	12354	1085		
8339	8753	2380										
8364	7861	1100	8162	868								
8389	5153	1033	3644	769	3804	774	4193	828	3060	766	3066	766
	9100	2287										
8408	10890	500										
8413	6799	1413										
8420	11251	1531	8330	1830	10508	1807	10471	1807	12354	1058		
8434	6525	2234										
8454	7826	1842	9030	334								
8464	6650	1136	6579	467	6948	839	10631	209	10708	1061	303	481
	155	980	169	884	230	964	216	611				
8490	8807	2566										
8501	9508	1189										
8503	8146	1183										

GRID0	GRID1	OVLP	GRID2	OVLP	GRID3	OVLP	GRID4	OVLP	GRID5	OVLP	GRID6	OVLP
8513	7092	1707										
8528	10593	1221										
8546	8603	904										
8550	543	1989	9144	1193								
8562	10000	1875										
8595	8059	1210										
8603	8546	859										
8618	8017	2482										
8631	8828	2443	11407	1372	8799	1425	8944	2519				
8633	10118	183										
8651	8045	154										
8693	8223	2514	8292	1237	121	1394	6744	1169	6579	209	8274	474
	8236	455										
8741	8032	2668										
8753	8339	2377										
8757	9502	1563	4294	872	15536	811						
8785	9015	1628	8915	251								
8799	8631	1391	8828	1412	11407	1198	8944	1407				
8807	8490	2652										
8818	13140	947	10761	1514	10026	263						
8820	10781	1148	9355	286								
8828	11407	1399	8631	2456	8799	1418	8944	2507				
8860	1183	1315	7603	1682	8876	2607	14239	808				
8876	8860	2577	1183	1339	7603	1661	14239	814				
8895	482	2477	9235	388								
8915	9015	331	8785	283								
8944	8799	1402	8631	2494	8828	2455	11407	1408				
8948	9235	294	482	259	10696	169						
8969	10619	1971										
8998	9301	490										
9015	8785	1674	8915	299								
9030	7826	205	8454	353								
9051	9075	371										
9075	9051	314										
9092	3420	467	9714	2556	12804	1027	1925	979	1430	803	580	389
	4043	253										
9100	8389	2273	5153	926	3644	745	3804	765	4193	787	3060	775
	3066	776										
9144	543	1750	8550	1253								
9171	9311	2500										
9219	10615	1274	10425	1321								
9221	9235	352	9278	316	9355	372						
9235	482	2781	8895	353	9347	382	9221	388	8948	359		
9261	6338	287	5849	322	7048	184						
9271	9955	676	8316	199	8106	439	9466	659	9630	632	13706	230
	12785	928										
9274	13743	893	1713	923								
9278	9588	372	9221	373								
9283	10723	2550	8282	1391								
9299	10517	2472										
9301	8998	506										
9305	9687	2518										
9311	9171	2509										

GRID0	GRID1	OVLP	GRID2	OVLP	GRID3	OVLP	GRID4	OVLP	GRID5	OVLP	GRID6	OVLP
9317	5963	1095	5747	930								
9339	9697	372	9347	373								
9347	9339	316	482	469	9235	449						
9355	9221	307	10781	220	8820	323						
9385	10325	385										
9391	12139	266										
9428	65	1011										
9466	9271	700	9955	2652	8316	1674	6874	1448	8106	1769	9630	2562
	13706	1060	12785	998								
9502	8757	1564	4294	814	15536	776						
9508	8501	1252										
9512	9707	1689	14689	830								
9588	9659	485	9278	429								
9590	10266	1416										
9615	1197	1037										
9630	9466	2551	9271	671	9955	2557	8316	1714	6874	1518	8106	1822
	13706	1028	12785	1003								
9659	9697	379	9963	226	9588	551						
9687	9305	2489										
9693	195	937										
9697	9711	347	9659	413	9339	429						
9707	9512	1700	14689	837								
9711	9881	368	9697	404								
9714	9092	2558	3420	456	12804	1102	1925	1073	1430	713	580	480
	4043	267										
9720	7944	2295	13088	833								
9734	10431	1010										
9786	9794	361	9963	434								
9794	10325	335	9786	418								
9800	10673	367	9881	364								
9820	2918	610										
9827	10456	1700										
9841	12286	1717										
9850	6882	887										
9854	10456	380										
9881	9800	301	9711	434								
9885	10856	2333	9998	284								
9955	8316	1671	6874	1444	8106	1790	9271	716	9466	2566	9630	2546
	13706	1057	12785	989								
9963	9786	368	9659	284								
9998	10856	161	9885	308								
10000	8562	1865										
10016	10402	250										
10026	8818	275	3885	178								
10087	7716	1576										
10118	8633	158										
10176	12096	2007										
10193	10523	514	10402	111								
10218	10606	672										
10220	6208	990	6405	880	6300	874						
10228	10771	2266	10688	532								
10238	13997	1001										
10266	9590	1408										

GRID0	GRID1	OVLP	GRID2	OVLP	GRID3	OVLP	GRID4	OVLP	GRID5	OVLP	GRID6	OVLP
10325	10673	360	9385	327	9794	401						
10365	1469	1269										
10392	10541	116										
10402	10193	130	10523	272	10016	226						
10425	9219	1325	10615	2309								
10427	2035	1199	15308	821								
10431	9734	1032										
10437	10462	1451	12763	1199								
10456	9854	368	9827	1742								
10462	10437	1417	12763	1331								
10466	10688	339										
10471	10508	2623	8330	1564	11251	2339	8420	1804	12354	1385		
10508	8330	1564	11251	2339	8420	1804	10471	2593	12354	1384		
10517	9299	2494										
10523	10193	553	10402	249								
10541	10392	116										
10580	262	1274										
10593	8528	1208										
10600	11834	1519										
10604	12039	192										
10606	10218	718										
10615	9219	1294	10425	2390								
10619	8969	1964										
10631	10708	311	164	1045	169	825	6948	142	6744	515	6579	996
	6650	842	8464	238	8274	231						
10673	10943	307	10325	379	9800	424						
10684	12079	2006										
10688	10228	484	10771	288	10466	391						
10696	10781	233										
10708	303	427	155	948	169	926	10631	288	6948	895	6579	427
	6650	901	8464	1087	230	913	216	557				
10723	8282	1368	9283	2558								
10761	13140	1532	8818	1514								
10771	10854	332	10228	2346	10688	349						
10781	10696	212	9355	161	8820	1142						
10848	774	200										
10854	10771	394	10228	170								
10856	9998	166	9885	2331								
10871	12167	247	12557	385								
10884	1414	1304	12113	1491								
10890	8408	464										
10920	11600	1477										
10943	10673	372										
10951	1067	1230	12167	107								
10956	763	382										
11045	14473	1031										
11241	1679	332	1257	317								
11247	12230	134										
11251	8420	1531	8330	1413	10508	2316	10471	2317	12354	1489		
11253	13150	2171										
11355	2414	307	1564	176	11580	2515						
11407	8828	1402	8631	1373	8799	1202	8944	1413				
11409	2408	1130	14316	1141								

GRID0	GRID1	OVLP	GRID2	OVLP	GRID3	OVLP	GRID4	OVLP	GRID5	OVLP	GRID6	OVLP
11525	2908	1299										
11547	1073	991	11718	2106								
11577	11884	2539	12566	2314								
11580	11355	2447	2414	193								
11587	2120	1277										
11589	4894	784	3139	1020								
11600	10920	1441										
11701	495	523										
11718	11547	2029	1073	841								
11763	14589	1209										
11800	2214	1190										
11816	1268	527										
11834	10600	1514										
11884	12566	2332	11577	2508								
11906	92	1089	95	214	90	1079	12205	1023	814	665		
11919	1367	889										
12039	10604	196										
12079	10684	1990										
12094	2308	1789										
12096	10176	2008										
12113	10884	1489	1414	1213								
12135	12139	1452										
12139	9391	238	12135	1517								
12167	1067	623	10951	107	10871	250						
12205	98	383	325	1000	90	631	95	1095	92	1304	11906	983
	814	1624										
12230	11247	117										
12232	12311	212										
12246	1294	543	1449	1789								
12269	12294	1657										
12286	9841	1702										
12294	12269	1647										
12311	12232	199										
12333	12339	2226	12750	854								
12339	12333	2203	12750	1128								
12354	10471	1391	10508	1391	8330	1090	11251	1496	8420	1066		
12362	2813	1394										
12396	12461	1741										
12454	1187	1627										
12461	12396	1675										
12473	12604	2417										
12477	13384	2203	3724	968								
12557	10871	356										
12566	11884	2297	11577	2281								
12604	12473	2501										
12609	13320	2272	2150	1543								
12710	2766	1429	13682	2076								
12750	12339	1084	12333	815								
12752	6152	313										
12763	10462	1337	10437	1209								
12785	13706	783	9630	1010	9466	1007	9271	946	9955	999	8316	698
	6874	829	8106	770								
12796	14171	1327										

GRID0	GRID1	OVLP	GRID2	OVLP	GRID3	OVLP	GRID4	OVLP	GRID5	OVLP	GRID6	OVLP
12804	9714	1093	9092	1024	1925	1133	580	878	601	136		
12808	1852	966										
12816	14163	1349										
12822	636	280	1835	583								
12852	14342	1372										
12871	12899	1042	14386	637	15055	315	13627	323				
12878	3885	516										
12899	14386	313	15055	613	12871	992	13627	509				
12950	13904	2107	4100	1060								
13011	2378	1502	14283	1969								
13053	1551	1765										
13057	14386	568	13118	580								
13080	13990	155	2366	228								
13088	7944	880	9720	835								
13118	14386	704	13057	619								
13140	8818	947	10761	1528								
13147	3428	698	2270	977	1872	968						
13150	11253	2161										
13156	13329	1185										
13216	13772	2461										
13230	2912	1343	2072	1235								
13256	2702	1519	3428	940								
13295	15043	2331										
13320	12609	2298	2150	1423								
13325	13990	2266	2366	1308								
13329	13156	1132										
13358	1204	1244										
13384	12477	2208	3724	1144								
13426	15532	1812										
13462	2512	1435										
13592	2611	1730										
13627	12871	344	12899	573								
13659	1301	1276										
13682	12710	2083	2766	1497								
13698	14058	1663										
13706	9630	1028	9466	1062	9271	239	9955	1061	8316	864	6874	782
	8106	857	12785	746								
13743	1713	944	9274	892								
13762	15065	2591	2362	1394	3734	1778						
13772	13216	2461										
13783	14332	2566	13792	553								
13792	14332	515	13783	512								
13844	14046	2456										
13852	3455	1020										
13895	2778	1149										
13904	12950	2115	4100	1357								
13963	14918	1385										
13990	2366	1277	13325	2258								
13997	10238	1001										
14046	13844	2374										
14058	13698	1666										
14160	8211	788										
14163	12816	1360										

GRID0	GRID1	OVLP	GRID2	OVLP	GRID3	OVLP	GRID4	OVLP	GRID5	OVLP	GRID6	OVLP
14167	15062	213										
14171	12796	1333										
14223	1494	929	851	701	1456	182	15458	456	3589	889	3607	115
14239	8876	813	8860	809	1183	1261	7603	764				
14250	5520	836	6263	811								
14283	13011	1973	2378	1393								
14316	11409	1141	2408	1460								
14332	13783	2652	13792	556								
14342	12852	1372										
14352	14666	1636										
14386	15055	815	13057	637	13118	716	12899	291	12871	572		
14447	1670	391										
14464	3709	1807	2914	1811								
14469	2188	426										
14473	11045	1028										
14475	3046	1657										
14479	14922	1343										
14568	3496	1812										
14589	11763	1214										
14655	3808	1688										
14666	14352	1640										
14689	9512	831	9707	840								
14857	2971	1376	1713	364								
14875	4049	1865	3693	1833	3548	1834	2402	1798				
14905	14976	1426										
14918	13963	1381										
14922	14479	1310										
14976	14905	1415										
14998	3958	1436										
15011	15024	1432										
15024	15011	1400										
15028	15497	1400										
15043	13295	2351										
15055	13057	161	14386	817	12899	561	12871	287				
15062	14167	243										
15065	13762	2571	2362	1433	3734	1817						
15108	3326	901										
15157	3693	157	4049	163								
15165	3730	1451										
15182	3201	1825										
15212	3257	1768										
15276	15354	740										
15300	4212	244										
15308	10427	821	2035	1174								
15354	15276	784										
15376	2598	785	5436	1103	2588	360						
15450	2756	6022	2749	2323	851	1016	2433	563	1494	1315	15458	3847
15458	1456	1166	15450	4049	851	1009	1494	1506	3589	1396		
15497	15028	1405										
15512	3544	2513	4105	2074								
15532	13426	1809										
15536	4294	2374	8757	812	9502	778						
15552	3837	2423	4595	1742								

```
GRIDO GRID1 OVLP GRID2 OVLP GRID3 OVLP GRID4 OVLP GRID5 OVLP GRID6 OVLP

15556  5067 1564  4696 1178  4770 1116
```